Aalto University
School of Chemical
Engineering

Pihla Ahola

MITOCHONDRIAL DYSFUNCTION AS A SOURCE FOR MISLEADING POSITIVES IN *IN VITRO* DNA DAMAGE ASSAYS

Master´s Programme in Life Science Technologies
Major in Biosystems and Biomaterials Engineering

Master's thesis for the degree of Master of Science in Technology
submitted for inspection, Espoo, 27 July, 2018.

Supervisor	Professor Alexander Frey
Instructors	Ph.D. Mikko Karjalainen
	Ph.D. Pekka Heikkinen

Aalto University
School of Chemical
Engineering

Aalto University, P.O. BOX 11000, 00076 AALTO
www.aalto.fi

Abstract of master's thesis

Author Pihla Ahola

Title of thesis Mitochondrial dysfunction as a source for misleading positives in *in vitro* DNA damage assays

Degree Programme Life Science Technologies

Major Biosystems and Biomaterials Engineering

Thesis supervisor Professor Alexander Frey

Thesis advisor(s) / Thesis examiner(s) Ph.D. Mikko Karjalainen, Ph.D. Pekka Heikkinen

Date 27.07.2018 **Number of pages** 85+13 **Language** English

Abstract

Drug toxicity testing is a necessary part of the drug development process and it is required by the regulatory authorities. Genotoxicity, the ability of drugs to cause DNA damage, is tested by both *in vivo* and *in vitro* tests. *In vitro* DNA damage assays have high sensitivity but low specificity and hence they cause misleading positive results, which leads to unnecessary animal testing. Animal testing is expensive and causes ethical issues.

Drugs that cause dysfunction in mitochondria are called mitochondrial toxins. Since the majority of the ATP is produced in mitochondria, mitochondrial toxins may cause insufficient energy production in mammalian cells. Since many processes in the cell, such as the cell cycle regulation, DNA damage repair and cytoskeleton dynamics, are energy dependent, the ATP depletion could possibly lead to indirect DNA damage response. The aim of this study was to investigate if the ATP depletion caused by the mitochondrial toxins induces the DNA damage indirectly and hence lead to misleading positive results in genotoxic assays. The focus was on examining whether the ATP depletion would cause DNA damage via changed dynamics of cytoskeleton.

The study was conducted with High-content analysis (HCA). HepG2/C3A cells were treated with 16 compounds, 15 mitochondrial toxins and one genotoxic agent, paclitaxel. The cells were immunolabeled to detect tubulin and actin fibers, nuclei, DNA double strand breaks and mitotic cells. Excluding metformin, all of the mitochondrial toxins did increase the DNA damage response significantly ($p<0.05$) in HepG2/C3A cells. Most of these compounds seemed to increase the DNA damage due to the cell death. However, most of the compounds that interfere with ATP production via uncoupling, increased DNA damage response without the cell death. Paclitaxel was the only compound that increased both the DNA double strand break marker and the mitotic marker simultaneously. Since the DNA damage marker and mitosis marker had a negative correlation it can be concluded that energy depletion did not cause dysfunction in the cell cycle regulation. Paclitaxel and most of the mitochondrial toxins seemed to affect the tubulin and actin dynamics. There appeared to be association between DNA damage and changed cytoskeleton dynamics but the causality of the two was not verified and requires further investigation. Whether the responses were due to the ATP depletion or general cytotoxicity of the mitochondrial toxins, was not confirmed in this study.

Keywords Mitochondrial toxicity, ATP depletion, DNA damage, cytoskeleton dynamics, High-content analysis (HCA).

Aalto-yliopisto
Kemian tekniikan
korkeakoulu

Aalto-yliopisto, PL 11000, 00076 AALTO
www.aalto.fi
Diplomityön tiivistelmä

Tekijä Pihla Ahola

Työn nimi Mitokondrioiden vajaatoiminta lähteenä *in vitro* DNA-vaurioanalyyseissä ilmenneille harhaanjohtaville positiivisille tuloksille

Koulutusohjelma Life Science Technologies

Pääaine Biosystems and Biomaterials Engineering

Työn valvoja Professori Alexander Frey

Työn ohjaaja(t)/Työn tarkastaja(t) FT Mikko Karjalainen, FT Pekka Heikkinen

Päivämäärä 27.07.2018 **Sivumäärä** 85+13 **Kieli** Englanti

Tiivistelmä

Lääkkeiden toksisuuden testaaminen on oleellinen osa lääkekehityskaarta ja lääkevalvontaviranomaiset velvoittavat sitä myyntilupaa hakevilta valmisteilta. Lääkkeet, jotka aiheuttavat vaurioita suoraan DNA:han, ovat genotoksisia. Genotoksisuutta tutkitaan niin *in vivo*- kuin *in vitro* -menetelmillä. DNA-vaurioiden tutkimista varten kehitellyt *in vitro* –testit ovat herkkiä, mutta epäspesifisiä, mistä johtuen ne antavat harhaanjohtavia positiivisia tuloksia. Tämä johtaa turhiin eläinkokeisiin, jotka ovat kalliita ja herättävät eettisiä kysymyksiä.

Mitokondrioihin vaikuttavat toksiinit aiheuttavat mitokondrioiden vajaatoimintaa ja koska suurin osa nisäkässolujen ATP-tuotannosta tapahtuu niissä, voi solujen altistuminen näille toksiineille johtaa riittämättömään energiatuotantoon. Monet solussa tapahtuvat prosessit, kuten solusyklin sääntely, DNA:n korjausmekanismit ja solutukirankadynamiikka, ovat energiariippuvaisia. Tämän tutkimuksen tarkoituksena oli selvittää, voiko mitokondriotoksisuudesta johtuva energiavaje johtaa epäsuorasti DNA-vaurioihin ja aiheuttaa siten harhaanjohtavia positiivisia tuloksia genotoksisuustesteissä. Työssä keskityttiin tutkimaan, aiheuttiko ATP:n puutos DNA-vaurioita nimenomaan muuttuneen solutukirankadynamiikan vuoksi.

Tämä tutkimus suoritettiin High-content analysis (HCA) –metodilla. HepG2/C3A-solut käsiteltiin 16:lla aineella, joista 15 oli mitokondriotoksisia ja yksi, paklitakseli, genotoksinen. Soluille suoritettiin vasta-ainevärjäys, jolla paikallistettiin solujen tumat, mikrotubulukset, aktiinisäikeet, DNA-katkokset ja mitoottiset solut. Metformiinia lukuun ottamatta kaikki mitokondriotoksiinit lisäsivät DNA-katkosten määrää merkitsevästi ($p<0.05$) HepG2/C3A-soluilla. Suurella osalla näistä toksiineista DNA-katkosten lisääntyminen näytti johtuvan solukuolemasta. Aineet, jotka aiheuttivat ATP:n puutosta irtikytkennästä johtuen, lisäsivät DNA-katkosten määrää, vaikka solukuolemien määrä ei lisääntynyt. Paklitakseli oli ainoa aine, joka lisäsi sekä DNA-katkosten että mitoottisten solujen osuutta samanaikaisesti. Muilla aineilla DNA-katkosten ja mitoottisten solujen esiintyvyydellä oli negatiivinen assosiaatio. Tästä voidaan päätellä, että ATP:n puutos ei aiheuttanut vajaatoimintaa solusyklin sääntelymekanismeissa. Paklitakseli ja suurin osa mitokondriotoksiineista näyttivät vaikuttavan tubuliinin ja aktiinin dynamiikkaan. DNA-katkoksilla ja solutukirankadynamiikan muutoksilla näytti olevan yhteys, mutta kausaliteettia näiden välillä ei tässä tutkimuksessa pystytty varmistamaan ja asia vaatii siten jatkotutkimuksia. Tässä tutkimuksessa ei varmistunut, johtuivatko mitokondriotoksiineiden aiheuttamat muutokset solutukirankadynamiikassa ja DNA-katkosten määrässä ATP;n puutoksesta vai kyseisten aineiden yleisestä solutoksisuudesta.

Avainsanat Mitokondriotoksisuus, ATP:n puutos, DNA-vaurio, solutukirankadynamiikka.

PREFACE

This master's thesis was conducted for Investigative Toxicology group at Orion Oyj, Espoo.

I would like to express my sincere gratitude to the advisors of my thesis, Mikko Karjalainen and Pekka Heikkinen. It has been inspiring to learn from the best. My deepest thanks to Mikko Karjalainen for the incredible amount of mentoring and support and for taking the time to help and advise me whenever needed. I am grateful to Pekka Heikkinen for sharing his expertise and for his positive and encouraging attitude throughout the project. I am thankful to Professor Alexander Frey for supervising my master's thesis and for the valuable comments and instructions.

I would like to thank the team leader Teija Oinonen and all the members of the Investigative Toxicology group for always being very helpful and taking me as a part of the group. I would like to thank Saila Pajari for teaching me many of the laboratory techniques and helping me to get started with the laboratory work. Thanks to Saila Pajari, Merja Valovirta and Teija Malen for all the help in conducting the experimental part of my thesis and for all the helpful tips that made my work easier.

I would like to thank Lassi Paavolainen at FIMM for providing the confocal microscopy images for my thesis and helping with the use of ACC.

Thanks to my family and friends for all the encouraging words and peer support during this project. Finally, I would like to thank my fiancé Tuomo for all the love, cheering and support not only throughout this project but also during my entire studies. Thank you, Tuomo, for being there for me.

Helsinki, 27.7.2018
Pihla Ahola

TABLE OF CONTENTS

ABBREVIATIONS

ACC	Advanced cell classifier
Acetyl CoA	Acetyl coenzyme A
ADP	Adenosine diphosphate
APC	Anaphase promoting complex
ATP	Adenosine triphosphate
BSA	Bovine serum albumin
CAK	Cdk-activating kinase
Cdk	Cyclin-dependent kinase
CKI	Cdk inhibitor protein
DMEM	Dulbecco's modified eagle medium
DMSO	Dimethyl sulfoxide
ER	Endoplasmic reticulum
ETC	Electron transport chain
$FADH_2$/FAD	Flavin adenine dinucleotide
FC	Flow cytometry
FMN	Flavin mononucleotide
GDP	Guanosine diphosphate
GTP	Guanosine triphosphate
HCA	High-content analysis
HCS	High-content screening
IF	Immunofluorescence
LEC	Lowest effective concentration
MPT	Mitochondrial permeability transition
MPTP	Mitochondrial permeability transition pore
mtDNA	Mitochondrial DNA
$NADH/NAD^+$	Nicotinamide adenine dinucleotide
PBS	Phosphate buffered saline
PFA	Paraformaldehyde
pH3	Phospho-histone H3
Q	Ubiquinone
QH_2	Ubiquinol
ROS	Reactive oxygen species
VDAC	Voltage-dependent anion channels

I INTRODUCTION

Toxicology screening is an important part of the drug development when performing the risk-benefit assessment (Bluemel, 2012). Screening can be done *in vivo* by animal testing and *in vitro* by using cell lines or primary cells (Parasuraman, 2011). Investigation of drug toxicology is required by the regulatory authorities and there are generally accepted guidelines available for toxicology testing (Whitebread et al., 2005). Approximately 30% of drug candidates never reach the market due to their toxicity (Guengerich, 2011; Whitebread et al., 2005). Drug toxicity is also a significant reason for drug withdrawal and addition of black box warnings after the approval (Abraham et al., 2008). Failing of the drug candidate in the late stage of drug development is highly expensive and therefore optimization of early-stage preclinical toxicology studies is important (Verbist et al., 2015).

All drugs are toxic if the dose is high enough and thus drug toxicity that leads to candidate failing refers to toxic effects that are expressed at therapeutic doses (Guengerich, 2011). The mechanisms of different toxins vary greatly. Cytotoxicity refers to toxicity that reduces the viability of the cells by decreasing the proliferation or leading to cell death (Nicolette, 2012). Mitochondrial toxicity is one form of cytotoxicity and it refers to toxic effects that pharmaceuticals may have on mitochondria (Meyer et al., 2018). Since mitochondria produce most of the energy that is used by the cell, mitochondrial toxins may cause energy depletion in the cell and this may lead to apoptosis (Wallace & Starkov, 2000).

Genotoxicity refers to ability of compounds to cause DNA damage and it may lead to inheritable defects or cancer formation (Nicolette, 2012). The International Council for Harmonisation of Technical Requirements for Pharmaceuticals for Human Use (ICH) has set a guideline for adequate genotoxicity testing. According to this guideline, all pharmaceuticals need to go through a test for gene mutation in bacteria (AMES test) and either two separate *in vivo* genotoxicity tests or one *in vivo* and one *in vitro* genotoxicity test. (ICHS2(R1), 2011) The Organization for Economic Co-operation and Development (OECD) has set more detailed guideline for each *in vitro* and *in vivo* test (OECD, 2015).

The currently used *in vitro* tests for genotoxicity have high sensitivity but low specificity, which leads to high rate of false positives (Corvi & Madia, 2017). The false and misleading positives in *in vitro* tests lead to follow-up *in vivo* tests and to unnecessary animal testing (Kirkland et al., 2007). This is problematic due to the ethical issues and high costs (Benigni & Bossa, 2011). The ways to decrease the false positives in *in vitro* tests have been investigated (Corvi & Madia, 2017). It seems that the rate of misleading positives can be reduced e.g. by adjusting the top concentration of the compound and by choosing a suitable cell type (Fowler et al., 2012a; Fowler et al., 2012b; Parry et al., 2010).

The aim of this research was to investigate if energy depletion caused by mitochondrial toxicity may be responsible for the misleading positives in DNA damage assays. If the energy production is insufficient, the cell may not be capable of performing all its functions properly and this might lead indirectly to DNA damage. An indirect induction of DNA damage is not considered as an indication of genotoxicity and hence this type of actual but indirect response of DNA damage is not considered straightforwardly as “positive”. The focus in this research was on examining the impact of energy deprivation on cytoskeletal dynamics during mitosis, and estimating whether it might mediate the genotoxic effect.

II LITERATURE REVIEW

1 Mitochondrial toxicity

1.1 Structure of mitochondria

Mitochondria are cytosolic organelles with a diameter of 0.5–1 μm (Alberts et al., 2015d, p. 755). They are found in every human cell, apart from mature erythrocytes. Their number per cell depends on the energy need of the cell type. Metabolically active cells, such as the ones found in liver and heart, have high number of mitochondria. (Neustadt & Pieczenik, 2008) The shape of the mitochondria may be constantly changing and varies depending on the tissue (Alberts et al., 2015d, p. 755). Mitochondria also interact with other cellular components, mainly with cytoskeleton and endoplasmic reticulum (ER) (Frey & Mannella, 2000). They consist of an outer and inner membrane. Both of these membranes consist of phospholipid bilayer and membrane proteins. (Krauss, 2001) The membranes confine the two mitochondrial compartments: intermembrane space that lies between the outer and inner membranes and the matrix that is located inside the inner membrane. (Harris & Thompson, 2000) The structure of a mitochondrion is illustrated in figure 1.

The outer membrane of the mitochondria is permeable to molecules smaller than 5000 Daltons. The high permeability is enabled by porins, also known as voltage-dependent anion channels (VDACs). VDACs are the most abundant proteins in the outer membrane. (Harris & Thompson, 2000) The protein-to-lipid ratio for the outer mitochondrial membrane is about 50:50 (Krauss, 2001). Due to the high permeability, the pH and ionic composition of the intermembrane space is equivalent to cytosol (Alberts et al., 2015d, p. 757). However, the outer membrane is impermeable to apoptosis promoting proteins, which are present in the intermembrane space. This impermeability enables the regulation of apoptosis. (Harris & Thompson, 2000)

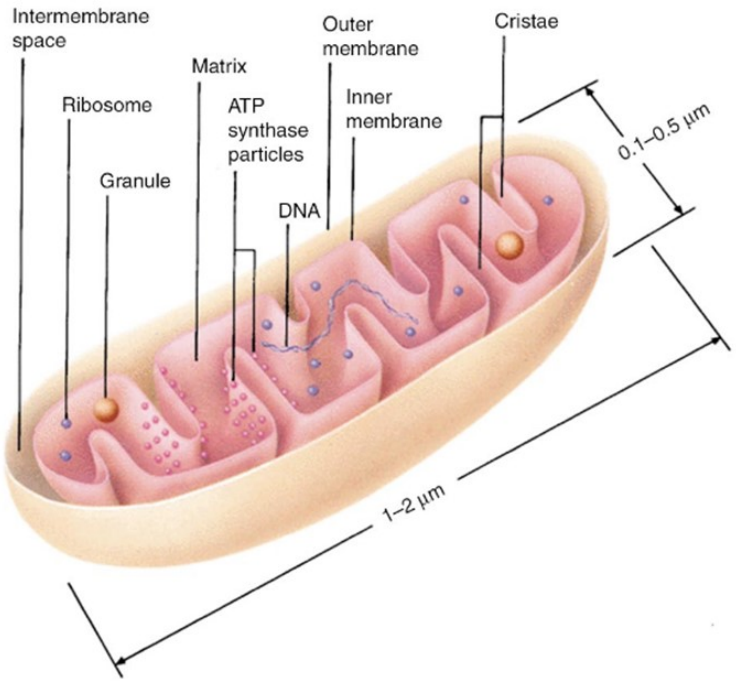

Figure 1. The structure of the mitochondria. Mitochondria consist of an outer and inner membrane, intermembrane space and matrix. Inner membrane is folded into cristae. Mitochondria contain their own DNA (mtDNA) and ribosomes and granules participate the synthesis of mitochondrial proteins. Mitochondria produce ATP by ATP synthase that is located in the inner membrane. (Frey & Mannella, 2000)

The transportation across the inner membrane is more tightly regulated than transport through the outer membrane (Harris & Thompson, 2000). The inner membrane is folded into cristae and has a large surface area. It contains several transport proteins, including electron transport chain (ETC) and ATP synthase, and the protein-to-lipid ratio is approximately 80:20. (Amacher, 2005; Krauss, 2001) The inner membrane is impermeable and small molecules can pass it only with the aid of membrane transport proteins. The content of the matrix can therefore be regulated and it enables the formation of electron gradient across the inner membrane. (Wallace & Starkov, 2000) The matrix contains e.g. several enzymes and mitochondrial DNA, RNA and ribosomes (Alberts et al., 2015d, p. 759; Frey & Mannella, 2000). Some of the inner membrane proteins are produced by the mitochondria themselves in the matrix (Frey & Mannella, 2000).

1.2 Energy production in eukaryotic cell

In order to function, the cells require energy. The energy is needed e.g. for growth, division, migration and maintenance of the cell structure. The cells need an external energy source that they can utilize to produce adenosine triphosphate (ATP). (Haug et al., 2009, p. 46) ATP is the main chemical energy currency of the cell (Alberts et al., 2015d, p. 754). The cells produce ATP via glycolysis or oxidative phosphorylation. A small amount of ATP is also produced in citric acid cycle.

1.2.1 Glycolysis

Glycolysis is a process where ATP is produced without the presence of oxygen. It occurs in the cytosol of the cell. In the glycolysis, a glucose molecule is degraded into two pyruvate molecules. This process consumes two and produces four molecules of ATP. Hence, the yield is two ATP molecules per one glucose molecule. (Alberts et al., 2015a, p. 74) Glycolysis consists of multiple steps that are shown in figure 2. ATP is produced in two different stages. The first ATP molecules are generated when phosphoglycerate kinase catalyses reaction where 1,3-bisphosphoglycerate donates one phosphoryl group to adenosine diphosphate (ADP). As a product, ATP is produced. The second stage where ATP is generated is the final stage of glycolysis where pyruvate is being produced. Pyruvate kinase catalyzes reaction where a phosphate group is transferred from phosphoenolpyruvate to ADP, generating ATP. During glycolysis, also two molecules of coenzyme nicotinamide adenine dinucleotide (NADH) are produced. (Berg et al., 2002c)

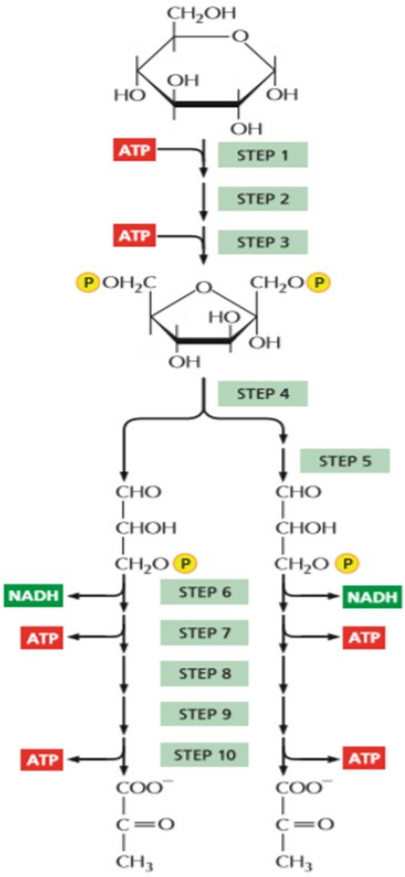

Figure 2. Glycolysis. In glycolysis, glucose is degraded via several steps into two pyruvate molecules. During the first steps of glycolysis, two ATP molecules are consumed and at steps 7 and 10, four ATP molecules are produced. The total yield in glycolysis is two molecules of ATP per one glucose molecule. In addition, two molecules of NADH are produced during glycolysis. (Adapted from Alberts et al., 2015a, p. 75.)

1.2.2 Oxidative Phosphorylation

Over 90% of the ATP is produced in the mitochondria via oxidative phosphorylation (Amacher, 2005; Neustadt & Pieczenik, 2008). This process is efficient and produces more ATP than glycolysis (Zheng, 2012). Oxidative phosphorylation takes place in the inner mitochondrial membrane and consists of two consecutive events. The first event is an electron flow through the electron transport chain that generates a proton gradient across the inner membrane. This is followed by the second event where ATP synthase utilizes the proton gradient to produce ATP from ADP. (Saraste, 1999)

The electrons for the ETC are gained from the coenzymes NADH and flavin adenine dinucleotide ($FADH_2$) (Neustadt & Pieczenik, 2008). As mentioned earlier, NADH is

produced in glycolysis in the cytosol (Berg et al., 2002c). NADH is transported into mitochondria through the malate-aspartate shuttle (Eto et al., 1999). In addition, NADH is formed in the citric acid cycle where also the $FADH_2$ is produced. Citric acid cycle takes place in the mitochondrial matrix and it utilizes acetyl Coenzyme A (acetyl CoA) as its fuel to produce NADH and $FADH_2$. (Neustadt & Pieczenik, 2008) Acetyl CoA is produced either by β-oxidation of fatty acids or by oxidative decarboxylation of the pyruvate generated from glycolysis (Berg et al., 2002a; Neustadt & Pieczenik, 2008). One round of citric acid cycle produces three molecules of NADH and one molecule of $FADH_2$. In addition, one molecule of ATP is produced. (Modica-Napolitano et al., 2007) The overview of energy production in mitochondria is described in figure 3.

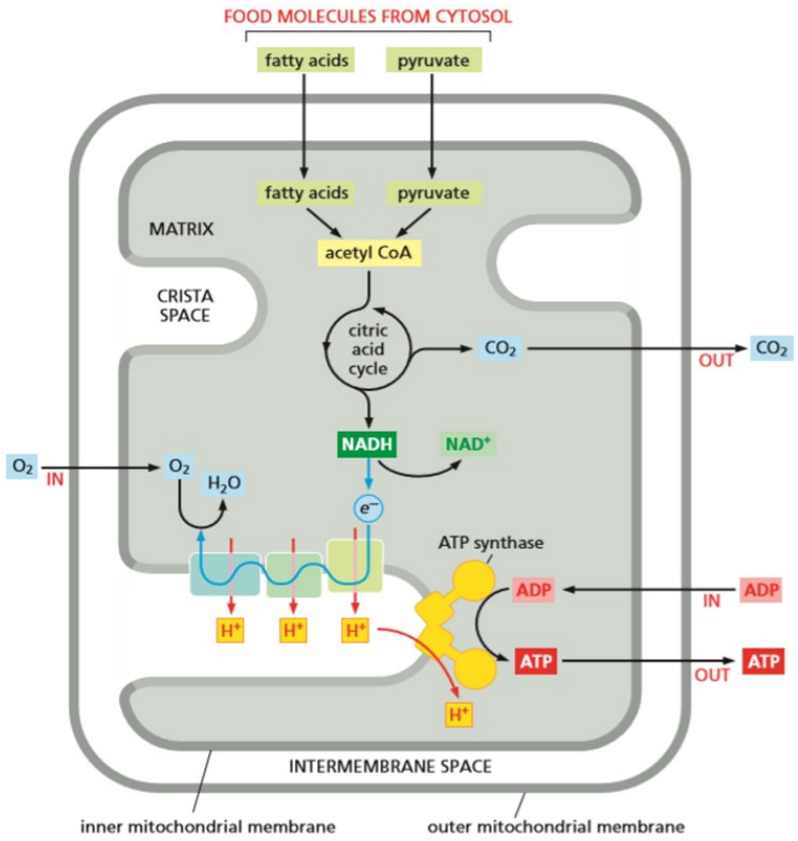

Figure 3. Overview on energy production in mitochondria. Fatty acids and pyruvate enter mitochondria where they are transformed into acetyl CoA. Acetyl CoA is fuel for citric acid cycle that produces NADH. NADH donates two electrons that flow through ETC producing proton gradient across the inner mitochondrial membrane. ATP synthase utilizes proton gradient to produce ATP from ADP. ATP is transported from the mitochondria to cytosol by ADP/ATP carrier proteins. (Alberts et al., 2015d, p. 759)

The electron transport chain includes four complexes, each of which consist of several proteins (Brinkman et al., 1998). These complexes are NADH:ubiquinone oxidoreductase (complex I), succinate:ubiquinone reductase (complex II), cytochrome bc_1 (complex III) and cytochrome c oxidase (complex IV). The complexes transport the electrons from NADH and $FADH_2$ to oxygen and H_2O is formed. (Huttemann et al., 2007) These reactions are highly energy-yielding and the energy is released gradually in each step of the transportation chain (Lodish et al., 2000). The released energy is used for pumping protons from matrix to intermembrane space and this is done by complexes I, III and IV. The evolved proton gradient is utilized by the ATP synthase (complex V). (Brand, 2000) The ETC and ATP synthase are shown in figure 4.

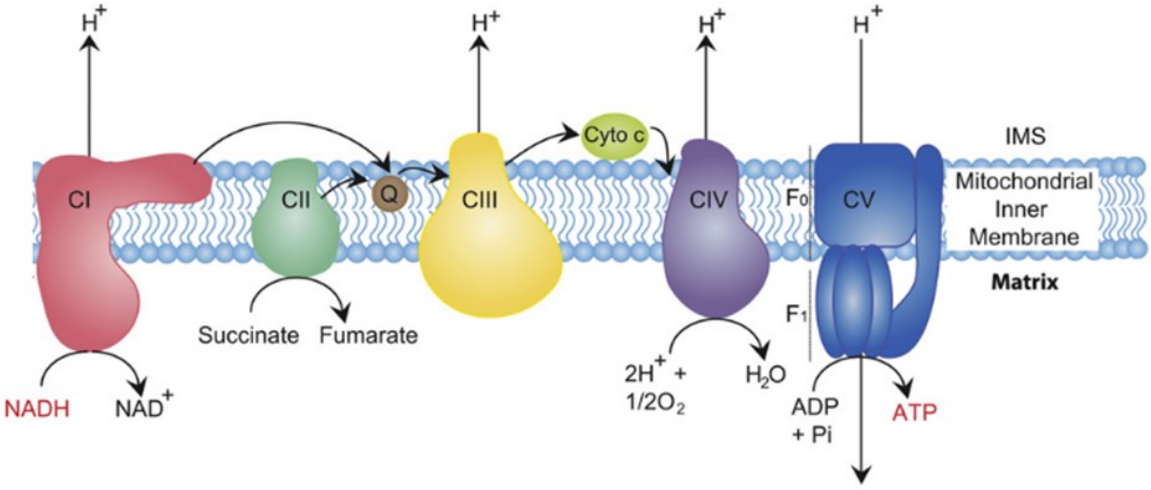

Figure 4. Complexes I-IV of ETC and ATP synthase (complex V). Complex I accepts electrons from NADH and complex II from $FADH_2$ that is produced when succinate oxidizes to fumarate. Electrons flow via ubiquinone (Q) to complex III and via cytochrome c to complex IV. At complex IV electrons reduce oxygen to water. Complexes I, III and IV pump protons from mitochondrial matrix to intermembrane space and ATP synthase utilizes formed proton gradient to produce ATP from ADP. (Adapted from Osellame et al., 2012)

Each complex in ETC has their own specific function. Complex I is a L-shaped structure consisting of over 40 different subunits (Guenebaut et al., 1998; Huttemann et al., 2007; Sled et al., 1994). It is the largest and most complicated of the ETC complexes (Estornell, 2000). NADH enters ETC in complex I and it is oxidized to NAD^+ by cofactor flavin mononucleotide (FMN). Two electrons are released and they flow through eight iron-sulfur clusters to reduce ubiquinone (Q) to ubiquinol (QH_2). (Hirst, 2009) QH_2 is transported to the complex III (MacAskill & Kittler, 2010). Complex I

pumps four protons per NADH from mitochondrial matrix to the intermembrane space (Hirst, 2009).

Complex II is a part of citric acid cycle. One of its four subunits is responsible for the generation of $FADH_2$ that is produced when succinate is oxidized to fumarate. Complex II also feeds electrons from $FADH_2$ into the ETC. (Modica-Napolitano et al., 2007) Hence, $FADH_2$ never leaves the complex but it is oxidized to FAD and two electrons are released and transported through three iron-sulfur clusters (Lodish et al., 2000; Tomitsuka et al., 2003). The electrons flow to ubiquinone and reduce it to ubiquinol which is transported to complex III (Lodish et al., 2000). Complex II does not transport protons across the inner membrane (Huttemann et al., 2007).

Complex III has 11 subunits and it catalyzes the reaction where electrons from QH_2 are transferred to cytochrome c. Cytochrome c is an electron carrier that is located on the outer surface of the inner membrane and it transfers one electron at a time from complex III to complex IV. (Modica-Napolitano et al., 2007) Complex III itself contains three electron transfer proteins, cytochrome c_1, cytochrome b and an iron-sulfur protein (Trumpower, 1990). Complex III transfers electrons and pumps protons to the intermembrane space by a mechanism called the protonmotive Q cycle (Grossman et al., 2004). Complex III pumps four protons to the intermembrane space. (Trumpower, 1990)

Complex IV is the final complex in the ETC and it consists of 13 subunits (Grossman et al., 2004). In complex IV, cytochrome c is oxidized and the electron flows via copper ions and cytochrome a and a_3 to O_2, which is the final electron acceptor (Saraste, 1999). One electron pair reduces only one oxygen atom and one water molecule is produced. Therefore, four electrons are needed to reduce one O_2 molecule. Complex IV pumps two protons to the intermembrane space per one electron pair. (Lodish et al., 2000)

The final step in oxidative phosphorylation is the production of ATP by the ATP synthase. ATP synthase, or F_1F_0ATPase, is also called complex V even though it is not part of the ETC. It is functionally reversible enzyme, meaning that it can both produce and hydrolyze ATP. ATP synthase consists of two functional domains: F_1 and F_0. F_1 is located in mitochondrial matrix and has five different subunits: three copies

of α and β and one copy of γ, δ and ε. (Saraste, 1999) F_1 domain is responsible for the production of ATP from ADP and inorganic phosphate P_i. F_0 is bound to the inner mitochondrial membrane and includes ten different subunits: a, b, c, d, e, f, g, A6L, F_6 and OSCP. Subunit c is thought to have eight copies that form a ring-shaped structure but other subunits have only one copy of each. (Jonckheere et al., 2012) F_0 domain forms a proton channel across the inner membrane (Saraste, 1999). The subunits of ATP synthase are shown in figure 5.

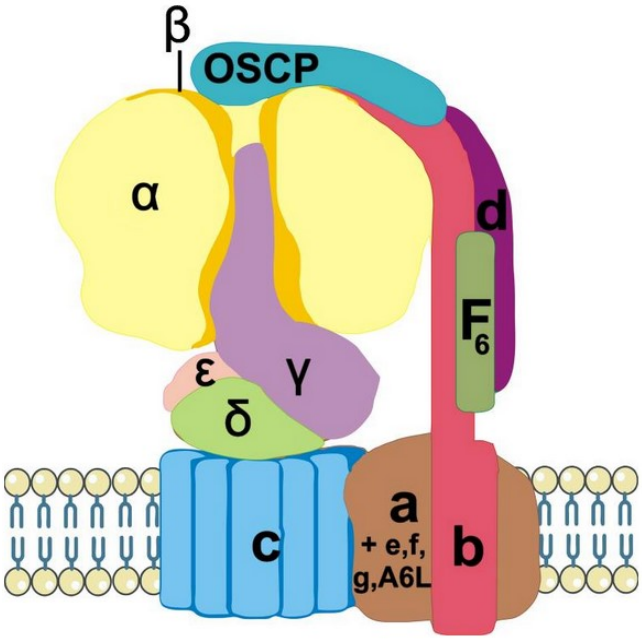

Figure 5. Human mitochondrial ATP synthase and its subunits. F_1 domain is located in the mitochondrial matrix and consists of α, β, γ, δ and ε subunits. F_0 domain is in the inner mitochondrial membrane and includes a, b, c, d, e, f, g, A6L, F_6 and OSCP subunits. (Jonckheere et al. 2012)

The proton gradient produced by the ETC drives protons to flow from mitochondrial intermembrane space to the matrix. The protons flow across the inner membrane via the subunits a and c. This proton flow releases energy and causes rotation of the c subunit ring and subunits ε, δ and γ. (Jonckheere et al., 2012) The rotation causes conformational changes in the β subunits which are the catalytic sites for ATP production. The binding sites for ADP, P_i and ATP are located in the interface of α and β subunit. β subunits have three different conformations: open (O), loose (L) and tight (T). In open conformation ADP and P_i enters the binding site and their binding affinity increases in the L state. In T state ADP and P_i approach each other and form

spontaneously ADP. ADP is then released to the mitochondrial matrix in the O state. (Faccenda & Campanella, 2012)

In oxidative phosphorylation 2.5 ATP molecules are produced per electron pair donated by NADH and 1.5 ATP molecules per electron pair from $FADH_2$ (Alberts et al., 2015d, p. 775). $FADH_2$ produces less ATP since complex II doesn't participate in the formation of the proton gradient across the inner membrane (Huttemann et al., 2007). The produced ATP can be transported from the matrix by ADP/ATP carrier proteins that are located in the inner membrane. They release ATP via intermembrane space to the cytosol and ATP can be used for energy-requiring processes everywhere in the cell. (Alberts et al., 2015d, pp. 779-782)

1.3 Targets of mitochondrial toxicity

As mentioned in the chapter 2.1 the number of mitochondria varies within different cell types. The cells that have highest amount of mitochondria are also more easily affected by diverse effects caused by the mitochondrial toxins. (Amacher, 2005) Also tissues that are exposed to higher concentrations of pharmaceuticals, such as the liver, are more easily affected (Dykens & Will, 2007). There are several different mechanisms for mitochondrial toxicity that can cause harm for the host cell. Mitochondrial toxins may induce apoptosis in the cell and increase the production of DNA damaging reactive oxygen species (ROS). (Amacher, 2005) Since mitochondria are responsible for the energy production in the cell, one major consequence of mitochondrial toxicity is insufficient energy production (Wallace & Starkov, 2000). Even though glycolysis can partly compensate the energy loss caused by mitochondrial dysfunction, oxidative phosphorylation is often needed to cover the energy requirements of the functioning cell (Salazar-Roa & Malumbres, 2017). Energy deprivation may cause dysfunction in ATP-dependent processes, such as cell cycle regulation and cell division (Peyressatre et al., 2015; Salazar-Roa & Malumbres, 2017).

1.3.1 Inhibitors of ETC and ATP synthase

Mitochondrial toxicity can be caused by the inhibition of the electron flow across the ETC (Amacher, 2005). When one or more complexes of the ETC are inhibited, it affects the generation of the proton gradient across the inner membrane and interferes with the production of ATP.

Complex I is very vulnerable to mitochondrial toxins and there are more than 60 different types of compounds that inhibit its activity (Amacher, 2005; Wallace & Starkov, 2000). Due to its complexity, there has been a lot of debate about the mechanisms and binding sites of complex I inhibitors (Degli Esposti, 1998; Estornell, 2000; Murai & Miyoshi, 2016). Even though the binding sites and affinities of different inhibitors may vary, it seems that most of the inhibitors affect in the ubiquinone binding pocket. Binding to this pocket disturbs the electron flow from iron-sulfur clusters to the ubiquinone. (Estornell, 2000)

Complex II inhibition has been described much less than inhibition of other ETC complexes (Miyadera et al., 2003). There are some inhibitors that seem to interfere with the binding of electrons to the ubiquinone and inhibit the reduction of ubiquinone to ubiquinol (Hagerhall, 1997). Complex III inhibitors can be categorized based on their binding sites in the Q cycle (Esser et al., 2004). Regardless of the binding site, the inhibitors block the electron flow in the Q cycle and interfere with the generation of proton gradient (Ma et al., 2011).

The inhibition of complex IV may occur via several different mechanisms (Wallace & Starkov, 2000). Some toxins prevent the proper binding of cytochrome c by binding close to its oxidation site and thus blocking the electron flow. The electron flow can also be inhibited inside the complex IV by the reaction with cytochrome a_3 or copper ions. (Sarti et al., 2003; Wallace & Starkov, 2000)

Toxins can inhibit ATP synthase by binding to its F_o or F_1 domain. Depending on the compound, the binding site may vary. (Zheng & Ramirez, 2000) Binding to F_o domain interferes with the proton flow across the ATP synthase and hence blocks the production of ATP (Devenish et al., 2000; Symersky et al., 2012). Binding to F_1 domain prevents the production of ATP from ADP and P_i. F_1 inhibitors seem to disturb the

conformational changes of β subunits that are critical for ATP synthase to function. (Abrahams et al., 1996)

1.3.2 Uncouplers of oxidative phosphorylation

The ATP production by oxidative phosphorylation can also be inhibited via uncoupling. Uncoupling refers to a mechanism where after the production of proton gradient the protons do not pass across the ATP synthase when flowing back to the mitochondrial matrix. Instead, they flow across the inner membrane directly and proton gradient collapses. Instead of ATP only heat is produced. (Amacher, 2005)

Most of the uncouplers are lipophilic weak organic acids or weak bases (Kadenbach, 2003; Krahenbuhl, 2001). These uncouplers are able to cross the inner membrane both in deprotonated and protonated forms. In the intermembrane space they bind protons and transport them across the membrane to the matrix. (Kadenbach, 2003) In the matrix uncouplers release the proton and are ready to go back to intermembrane space and bind another proton. This cycle collapses the proton gradient. (Wallace & Starkov, 2000)

1.3.3 Other possible targets of mitochondrial toxicity

Toxins that induce the mitochondrial permeability transition (MPT) or inhibit fatty acid β-oxidation or mitochondrial DNA (mtDNA) synthesis can also interfere with the energy production of mitochondria (Amacher, 2005).

As mentioned in the chapter 2.2.2. β-oxidation is an essential process to generate NADH and $FADH_2$. The prevention of the NADH and $FADH_2$ production by β-oxidation results in the dysfunction of ETC and decreases the ATP formation in the cell. (Fromenty & Pessayre, 1997) Except for complex II, all the complexes in ETC and ATP synthase are partly encoded by mtDNA. Toxins that inhibit the mtDNA synthesis affect also the formation and function of the complexes of ETC. (Brinkman et al., 1998)

Some compounds may induce the mitochondrial permeability transition in the cell. MPT is induced when mitochondrial permeability transition pores (MPTPs) are opened. The structure of the MPTPs are not completely understood but they seem to be located at the contact sites of outer and inner mitochondrial membrane. When the pores are opened, molecules under 1500 Daltons can pass freely from the mitochondrial matrix to the cytosol of the cell. This disrupts the proton gradient and prevents the ATP production. (Halestrap, 2009) ATP depletion is not the only consequence of the MPT which also causes e.g. swelling of the matrix and imbalance of the ion gradients across the inner membrane. Depending on the duration and extent of MPTP opening, the cell may survive but often MPT leads to apoptosis or necrosis. (Honda & Ping, 2006; Labbe et al., 2008)

2. Cell cycle

2.1 Overview of the cell cycle

Cells reproduce by dividing. The content of the cell is first duplicated and the mother cell divides into two daughter cells. This process is continual and is known as a cell cycle. Cell cycle is a highly conserved process even though its details may vary depending on the cell type. (Alberts et al., 2015b, p. 963) Cell cycle consists of multiple energy-dependent processes as will be explained in chapter 2.3 (Salazar-Roa & Malumbres, 2017).

The cell cycle can be seen in figure 6. It consists of four main stages: G_1, S, G_2 and M phases (Vermeulen et al., 2003). M phase consists of mitosis and cytokinesis (Cooper, 2000). G_1, S and G_2 phases form together the interphase. The DNA replication occurs in the S phase and the division of the cell takes place in the M phase (Vermeulen et al., 2003). G_1 and G_2 phases are so called gap phases. Gap phases give the cell time to grow and to verify that it is prepared for the next phase. However, cell growth occurs throughout the interphase. (Alberts et al., 2015b, pp. 964-965) Mitochondria increase their mass in the G_1 phase and are segregated in the G_2 phase (Lee et al., 2007; Salazar-Roa & Malumbres, 2017).

Cells may reversibly exit the cell cycle into a resting, G_0, phase, where proliferating and growing stops (Oki et al., 2014; Vermeulen et al., 2003). Exit to the resting phase occurs when the extracellular conditions become unfavourable, e.g. there is depletion of nutrients or changes in cell adhesion (Oki et al., 2014). The duration of the G_0 phase varies greatly and it may take even years before the cell re-enters the cell cycle. Some cells remain in the resting phase permanently. (Alberts et al. 2015, pp. 965) Terminally differentiated cells that do not divide are irreversibly arrested at G_0 phase (Yao, 2014).

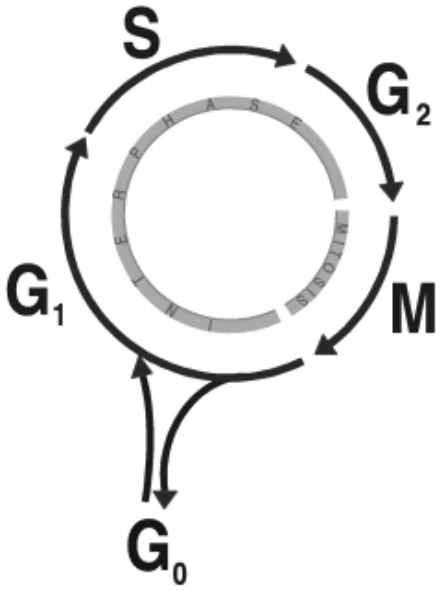

Figure 6. The stages of the cell cycle. Interphase consists of G_1, S and G_2 phases. During interphase the cell e.g. grows and replicates its DNA. The cell division takes place in M phase, which consists of mitosis and cytokinesis (not shown in the figure). The cell may exit the cell cycle into a resting G_0 phase if the extracellular conditions do not favor the cell division. (Adapted from Vermeulen et al., 2003.)

2.1.1 Cytoskeleton

Cytoskeleton has an important role in the cell cycle and especially in the mitosis. The cell also maintains its shape, structures its inner components and migrates by its cytoskeleton. Cytoskeleton is composed of three different types of filaments: microfilaments, microtubules and intermediate filaments. Since cytoskeleton is responsible for the mechanical functions and spatial organization, it needs to be able

to rearrange itself very rapidly as the cell undergo big changes such as cell cycle. Especially microfilaments and microtubules, polymers that are composed of actin and tubulin, respectively, play a crucial role in mitosis. (Nakaseko & Yanagida, 2001)

The fast rearrangement capacity of microfilaments and microtubules is due to the constant polymerization and depolymerisation of the filaments. Polymerization and depolymerisation processes are slightly different with actin than with tubulin (figure 7). Microfilaments have plus end where the polymerization occurs and minus end that is depolymerizing. Actin polymerisation is ATP driven. Actin subunits bind ATP and when the actin is added to the polymer, ATP is hydrolysed to ADP. ADP bound actin dissociates from the polymer and this causes the depolymerisation. Microtubules consist of α- and β-tubulin dimers. (Kueh & Mitchison, 2009) Instead of ATP, tubulin dimers bind guanosine triphosphate (GTP) which drives the polymerization (Sept, 2007). GTP is produced in the citric acid cycle as a byproduct of the succinate production (Berg et al., 2002b). It is then hydrolysed to guanosine diphosphate (GDP) (Sept, 2007). Microtubules polymerize and depolymerize from their plus end since their minus ends are embedded in nucleatic centers that are called centrosomes (H. Yang et al., 2010). Depolymerization occurs when the concentration of GTP bound tubulin dimers decreases and the hydrolysis of GTP happens more quickly than the addition of GTP bound dimers. When the hydrolysis of GTP reaches the plus end, the polymer collapses and a very fast depolymerisation occurs. This phenomenon is called dynamic instability. (Sept, 2007)

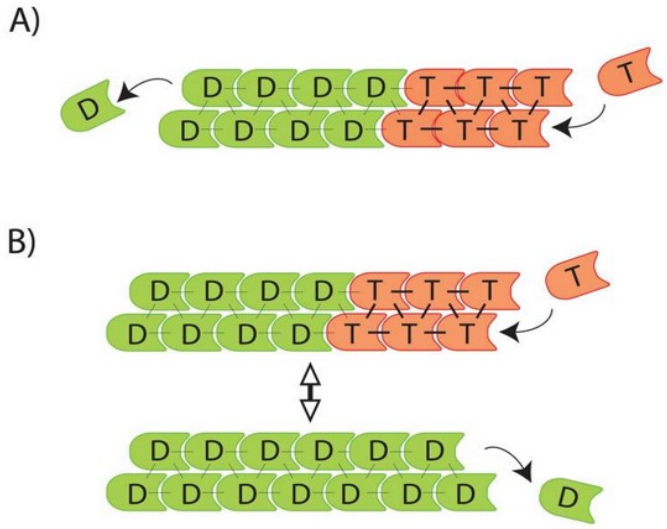

Figure 7. A) Polymerization of microfilaments from ATP bound actin monomers. Microfilaments polymerize from plus end and depolymerization from the minus end begins when ATP (T) is hydrolyzed to ADP (D). B) Microtubules polymerize from GTP bound tubulin dimers. When GTP (T) is hydrolyzed to GDP (D), depolymerization begins. Microtubules polymerize and depolymerize from plus end. (Modified from Kueh & Mitchison, 2009)

2.1.2 S phase

As mentioned above, the DNA replication takes place in the S phase. In DNA replication two genetically identical sister chromatins are formed and they stay connected through the interphase. The cohesion between sister chromatids is crucial since the premature separation may lead to genome instability. The cohesion is maintained by protein complexes called cohesins that have a multiphase regulatory system. An important part of the regulatory system is securin, which inhibits the inhibitors of cohesins. (Brooker & Berkowitz, 2014)

2.1.3 Mitosis and cytokinesis

Mitosis is divided into five stages: prophase, prometaphase, metaphase, anaphase and telophase that are presented with cytokinesis in figure 8. In the beginning of mitosis, the cell stops migrating and receives a spherical shape. This is due to the new arrangement of actin filaments. (Alberts et al., 2015c, p. 890) Mitosis begins with the prophase. In the prophase the chromosomes begin to condensate. (Hagstrom & Meyer, 2003) Protein complexes, condensins I and II, play an important role in

chromosome condensation and condensin II, which locates in nucleus, participates the condensation in prophase (Hirano, 2012). Cohesins are mostly removed from the arms of the chromosome but they remain in the centromere. The centrosomes move to the opposite sides of the cell and microtubules begin to polymerize from them. (O'Connor, 2008)

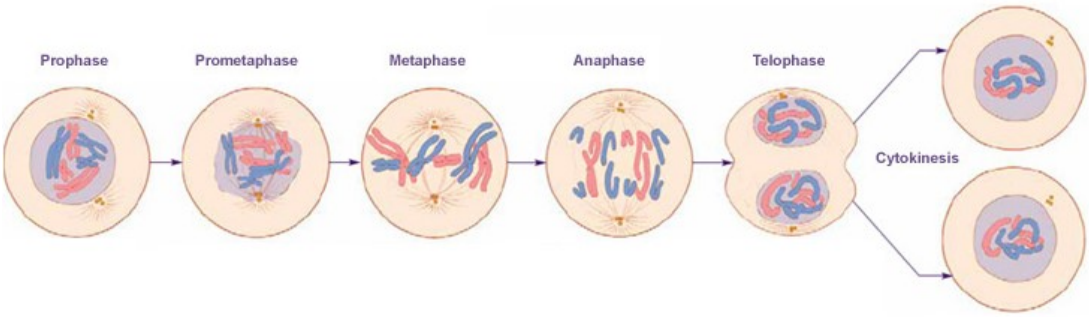

Figure 8. Mitosis and cytokinesis. In prophase, centromeres move to the opposite sides of the cell. In prometaphase, nuclear membrane is broken and microtubules reach the kinetochores of the chromatins. During metaphase, chromatins form metaphase plate in the center of the cell. In anaphase, the sister chromatins are pulled away from each other and in telophase, a new nuclear membrane is formed around both sets of chromosomes. The cytoplasm of the cell is divided in cytokinesis. (Adapted from Saltsman, 2005, p. 57)

Promethaphase begins when the nuclear membrane, also known as nuclear envelope, falls apart into several vesicles (Hagstrom & Meyer, 2003; O'Connor, 2008). After the disruption of nuclear envelope, cytosolic protein, condensin I, gains access to chromosomes and begins to collaborate with condensin II (Hirano, 2012). The polymerization of the microtubules continues and they begin to seek the attachment sites of the chromosomes (O'Connor, 2008). Microtubules attach to the kinetochores, protein complexes that are present at the surface of each centromere, and form a so called mitotic spindle (Cleveland et al., 2003). Chromosomes end up having bi-orientation where sister chromatines are attached to the microtubules from opposite centrosomes (O'Connor, 2008).

In metaphase the chromosomes are fully condensed and microtubules begin to pull them to the opposite sides of the cell. However, due to the condensation and presence of the cohesins, chromosomes are able to withstand the pulling (Brooker & Berkowitz, 2014; Hagstrom & Meyer, 2003). Chromosomes are aligned in the middle of the cell and form a so called metaphase plate (Hagstrom & Meyer, 2003).

In anaphase the cohesins are removed from the centromeres and the cohesion between sister chromatides is no longer maintained (Brooker & Berkowitz, 2014). Microtubules get shorter and centromeres move further apart and the chromosomes are pulled to the opposite sides of the cell (Alberts et al., 2015b, p. 981; O'Connor, 2008). Due to the movement of centromeres, caused by the pushing and pulling by non-kinetochore microtubules, the cell become elongated (Scholey et al., 2016). Actin plays also an important role in this since the cortical flow of actin enables the movement of centromeres (Heng & Koh, 2010).

The last phase of mitosis is the telophase in which the chromosomes reach the centrosomes (O'Connor, 2008). The nuclear membrane is formed around both sets of chromosomes creating two new nuclei (Webster et al., 2009). Chromosomes begin to decondensate (O'Connor, 2008).

Cytokinesis is the division of the cytoplasm (O'Connor, 2008). It is not a part of mitosis but it belongs to the M phase and is the last step of the cell cycle. It usually begins during the anaphase and ends after the completion of mitosis. (Alberts et al., 2015b, p. 996) The division of cytoplasm is performed by a contractile ring consisting of actin and myosin. The actomyosin contractile ring creates a groove, a so called cleavage furrow, that deepens as the ring contracts. (Glotzer, 2005) After the complete contraction of the actomyosin ring, the daughter cells still remain connected by cytoplasmic bridge. The bridge can be broken and the cell membranes sealed by the membrane insertion and fusion. (Finger & White, 2002) When the cells are completely divided, the actin cytoskeleton is rearranged and the cells regain their extended shape (Heng & Koh, 2010).

2.2 Regulation of the cell cycle

The cell cycle is highly regulated process. The cell needs to ensure it has completed the previous phase until it can proceed to the next phase. This includes ensuring e.g. the errorless replication, adequate cell size and uniformity of the chromosomes. (Barnum & O'Connell, 2014) The cell cycle has specific checkpoints, which work as binary switches, either allowing or preventing the cell cycle to continue (Alberts et al., 2015b, p. 967). The delaying of cell cycle gives time to the cell to finish the previous

phase and repair possible DNA damages. If the cell cannot do this, the cell cycle is arrested permanently, leading to cell death. (Lukas et al., 2004) The checkpoints arrest the cell cycle also if there is not enough energy to complete the next phase (Salazar-Roa & Malumbres, 2017). There are three major checkpoints in the cell cycle: restriction point (or start) in late G_1, G_2/M transition and spindle checkpoint in metaphase/anaphase transition (Alberts et al., 2015b, p. 968; Molinari, 2000). The main checkpoints are illustrated in figure 9.

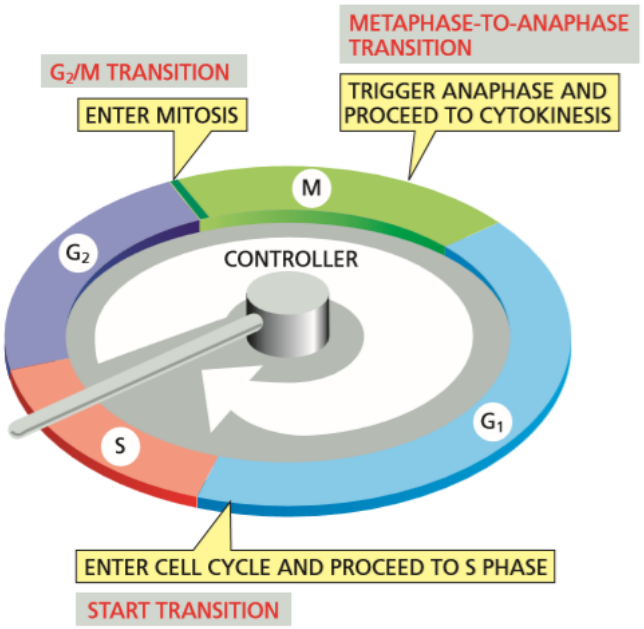

Figure 9. The main checkpoints of the cell cycle: the restriction point or start at the end of G_1 phase, G_2/M transition and spindle checkpoint between metaphase and anaphase. (modified from Alberts et al., 2015b, p. 968.)

2.2.1 Cell cycle checkpoints

Restriction point is the first main checkpoint in the cell cycle. It is located in the late G_1 phase and it acts as a starting point for cell division. Once the restriction point has been passed, the cell is committed to begin the DNA replication and once it is started, it must be finished. Restriction point is also the point after which the growth factors do not affect the cell cycle anymore (Blagosklonny & Pardee, 2002). In order to pass the restriction point, the DNA of the cell must be undamaged so that the cell will not replicate the damaged sequences. In addition, the extracellular environment must be favourable. (Alberts et al., 2015b, p. 973; Blagosklonny & Pardee, 2002)

G_2/M transition is located between the G_2 and M phase and it is a starting point for mitosis. It is an important checkpoint since it helps maintaining the genomic stability by preventing the proliferation of cells with damaged DNA. (Stark & Taylor, 2006) G_2/M transition verifies that DNA replication in S phase has been successful and offers time for DNA repair if necessary (Blagosklonny & Pardee, 2002).

The spindle checkpoint is the last of the main checkpoints in the cell cycle and it is located between metaphase and anaphase. The main responsibility of the spindle checkpoint is to maintain the genomic stability by ensuring that the chromosomes are segregated accurately. (Lara-Gonzalez et al., 2012) This checkpoint delays the progression to anaphase if the spindle microtubules are disrupted or they are not correctly attached to the chromosomes (Gorbsky, 2015). The spindle checkpoint recognizes the unattached kinetochores and allows the cell to continue to anaphase once all the kinetochores are attached to microtubules (Lara-Gonzalez et al., 2012).

2.2.2 Overview on checkpoint regulatory system

The cell cycle has a complicated regulatory system but its main participants are the cyclin-dependent kinases (Cdks) that are activated by cyclins (Molinari, 2000). Cyclin-Cdk complexes regulate e.g. the proceeding through the restriction point and G_2/M transition (Alberts et al., 2015b, p. 970). The activation of Cdks is dependent on the availability of specific cyclins, which is regulated during the cell cycle. Cyclins also direct the cyclin-Cdk complex to specific targets. (Molinari, 2000) There are several different types of cyclins that are categorized by the cell cycle stage they are present in: G_1/S cyclins, S cyclins and M cyclins. Their concentration varies during the cell cycle (figure 10). (Alberts et al., 2015b, p. 969) Cyclin-Cdk complexes are not fully activated until Cdk-activating kinase (CAK) phosphorylates them on specific threonine. (Molinari, 2000) Cdks can be inactivated by additional phosphorylation of tyrosin or by Cdk inhibitor proteins (CKIs) (Barnum & O'Connell, 2014). When activated, Cdks activate their target proteins by phosphorylating them and in that way regulate the occurrence of cell cycle events (Alberts et al., 2015b, p. 969). The phosphorylation of target proteins is driven by the hydrolysis of ATP that is bound to each Cdk (Peyressatre et al., 2015).

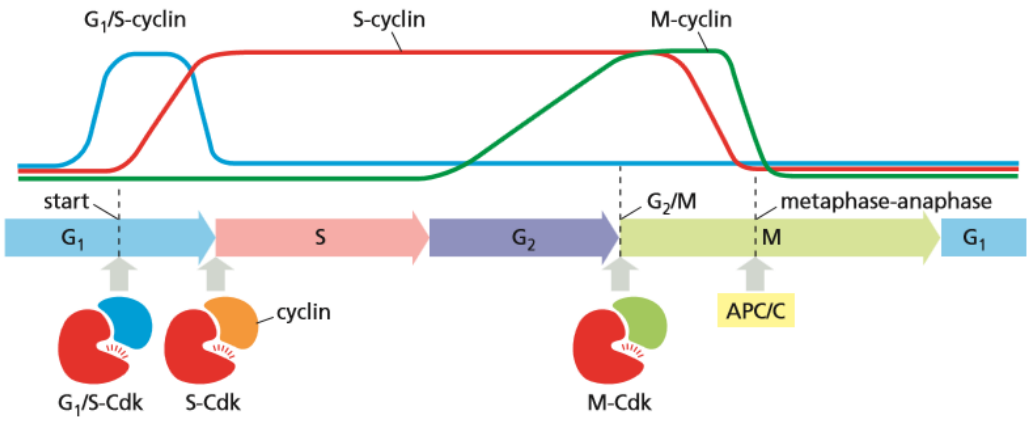

Figure 10. The cyclins activate and direct the cyclin-dependent kinases (Cdks) that regulate the cell cycle. The activation of Cdks is regulated by altering the concentrations of specific cyclins during the cell cycle. The cyclins are categorized based on the cell cycle phase they are present in. Cyclin bound Cdks control the proceeding through start checkpoint and G_2/M transition. Spindle checkpoint is controlled by anaphase promoting complex (APC). (Alberts et al., 2015b, p. 969.)

The spindle checkpoint is regulated by anaphase promoting complex (APC) (Alberts et al., 2015b, p. 970). APC is an ubiquitin ligase that marks its target proteins for degradation. The activator of the APC, Cdc20, is unable to activate APC until all the kinetochores are properly attached to the mitotic spindle. (Reddy et al., 2007) The regulation of the activation capability of Cdc20 seems to be ATP-dependent (Miniowitz-Shemtov et al., 2012; Miniowitz-Shemtov et al., 2010). After activation, APC degrades its targets, securin and S- and M-cyclins (Alberts et al., 2015b, p. 971; Reddy et al., 2007). The degradation of cyclins is essential for cell cycle to finish (Alberts et al., 2015b, p. 971). As described earlier, securin plays a role in regulatory system of the cohesion between sister chromatins and after its degradation, cohesins are inhibited and sister chromatins are able to detach from each other. This chain of events enable the transition to anaphase.

2.3 Energy consumption of the cell cycle

Cell division is a complex process consisting of multiple events and therefore it has high energy demands. DNA synthesis and mitosis are energy-dependent processes that require oxidative phosphorylation. In the case of ATP depletion, the cell cycle

checkpoints are activated, since the cell can proceed to the next phase of the cycle only if it has sufficient resources to finish it. Checkpoint activation due to the ATP depletion seems to be Cdk-mediated and thus the cell cycle arrests take place especially before the beginning of S phase or at G_2/M transition. (Salazar-Roa & Malumbres, 2017). However, defects in the cell cycle regulation may lead to checkpoint dysfunction, meaning that the cells may pass the checkpoint when they normally would not. This may lead to apoptosis or cancer. (Barnum & O'Connell, 2014) How well the cell can withstand the energy shortage, depends on the cell type (Wieser & Krumschnabel, 2001).

There are multiple energy-dependent processes in the cell cycle and here only few of them are briefly mentioned. Protein synthesis seems to be the most ATP consuming process in the cell (Buttgereit & Brand, 1995; Pontes et al., 2015). The protein synthesis can be inhibited due to the ATP shortage and this has direct effects on the cell cycle since many proteins play essential role in it (Freudenberg & Mager, 1971; Polymenis & Aramayo, 2015). Similarly, the replication and synthesis of DNA in S phase requires ATP and if there is a shortage of it, the DNA synthesis is inhibited (Enomoto et al., 1981). Also, the cell cycle regulation by Cdks and APC requires ATP as described in chapter 2.2.2.

One essential function during cell cycle is the DNA repair system that is activated when DNA is damaged or incorrectly replicated. The type of the DNA damage can vary and can be roughly categorized to single strand breaks and double strand breaks. There are different repair mechanisms for each type of damage. (Houtgraaf et al., 2006) Regardless of the mechanism, DNA repair requires the remodelling of the chromatin structure in order to succeed (Liu et al., 2012). Chromatin remodelling is highly ATP-dependent process since the chromatin-remodelling complexes need the energy from ATP hydrolysis to function (Lans et al., 2012). ATP dependent actin polymerization is also required in DNA repair (Andrin et al., 2012). If the DNA repair system does not function properly due to the energy shortage, the cell cycle is arrested in G_1/S or in G_2/M transition (Houtgraaf et al., 2006).

The cytoskeleton plays an important role in mitosis. As discussed in chapter 2.1.1, the polymerisation of actin and tubulin is driven by the binding of ATP and GTP, respectively (Kueh & Mitchison, 2009; Sept, 2007). It is thus clear that rearrangement

of microfilaments is an ATP-depending process and the disruption of actin filaments may delay the mitosis. Actin disruption has also been linked to cell cycle arrest at G_1 phase. (Heng & Koh, 2010) However, also depolymerisation of microtubules seems to require ATP and ATP depletion may result in microtubule stabilization, leading to mitotic arrest (Spurck & Pickett-Heaps, 1987).

2.4 Cell cycle affecting toxins

Many toxins affect cell cycle and its regulatory system often via DNA damage. Agents that damage DNA or cause chromosomal aberrations are called genotoxins (Phillips & Arlt, 2009). The DNA damage can lead to mutations and initiate carcinogenesis (Kaufmann, 2007). Cell cycle checkpoint system should not pass cells with damaged DNA content to S phase or mitosis, but when the checkpoint control is incompetent, e.g. due to the mutations, this may happen and lead to proliferation of malignant cells. Despite their potential carcinogenicity, many cell cycle affecting genotoxins can be utilized in cancer treatment due to their cell cycle arresting effects. (Shapiro & Harper, 1999) Genotoxins can interfere with the cell cycle via multiple mechanisms and some of the most relevant ones are introduced in the next chapter. Understanding these mechanisms is important when evaluating the underlying mechanisms of the possible association between mitochondrial toxins and DNA damage.

2.4.1 Mechanisms of cell cycle affecting genotoxins

Here, three groups of cell cycle affecting genotoxins are introduced: microtubule-targeting agents, topoisomerase inhibitors and DNA alkylating agents. Microtubule-targeting agents disrupt the mitotic spindle and arrest the cell cycle at metaphase/anaphase transition. These agents have been used in the treatment of cancer and they can be divided into two categories based on their mechanism: microtubule stabilizers and destabilizers. (Fanale et al., 2015) Microtubule stabilizers prevent the depolymerization of the microtubules by binding directly to tubulin dimers. The most well-known binding site is the taxoid site, which is located in the β-tubulin subunit. When the depolymerization is prevented, microtubules are not able to pull the sister chromatins away from each other and the cell cycle is arrested. (Field et al.,

2013) Microtubule destabilizers prevent the polymerization of microtubules and stop the formation of mitotic spindle (Fanale et al., 2015). Destabilizers bind to colchicine or vinca alkaloid site, which are both located in β-tubulin subunit of the dimer (Bates & Eastman, 2017). How the microtubule stabilizers and destabilizers prevent the depolymerization and polymerization of microtubules, is not fully understood (Wang et al., 2017; H. Yang et al., 2010).

Topoisomerase I and II are nuclear enzymes that can make a single strand and double strand break, respectively, to DNA in order to allow relaxation of supercoiled DNA. After the relaxation, the strands ligate back together and the structure of the DNA is restored. The topoisomerase I and II inhibitors can disturb this activity by preventing the religating of the DNA strands and thus inducing the formation of DNA strand breaks. (Ewesuedo & Ratain, 1997; Hande, 2008) These breaks arrest the cell cycle or delay it at the G_2/M transition (Poot et al., 1992). Due to this activity, topoisomerase I and II inhibitors are used as anticancer drugs (Ewesuedo & Ratain, 1997; Mikhailov et al., 2004).

DNA alkylating agents are a wide group of compounds that cause DNA damage by adding alkyl groups to bases of the DNA strand. The alkyl group added depends on the agent. (Grady & Ulrich, 2007) The addition of alkyl groups can cause base mispairing and block the replication (Lundin et al., 2005). Even though the DNA repair mechanisms of the cell can repair some of the caused DNA damage, DNA alkylation can lead to cell cycle arrest at G_2/M transition or apoptosis (Kondo et al., 2010).

2.4.2 Markers for genotoxicity

Genotoxicity can be detected with the aid of specific markers. These markers are developed to tag the targets that are predominantly present when cells are affected by genotoxins. (Khoury et al., 2016) Markers that target the phosphorylated histone H3 and H2Ax are very common in the detection of genotoxicity.

The chromosome condensation in mitosis is correlated with the phosphorylation of histone H3. In mammalian cells, this phosphorylation occurs at a specific spot, at the serine 10 of histone H3. Phosphorylation of H3 takes place almost exclusively in

mitosis. It begins in prophase, becomes maximal during metaphase and is lost during telophase. Antibodies that specifically recognise the phosphorylated serine 10 in histone H3 can be used to detect mitotic cells. (Hendzel et al., 1997) As described in previous chapter, some genotoxic agents arrest the cell cycle during mitosis. The cell population treated with this kind of toxicant contains more mitotic cells than the unexposed cell population. Hence, the amount of phospho-histone H3 (pH3) is increased when the cells are damaged by mitosis arresting genotoxins. (Khoury et al., 2016)

When DNA double strand breaks are formed as a result of DNA damage, it is always followed by phosphorylation of histone H2Ax (Kuo & Yang, 2008). This phosphorylation occurs specifically at serine 139 of H2Ax (Podhorecka et al., 2010). In normal cells, the amount of phosphorylated H2Ax increases during S phase and reaches maximal level at G_2/M transition due to the function of topoisomerase II (McManus & Hendzel, 2005). However, when the cells have been damaged by the double strand break inducing genotoxins, the level of phosphorylated H2Ax is clearly increased. Phosphorylated H2Ax is called γ-H2Ax and there are antibodies available that recognise it specifically. These antibodies detect DNA double strand breaks and can be used to investigate DNA damaging potency of drugs. (Kuo & Yang, 2008)

3. High-content analysis and flow cytometry in drug toxicity testing

3.1 Overview on drug toxicity testing

The failure of candidate drugs at the late stage of drug development is very expensive and is usually due to the discovery of adverse effects (Verbist et al., 2015). Hence, there is a demand for predictive assays than can be used for drug safety assessment at the early stage of drug development (Bluemel, 2012). Drug toxicity has been traditionally tested *in vivo* by using animal models at relatively late stages of drug development. Animal testing is expensive and animal models do not replicate the human biology comprehensively. In addition, it is very slow since only one compound at the time can be investigated. (Shukla et al., 2010; Verbist et al., 2015)

Moving from *in vivo* tests to *in vitro* high-throughput techniques that are able to measure multiple parameters from several compounds simultaneously has been necessary to investigate the toxicology of compounds effectively (Verbist et al., 2015). The use of human-derived cell lines may provide better biomarkers of exposure to toxicants and lead to better understanding of the mechanisms of toxicity (Shukla et al., 2010; Verbist et al., 2015). In addition, *in vitro* assays are less expensive and can be performed at the earlier stage of development (Verbist et al., 2015).

Even though it is desired to have a lot of data in a short period of time, the data amount is also one of the biggest challenges of high-throughput techniques. The large amount of data is not only laborious and slow to handle but makes it difficult to find the relevant information. (Pedreira et al., 2013; Zanella et al., 2010) The development of data analysing tools that are able to extract the relevant data, is essential but difficult (Pedreira et al., 2013). Also the development of toxicity assays, including the choice of cell source, requires careful planning and may be challenging (Zanella et al., 2010).

The mechanisms of two high-throughput techniques, high-content analysis (HCA) and flow cytometry (FC), will be briefly explained later. Both of these techniques are based on the utilization of fluorescence, which will be covered next.

3.2 Immunofluorescence

Immunofluorescence (IF) is a technique that can be used to determine the structure or the processes of the cell (Hoff, 2015). It is based on fluorochrome bound antibodies that bind to their specific targets, antigens. The level of selectivity and affinity that antibodies have for the epitopes of their antigens determines the accuracy and sensitivity of the assay. However, the preservation of the cells and their possible autofluorescence as well as the quality of the fluorescence detection device are factors that influence optimal detection. (Fritschy & Härtig, 2001) Monoclonal antibodies that bind only to one epitope give better results than polyclonal antibodies that bind to several epitopes (Hoff, 2015).

Immunofluorescence can be either direct or indirect (figure 11). In direct IF the primary antibody is tagged with a fluorochrome and it binds to its antigen directly. The indirect IF has two separate steps. First, the primary antibody, without a fluorochrome attached to it, binds to the antigen. In the second step, the fluorochrome-tagged secondary antibody binds to the primary antibody. Indirect IF requires two incubation steps and is therefore slower than direct IF. However, in indirect immunofluorescence more than one secondary antibody can bind to the primary antibody. This leads to the amplification of the signal and less primary antibody can be used. (Hoff, 2015)

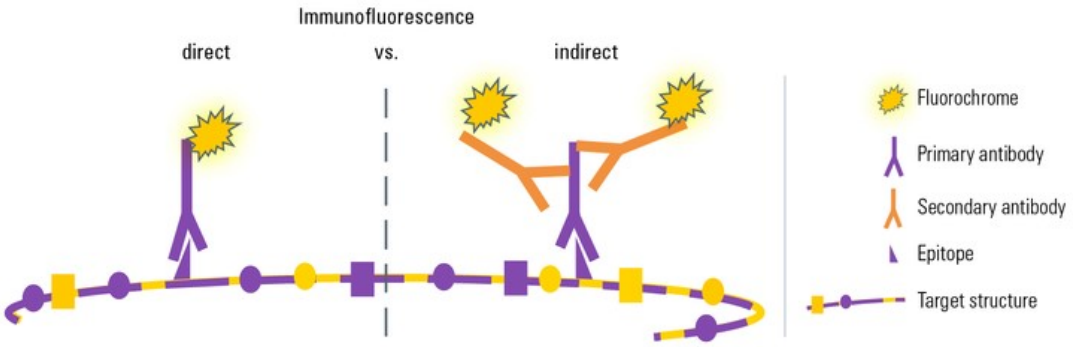

Figure 11. The difference of direct and indirect immunofluorescence (IF). In direct IF, the fluorochrome bound antibody binds directly to its target epitope. In indirect IF, primary antibody binds to its epitope and secondary antibody that is bound to the fluorochrome, binds to the primary antibody. (Hoff, 2015)

In order to bind to the primary antibody, the secondary antibody needs to be targeted against the host species of the primary antibody. For this reason, the matching primary and secondary antibodies can never be derived from the same host species. (Donaldson, 2015) Similarly, if there are more than one target that is detected, the host species of the used primary antibodies need to be different. Otherwise the secondary antibody will bind to all of them and the different targets cannot be distinguished. (Hoff, 2015)

Not all fluorescent dyes are conjugated to antibodies. Some fluorescent dyes bind directly and specifically to their target. An example is Hoechst DNA stains that bind directly to DNA. (Greb, 2012) Fluorescent dyes can also be conjugated with other compounds that have the ability to bind specifically to their cellular targets. An example is phalloidin, a toxin that binds directly to filamentous actin. When phalloidin is conjugated with fluorochrome, it can be used to detect actin. (Tang et al., 1989)

3.3 High-content analysis

High content analysis (HCA) or high-content screening (HCS) is a technique that integrates cell sample preparation, immunofluorescence, automated fluorescence microscopy and image analysis (Abraham et al., 2004). It enables large-scale screening of cells with subcellular spatial resolution. It is possible to measure simultaneously multiple cell features, such as nuclear area, proliferation, morphology and mitochondrial function. (Abraham et al., 2008) Several integrating HCA tools have been developed in addition to imaging instrumentation, including software with different bioapplications and data analysis tools. With these tools, both living and fixed cells can be analysed. (Abraham et al., 2004) Live-cell imaging enables also the kinetic monitoring of the cell in real time (O'Brien et al., 2006). In pharmaceutical industry, HCA is used e.g. for an early drug discovery and for toxicology screening (Abraham et al., 2008).

The HCA is based on the imaging of the fluorescent-dyed cells that are plated to microtiter plates (O'Brien et al., 2006). The images are taken by the automated, camera containing fluorescent microscope system that is located in a box (Buchser et al., 2004). The pixels of the images are segmented into objects. The features of the objects, such as intensity, size, count or shape, are then determined. (Trask & Johnston, 2015) What the object is, depends on the fluorescent-dyed target. For example, when nuclear specific stain is used, the object is the nucleus. Nuclear specific stains are commonly used to identify independent cells from the images and to determine an object mask, which defines the borders of the cells. The objects in other channels, e.g. tubulin fibers, are measured only inside these masks and the data can be linked to the correct cell. In HCA, multiple imaging channels can be used for different fluorescent stains with different wavelengths and several features from multiple cell compartments can be measured simultaneously. (Buchser et al., 2004)

3.4 Flow cytometry

In vitro drug toxicity can be measured by using flow cytometry (FC). It is a quick and accurate method to investigate both cytotoxic and genotocix effects. (Dallas & Evans, 1990) Flow cytometry utilizes light-scattering and fluorescence emission to analyse

single cells in a cell population (Díaz et al., 2010). It is possible to determine several cellular parameters, such as size, count, viability and data about cell cycle, very rapidly (McFarland & Harkins, 2010). The capacity of the technique depends on the sophistication of the device but even the conventional cytometers can analyse 5000 cells per second (Díaz et al., 2010). However, also the type of the cells affect the rate of the analysis. For example, large and easily aggregated cells must be processed slower than small, individual ones in order to avoid blockages in the device. (Edwards et al., 2007)

In FC, the sample is a suspension containing detached cells usually in a microtiter plate. Even though FC has conventionally been used for detecting characteristics of cells, also other particles such as chromosomes, can be used as a sample. (Edwards et al., 2007) The cells flow individually through a light beam in a narrow capillary. The light scattering and fluorescence emissions are collected by the detectors and the information is correlated to various cell parameters. For example, the forward-scattered light correlates with the cell size and the side-scattered light give information about the internal complexity of the cell. The light-scattering gives information of the intrinsic properties of the cell. (Alvarez-Barrientos et al., 2000) Additional information about extrinsic properties, such as intra- and extracellular content and processes, can be gained when combining immunofluorescence with FC. (Krutzik & Nolan, 2006).

III EXPERIMENTAL PART

4. Materials and methods

4.1 Cell lines

The cell line used in this thesis was C3A, a clonal derivative of human hepatocellular carcinoma HepG2 ([HepG2/C3A, derivative of Hep G2 (ATCC HB-8065)] ATCC® CRL-10741™). The cell line was acquired from ATCC and the passage number before thawing was unknown. Another cell line used in this research was TK6 (ATCC CRL-8015), a thymidine kinase heterozygote cell line isolated from the human lymphoblastoid line HH4. HH4 line was derived from the WIL-2 cell line. The cells were acquired from ATCC. The TK6 cells were provided and cultivated by Research Associate Merja Valovirta.

Since the focus in this research was in HepG2/C3A cells, in this thesis the term *cell* refers to them unless stated otherwise.

4.2 Cultivation and subculturing

HepG2/C3A cells were cultivated in 75 cm^2 flasks in Dulbecco's Modified Eage Medium (DMEM) with supplements. The composition of medium is shown in table 1. The cells were grown in an incubator (HERAcell, Heraeus, Kendro Laboratory Products, UK) at +37 ˚C and 5% CO_2. The handling of the cells was done in laminar flow hood (Kojair, Finland).

Table 1. The content of the medium.

Proportion	Substance
86.5%	Dulbecco's Modified Eagle Medium, Cat.no. 41965, Gibco, UK
1%	100 mM Sodium Pyruvate, Gibco, UK
0.5%	1M HEPES Buffer, Sigma, UK
1%	100x MEM NEAA (Minimum Essential Medium, Non-Essential Amino Acids), Gibco, UK
10%	Heat Inactivated FBS (Fetal Bovine Serum), Gibco, South America
1%	Penicillin-Streptomycin, Sigma, Israel

The cells were subcultivated twice a week, after the confluency was approximately 60% (figure 12). The confluency was estimated by observing the cells with microscope (Olympus CKX53, Japan). The medium, sterile Dulbecco's phosphate-buffered saline (PBS, Gibco, UK) and 0.05% Trypsin-EDTA (Gibco, Canada) were preheated to +37 ˚C in a water bath (Julabo, Germany). The old medium was removed and the cells were washed twice with 10 ml of PBS. To detach the cells, 5ml of Trypsin-EDTA was added to the flask. The cells were incubated first at room temperature for 1–2 minutes after which most of the trypsin was removed from the flask. The incubation was continued at +37 ˚C and 5% CO_2 for 6 minutes. 5 ml of fresh medium was added to the flask and the cell suspension was mixed roughly through a 300 µl pipette tip in order to break aggregates.

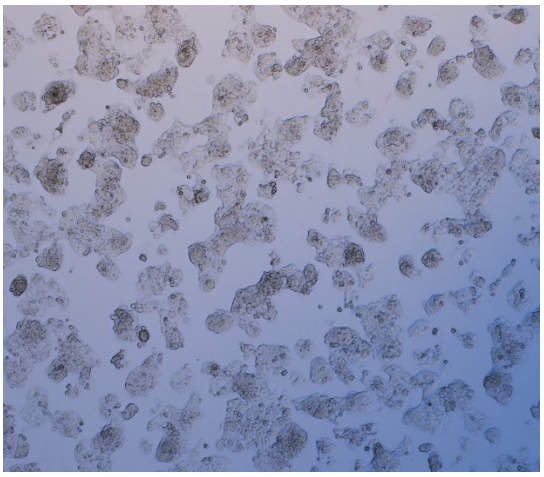

Figure 12. Phase-contrast image of HepG2/C3A cells with 100x magnification in the cultivation flask. The confluency of the cells is approximately 60% and the cells can be subcultivated.

For the cell count, 1:5 dilution was made by mixing 10 µl of cell suspension with 40 µl of PBS. C-chip was used for the cell count and 10 µl of the diluted suspension was pipetted into it. The average of the cell counts from the four corner squares was used as a final cell count. The needed volume of undiluted cell suspension was calculated based on the cell count and added to a new cultivation flask with fresh medium. The total volume of medium and cell suspension was 15 ml. The subcultivation ratio was dependent on when the cells were needed the next time and for this, table 2 was used as guidance. After each subcultivation the passage number of the cells increased by one. The cells were not subcultivated over passage number 30 in order to prevent any changes in the cell line.

Table 2. The subcultivation ratio for different cultivation times.

Growth Time	**Cell count per 15 ml**
2 days	$6*10^2$
3 days	$3*10^2$
4 days	$1.5*10^2$
5 days	$0.75*10^2$

4.3. Cell plating

For the assays, the cells were plated to poly-d-lysine coated 96-well plates (Biocoat, Corning, USA). The trypsinization protocol was identical to the one described in previous chapter. Before cell counting the cell suspension was passed through a 21 G needle to ensure that the cells have detached from each other. After cell counting the cell suspension was diluted with fresh medium and spread to the plates. The dilution ratio was dependent on the incubation time. The incubation times were 24 h and 48 h, and the number of cells per well was 11 000 and 8 000, respectively. The total volume of the cell suspension in each well was 100 µl. The plates were incubated at room temperature for one hour and placed in the incubator (+37 ˚C, 5% CO_2).

The TK6 cells were plated by pipetting robot Microlab Star (Hamilton, USA). The cell plating protocol of the pipetting robot was part of the FC procedure for TK6 cells that has been established at Orion.

4.4 Addition of compounds to the cells

The cells were treated with selected compounds and controls that are introduced later. All the compounds used were of analytical grade. Stock solutions were prepared by dissolving the compounds in dimethyl sulfoxide (DMSO, Sigma, UK). The concentration of the stock solutions was 100 times stronger than the top concentration added to the cells.

For the HCA the dilution series were done by diluting stock solutions with DMSO. Dilution series were further diluted in medium so that the final concentration of each solution was three times stronger than the concentration added to the cells. The compounds were added to the cells after 24 h incubation. The old medium was discarded, the cells were washed twice with 100 µl PBS and 100 µl of new, pre-heated medium was added to each well. The compound solutions were diluted into intended concentrations when 50 µl of them was added to the cells and mixed with the medium. At least one column in each microtiter plate was left without compounds and it acted as a negative control. The final DMSO concentration in each well was 1%. An example of the dilution protocol for HCA can be seen in figure 13. After the addition of compounds to the cells, the plates were incubated at incubator for 4 h, 6 h or 24 h. The plates that initially contained 11 000 cells per well were incubated either 4 h or 6 h and the plates with initial number of 8 000 cells per well were incubated for 24 h.

For the FC the same stock solutions were used as for HCA but the dilution series and the addition of the compounds to the cells were done by the pipetting robot. The procedure of the pipetting robot for both HepG2/C3A and TK6 cells has been established at Orion. Four wells per plate were left without compounds and contained 1% DMSO in medium. The plates for FC were incubated for 24 h.

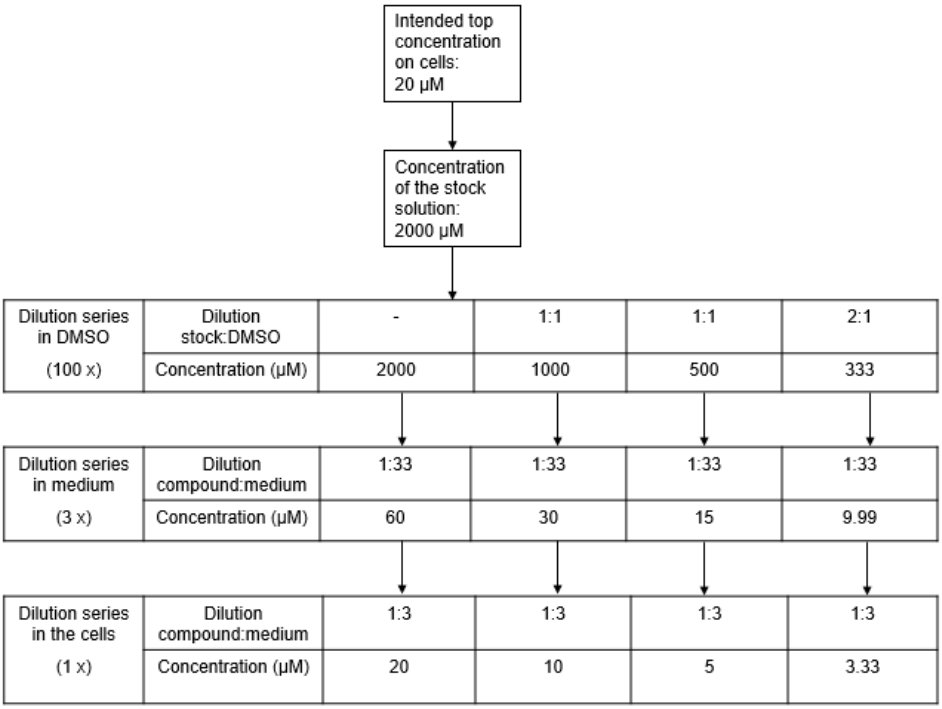

Figure 13. An example of the dilution protocol of concentration series for the HCA. The concentration of stock solution was 100 times stronger than the top concentration at the cells. The concentration series were diluted from the stock solution with DMSO. The series were further diluted with medium so that the concentration was three times stronger than the final concentrations at the cells. Finally, the compounds were diluted to the final concentrations when they were applied to the cells.

4.5 HCA assay

In this research, 16 different compounds were tested. In addition, five positive controls were used. The mechanisms of toxicity and the top concentrations of the used compounds are listed in table 3. The chosen concentrations of controls are listed in table 4.

The cells were plated as described in chapter 4.3 and the compounds were added to the cells the next day. The dilution series of four compounds were applied to the plates at once. The plate map of the assays and the dilution series of the compounds are illustrated in figure 14. The compounds were added as described in chapter 4.4. Two sets of three parallel plates per both time points, 6 h and 24 h, were handled simultaneously, meaning that each compound was applied to 12 plates.

Table 3. The compounds used in the research, their maximum concentration at the cells and their mechanism of toxicity.

Compound	Top concentration (μM)	Supplier, Country	Stock keeping unit	Mechanism of toxicity	Reference
2,4-dinitrophenol	200	Aldrich, USA	D198501	Uncoupler	(Grundlingh et al., 2011)
Amiodarone HCl	20	Sigma, USA	A8423	Uncoupler, complex I inhibitor, β-oxidation inhibitor	(Serviddio et al., 2011)
Buspirone HCl	200	Sigma, USA	B7148	Negative control, complex I inhibitor	Dykens et al. (2008b)
Entacapone	200	Sequoia, UK	SRP10885e	Negative control, uncoupler	(Grunig et al., 2017; Longo et al., 2016)
Fluoxetine	100	Sigma, USA	F0253000	Uncoupler, complex V inhibitor	(de Oliveira, 2016)
Levosimendan	200	Orion, Finland	-	Uncoupler	
Metformin HCl	200	Sequoia, UK	SRP02280m	Negative control, complex I inhibitor	(Dykens et al., 2008a)
Nefazodone HCl	50	Sequoia, UK	SRP03327n	Complex I and IV inhibitor	(Dykens et al., 2008b)
Nimesulide	200	Sigma, Italy	N1016	Uncoupler, MPT inducer	(Mingatto et al., 2002)
Oligomycin	2.5	Agilent*, USA	103015-100	Complex V inhibitor	(Jonckheere et al., 2012)
Paclitaxel	8	Sigma, USA	T7402	Microtubule stabilizer	(L. Yang et al., 2010; Zacharaki et al., 2013)
Phenformin HCl	200	Sigma, China	P7045	Complex I inhibitor	(Dykens et al., 2008a)
Rotenone	1	Sigma, USA	R8875	Complex I inhibitor	(Heinz et al., 2017)
Staurosporine	2	Enzo, USA	ALX380014M005	respiratory inhibition, Cdk1 inhibitor	(Duan et al., 2003; Vermeulen et al., 2003)
Tolcapone	200	Sequoia, UK	SRP02376t	Uncoupler	(Grunig et al., 2017; Longo et al., 2016)
Troglitazone	100	Sigma, USA	T2573	Complex II-V inhibitor, MPT inducer	(Masubuchi et al., 2006; Nadanaciva et al., 2007)

* From Seahorse XF Cell Mito Stress Test kit

Table 4. The positive controls, their concentrations at the cells and their mechanism of toxicity. All five controls were used in HCA assay. In FC assay, CCCP, MMS and Vinblastine were used

Control	Concentration (µM)	Supplier, Country	Stock keeping unit	Mechanism of toxicity	Reference
CCCP	50	Alfa Aesar, Germany	L06932	Cytotoxicant, Uncoupler	(Ganote & Armstrong, 2003)
Griseofulvin	50	Sigma, China	G4753	Microtubule stabilizer	(Zacharaki et al., 2013)
MMS	1000	Aldrich, USA	129925	DNA methylator	(Lundin et al., 2005)
Paclitaxel	2	Sigma, USA	T7402	Microtubule stabilizer	(Zacharaki et al., 2013)
Vinblastine	0.01	Sigma, USA	V1377	Microtubule destabilizer	(Weaver & Cleveland, 2005)

	1	2	3	4	5	6	7	8	9	10	11	12
A	Griseofulvin/ Paclitaxel	DMSO	Compound a -	a 2	a 2	a 1.5	a 2	a 2	a 2	a 3	a 3	CCCP
B	Griseofulvin/ Paclitaxel	DMSO	Compound a -	a 2	a 2	a 1.5	a 2	a 2	a 2	a 3	a 3	CCCP
C	Griseofulvin/ Paclitaxel	DMSO	Compound b -	b 2	b 2	b 1.5	b 2	b 2	b 2	b 3	b 3	CCCP
D	Griseofulvin/ Paclitaxel	DMSO	Compound b -	b 2	b 2	b 1.5	b 2	b 2	b 2	b 3	b 3	CCCP
E	Vinblastine	DMSO	Compound c -	c 2	c 2	c 1.5	c 2	c 2	c 2	c 3	c 3	MMS
F	Vinblastine	DMSO	Compound c -	c 2	c 2	c 1.5	c 2	c 2	c 2	c 3	c 3	MMS
G	Vinblastine	DMSO	Compound d -	d 2	d 2	d 1.5	d 2	d 2	d 2	d 3	d 3	MMS
H	Vinblastine	DMSO	Compound d -	d 2	d 2	d 1.5	d 2	d 2	d 2	d 3	d 3	MMS

Figure 14. The plate map of the HCA assay. The concentration series of four compounds were on one plate. The top concentration was in column 3 and the numbers in columns 4–11 are the dilution factors. The positive controls were on the sides of the plate and the negative control (untreated cells) in column 2.

After the cells had been incubated with the compounds for the correct amount of time, the cells were fixed. The medium and the compounds were discarded from the wells at the time points 4 h, 6 h or 24 h. The cells were fixed by adding 100 µl 4% (v/v) paraformaldehyde (PFA) to the wells. PFA was diluted from 16% (w/v) PFA (Electron Microscopy Sciences, USA) with non-sterile PBS. Non-sterile PBS was prepared by mixing 100 ml of Dulbecco's Phosphate Buffered Saline (10x) (Gibco, UK) with 900 ml of sterile water (Baxter, Switzerland). The cells were incubated with PFA for 15 minutes at room temperature. PFA was discarded and the cells were washed three times with 100 µl non-sterile PBS.

Before the immunolabeling, the permeabilization and blocking of the cells was performed. Permeabilization was done by adding 100 µl of 0.2% (w/v) TritonX-100 (Sigma, USA) in PBS to the wells. The cells were incubated for 15 minutes at room temperature. TritonX-100 was poured away and the cells were blocked with 3% (w/v) bovine serum albumin (BSA, Sigma, USA) in PBS. The cells were incubated with BSA for 15 minutes at room temperature. BSA was discarded from the cells.

Antibodies used in this research can be seen in table 5. The concentrations of the antibodies are presented in table 8. The primary antibodies were diluted with 3% BSA and 50 µl was added per well. The plates were set into microplate shaker and the cells were incubated with the primary antibodies overnight at +4 ˚C and shaking 250 rpm. Since there were three different primary antibodies from two different hosts, it was not possible to apply all of them to same plates. Hence, one set of three parallel plates per one time point was labelled with γH2Ax and the other set with pH3. Both sets included anti-tubulin, phalloidin and Hoechst.

Next day, the assay was continued. The primary antibodies were poured away and the cells were washed three times with 100 µl PBS. The secondary antibodies and fluorescence dyes were diluted with 3% BSA and added to the cells, 50 µl per well. Plates were incubated for 1 h in the dark and at room temperature. The cells were washed four times with 100 µl PBS and 150 µl PBS was left in the wells. The plates were sealed with non-transparent tape and stored in the dark, at +4 ˚C.

Cellomics ArrayScan VTI (Thermo Fischer Scientific, USA) was used for the imaging of the cells. All the plates were scanned with Cellomics by using bioapplication Morphology V.4. Approximately 500 cells per well was imaged. Nuclear stain, Hoechst, was selected for the channel 1 and was used for identifying the cells and determining the object mask (figure 15A). The objects in other channels were measured only inside the object mask (figure 15B). The parameters and the channels used in this research are listed in table 6.

Table 5. The antibodies and fluorescence dyes used.

Antibody	Host	Stock keeping unit	Supplier	Country
Primary antibodies				
Phospho-gamma γH2Ax pSer139	Rabbit	PA1-25001	Thermo Fischer Scientific	USA
Phospho-Histone H2Ax Ser139	Rabbit	LF-PA0025	Thermo Fischer Scientific	South Korea
Phospho-histone H3 (pH3) Ser10	Mouse	9706	Cell Signaling Technologies	USA
Anti-beta tubulin	Mouse	ab131205	Abcam	USA
Anti-beta tubulin	Rabbit	ab179513	Abcam	USA
Secondary antibodies				
Alexa Fluor® 546, anti-rabbit IgG	Goat	A11010	Thermo Fischer Scientific	USA
Alexa Fluor™ Plus 555, anti-mouse IgG	Goat	A32727	Thermo Fischer Scientific	USA
Alexa Fluor® 633, anti-rabbit IgG	Goat	A21071	Thermo Fischer Scientific	USA
Alexa Fluor™ Plus 647, anti-mouse IgG	Goat	A32728	Thermo Fischer Scientific	USA
Fluorescence dyes				
Hoechst 33342	–	H3570	Thermo Fischer Scientific	USA
Alexa Fluor™ 488 phalloidin	–	A12379	Thermo Fischer Scientific	USA

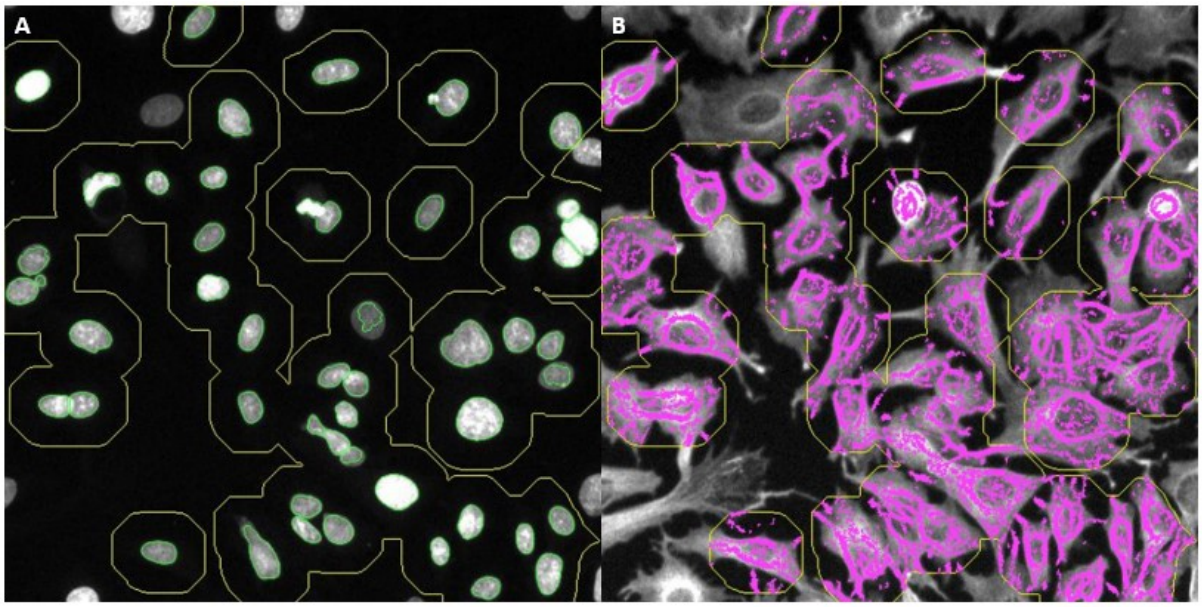

Figure 15. HepG2/C3A cells without compound treatment taken by Cellomics Array Scan VTI with 20x objective. A) Channel 1 shows the nuclear stain, Hoechst, that is used to define the borders of the nuclei (shown in green). Nuclei are used to determine the object mask (in yellow) that defines the cells. B) Channel 3 shows anti-tubulin and the image analysis measures the tubulin fibers (shown in pink) only within the object mask. Therefore, the data from different channels can be linked together to the correct cell.

Table 6. The list of features measured from different channels in image analysis. All features are included in Morphology V.4 bioapplication.

Fluorescent probe + primary antibody	Imaging Channel	Feature name
Hoechst 33342	Channel 1	Nuclear area
Hoechst 33342	Channel 1	Average intensity of nucleus
Hoechst 33342	Channel 1	Cell count per field
Alexa 546 + γH2Ax	Channel 2	Member count per cell
Alexa 546 + γH2Ax	Channel 2	Average intensity of the members per cell
Alexa 555 + pH3	Channel 2	Member count per cell
Alexa 555 + pH3	Channel 2	Average intensity of the members per cell
Alexa 647 + Anti-tubulin	Channel 3	Fiber alignment 1
Alexa 647 + Anti-tubulin	Channel 3	Fiber alignment 2
Alexa 647 + Anti-tubulin	Channel 3	Average intensity of the fibers
Alexa 647 + Anti-tubulin	Channel 3	Average area of the fibers
Alexa 647 + Anti-tubulin	Channel 3	Fiber count
Alexa 633 + Anti-tubulin	Channel 3	Fiber alignment 1
Alexa 633 + Anti-tubulin	Channel 3	Fiber alignment 2
Alexa 633 + Anti-tubulin	Channel 3	Average intensity of the fibers
Alexa 633 + Anti-tubulin	Channel 3	Average area of the fibers
Alexa 633 + Anti-tubulin	Channel 3	Fiber count
Alexa 488 phalloidin	Channel 4	Fiber alignment 1
Alexa 488 phalloidin	Channel 4	Fiber alignment 2
Alexa 488 phalloidin	Channel 4	Average intensity of the fibers

4.6 Flow cytometry DNA damage assay

Flow cytometry DNA damage assay was performed with both HepG2/C3A and TK6 cells. The cells from both cell lines were plated as described in chapter 4.3. The same 16 compounds that were used in HCA assay were tested also in FC. In FC, three positive controls were used: CCCP, vinblastine and MMS. The details of the compounds and controls are shown in tables 3 and 4 respectively. The compounds were plated as described in chapter 4.4. The plate map of the FC assay for HepG2/C3A cells is illustrated in figure 16.

For the DNA damage assay, Beta MultiFlow™ DNA Damage kit (Litron Laboratories, USA), containing p53, γH2Ax and pH3 markers, was used. The kit included materials for complete labelling solution that was prepared and its content is shown in table 7. The addition of complete labelling solution to the TK6 cells was done with pipetting robot and according to the previously established FC protocol. The TK6 cells were incubated at room temperature for 15 minutes before they were screened with flow cytometer (iQue screener, Intellicyt, USA). For the HepG2/C3A cells, the labelling

solution was mixed with StemPro® Accutase® (Gibco, USA) (2:1). The medium from the cells was discarded and 50 µl of the mixture of complete labelling solution and Accutase® was added to the cells. The cells were incubated at +37 ˚C, 5% CO_2 for 30 minutes. The detached cells were gently mixed with the solution to ensure their proper detachment. The cells and the solution was transferred into U bottom 96-well plates (Falcon™ Polystyrene, Corning, USA). The plates were screened using flow cytometer.

	1	2	3	4	5	6	7	8	9	10	11	12
A	Compound a 1	a 3	a 5	a 7	a 9	a 11	a 13	a 15	a 17	a 19	CCCP	CCCP
B	Compound a 2	a 4	a 6	a 8	a 10	a 12	a 14	a 16	a 18	a 20	CCCP	CCCP
C	Compound b 1	b 3	b 5	b 7	b 9	b 11	b 13	b 15	b 17	b 19	Vinblastine	Vinblastine
D	Compound b 2	b 4	b 6	b 8	b 10	b 12	b 14	b 16	b 18	b 20	Vinblastine	Vinblastine
E	Compound c 1	c 3	c 5	c 7	c 9	c 11	c 13	c 15	c 17	c 19	MMS	MMS
F	Compound c 2	c 4	c 6	c 8	c 10	c 12	c 14	c 16	c 18	c 20	MMS	MMS
G	Compound d 1	d 3	d 5	d 7	d 9	d 11	d 13	d 15	d 17	d 19	DMSO	DMSO
H	Compound d 2	d 4	d 6	d 8	d 10	d 12	d 14	d 16	d 18	d 20	DMSO	DMSO

Figure 16. The plate map of the FC assay for HepG2/C3A cells. The concentration series of four compounds (a-d) were pipetted on one plate. The number refers to the rank of the concentration: 1 meaning the top concentration and 20 the lowest concentration of the series. The controls were at columns 11 and 12.

Table 7. The content of the complete labelling solution per one 96-well plate.

Number of wells	Volume of Nuclei release solution with counting beads	Volume of DNA stain	Volume of RNAse solution	Volume of γH2Ax Alexa Fluor™ 647	Volume of pH3 PE	Volume of p53 FITC
96	5.5 ml	137.5 µl	27.5 µl	27.5 µl	11.0 µl	27.5 µl

4.7 Data analysis

Since the purpose in this research was to find connections between the features of used markers, all the data was normalized based on the DMSO control to simplify the presentation and comparison. The exceptions were the γH2Ax and pH3 responder analyses that were built on the original data.

Responder analyses were developed for pH3 and γH2Ax markers in order to investigate how many percent of the cells with different treatments were positive for these markers. Since pH3 marker is binary, the cell would be pH3 positive if the member count is greater than zero. To exclude the possible false signals, the cell was categorized as pH3 positive when the member count was greater than two. The responder analysis for γH2Ax was based on the average intensity of the γH2Ax. The cell was categorized as positive if its average intensity was greater than the set limit. The limit was two standard deviations from the mean of the average intensity of the DMSO controls.

The normalized data was used for calculating the lowest effective concentrations (LECs). In order to take only the actual events into account, the upper and lower limits of natural fluctuations were determined. Three standard deviations from the mean of the DMSO controls were chosen as limits. The decision was based on the 68-95-99.7 rule of normal distribution, meaning that 99.7% of natural fluctuation in the data should be within the determined limits. LECs were the lowest concentrations that either exceeded the upper limit or went below the lower limit.

The data gained from the HCA image analysis was analysed by Advanced cell classifier (ACC), a data analyser program (Piccinini et al., 2017). The cell images were used to train the program to classify the cells into created classes and the program based the classification on the similarity of the numeric data. The used classifier was MLP_Weka. The cells were classified into six classes: interphase, mitotic, rounded, stretched, damaged and unclassified cells. Percentage from all cells was calculated based on the output data of ACC. Validity of the classification was 75.5%.

The statistical analysis was conducted by Excel, Spotfire and R. The significances of the differences were determined by Mann-Whitney U-test since not all of the data was normally distributed and only independent variables were compared. The levels of significance were set at $p \leq 0.05$ (*, significant), $p \leq 0.01$ (**, very significant) and $p \leq 0.001$ (***, extremely significant).

5. Results

5.1 Setting up the HCA assay

The first part of this research was to set up the HCA assay that was used for investigating the genotoxicity markers and cytoskeleton dynamics. The positive controls for pH3 and γH2Ax markers and for mitochondrial toxicity had to be selected and their suitable concentrations and incubation times had to be investigated for the HCA assay. Similarly, the specificity and proper function of antibodies had to be confirmed and the concentrations for both primary and secondary antibodies adjusted. The compounds used in the set up were the positive controls of the HCA assay and are presented in table 4. All the primary and secondary antibodies were tested with each compound treatment and blank control to examine their proper binding and specificity. Concentration series were used to set the suitable concentration for each antibody (table 8). The concentration of Hoechst and fluorochrome bound phalloidin, were not tested since their concentrations for HCA assay has previously been adjusted at Orion. The concentrations of antibodies were chosen based on the reasonable exposure time and signal-to-noise ratio of the images acquired by Cellomics. The concentrations of the positive controls were selected based on their γH2Ax and pH3 responses that needed to be distinguishable from the negative control. However, the concentrations had to be low enough to not to kill all the cells.

Table 8. The concentration series used in the set-up for each antibody. The concentrations selected for the HCA assay are in red.

Primary antibodies					**Secondary antibodies**			
γH2Ax PA1-25001	**γH2Ax** LF-PA0025	**pH3**	**Anti-β tubulin** (m)	**Anti-β tubulin** (r)	**Alexa 546**	**Alexa 555**	**Alexa 633**	**Alexa 647**
1:500	1:400	1:1000	1:600	1:1000	1:1000	1:1000	1:1000	1:1000
1:1000	1:800	1:2000	1:800	1:2000	1:2000	1:2000	1:2000	1:2000
1:2000	1:1000	1:3000	1:1000	1:3000	1:3000	1:3000	1:3000	1:3000
1:3000	1:2000	1:4000	1:2000	1:4000	1:4000	1:4000	1:4000	1:4000
1:4000	1:3000	1:5000			1:5000			1:5000
1:5000	1:4000	1:6000			1:6000			1:6000
1:6000	1:5000	1:7000			1:7000			1:7000
	1:6000	1:8000			1:8000			1:8000

5.2 Describing the features by the cell images

To understand how the features that were measured in image analysis are linked to the appearance of the cells and markers, the data acquired from the image analysis and the cell images were compared. The γH2Ax and pH3 markers are presented in figure 17. γH2Ax, the marker for phosphorylated histone H2Ax, was seen as dots, each dot representing one DNA double strand break. The amount of γH2Ax correlated hence directly with the amount of DNA double strand breaks, either caused by topoisomerase II activity during interphase or by DNA damage. pH3, the marker for phosphorylated histone H3, was seen as ring-shaped and it was a binary marker, meaning that the cell is either pH3 positive (mitotic) or negative (non-mitotic).

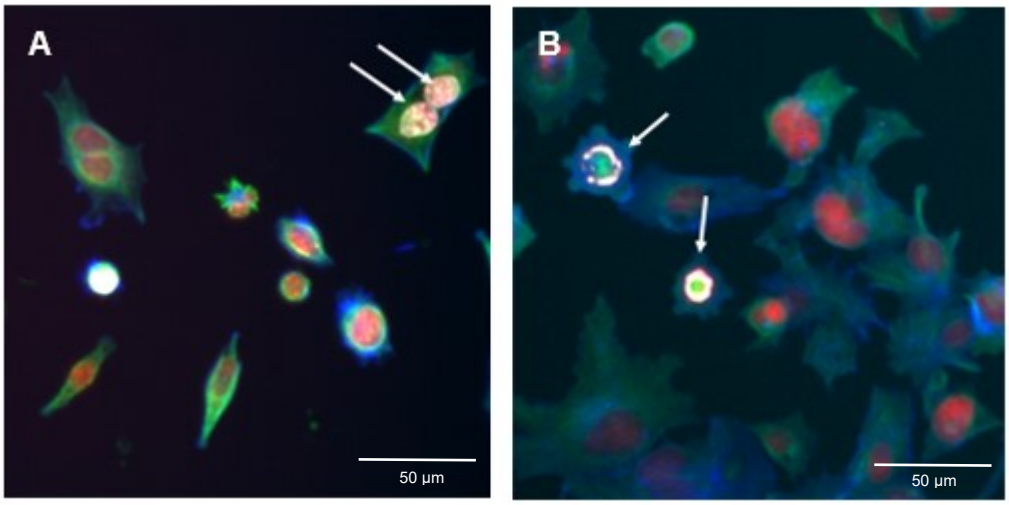

Figure 17. Overlays of 20x confocal images of HepG2/C3A cells taken with Opera Phenix HCS system (PerkinElmer, USA). The nucleus is seen in red, tubulin in green and actin in blue. A) Cells treated with MMS. The arrows point γH2Ax positive cells. γH2Ax can be seen as dots within the nucleus. B) Cells treated with paclitaxel. The arrows point pH3 positive (mitotic) cells. pH3 marker was usually seen as ring-shaped.

How the changes in parameters describing actin and tubulin were seen in the cell images, was investigated. Figure 18 shows how DMSO and metformin-treated cells differ from their actin and tubulin structure. It can be seen that both the data and image of metformin-treated cells looks very similar to the untreated cells. Since all of the data was normalized by the mean of DMSO, the averages of all the parameters of untreated cells were 100.

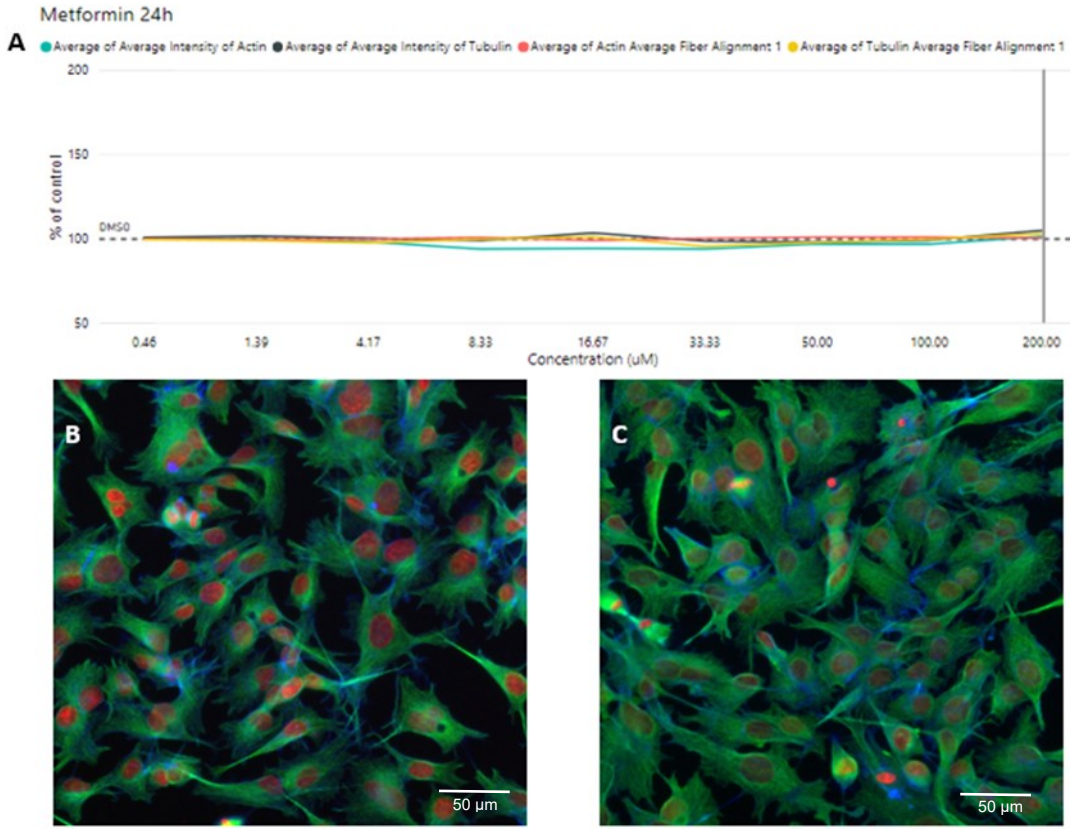

Figure 18. A) The tubulin and actin intensity and fiber alignment of metformin-treated cells in each tested concentration. The parameters did not differ from the untreated cells. The vertical line demonstrates the concentration of the metformin-treatment of the cells shown in figure C. B) 20x magnification of the normal, untreated HepG2/C3A cells. C) 20x image of metformin-treated cells. In images, the nucleus is seen in red, tubulin in green and actin in blue. The images were taken with Cellomics.

The data from nefazodone and paclitaxel-treated cells have been illustrated in figure 19. Nefazodone and paclitaxel increased the intensity of the tubulin and actin and decrease the alignment 1 parameters. Despite the similar behaviour of the parameters, the images of the cells look different: nefazodone-treated cells have elongated tubulin whereas the tubulin of paclitaxel-treated cells is brush-shaped.

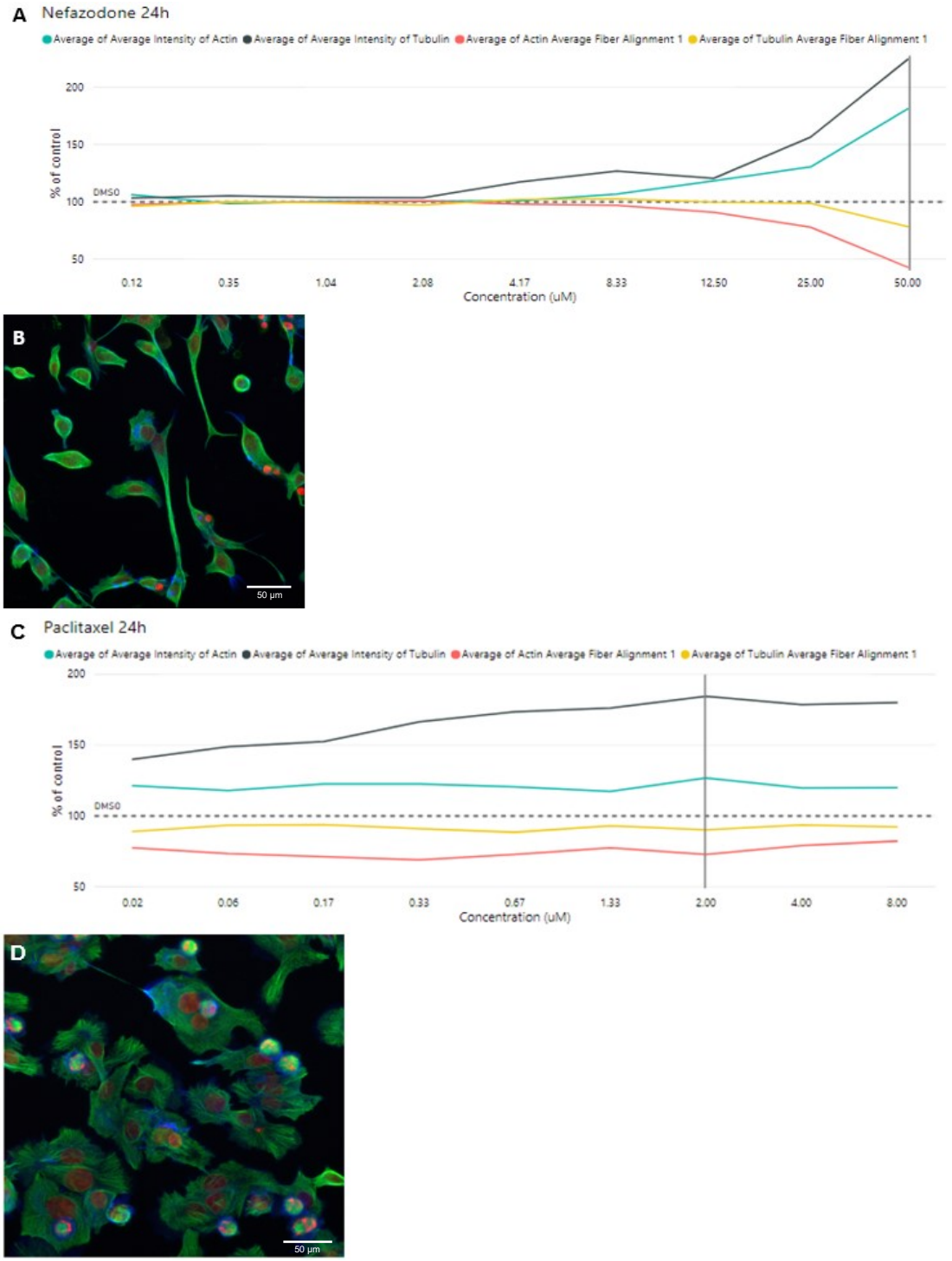

Figure 19. A) The tubulin and actin intensity and fiber alignment of nefazodone-treated cells in each concentration. The intensity of both actin and tubulin increased with the increasing concentration whereas the alignment parameters decreased. The vertical line represents the concentration of the nefazodone-treatment of the cells shown in figure B. B) 20x magnification of nefazodone-treated cells. The cells seemed elongated and it can be seen that the tubulin fibers were organized and aligned parallel. C) The intensity and fiber alignment data of actin and tubulin for paclitaxel-treated cells. The intensity parameters of paclitaxel are increased compared to DMSO level and the fiber alignment parameters are decreased, indicating the organization of the fibers. The vertical line demonstrates the concentration of paclitaxel-treatment of cells shown in figure D. D) 20x magnification of paclitaxel-treated cells. It can be seen that tubulin had a brush-shaped organization and some of the cells have rounded. In the images, the nucleus is seen in red, tubulin in green and actin in blue. The images were taken with Cellomics.

5.3 Selection of parameters for the data analysis

Several features were measured from each channel in the image analysis (table 6). Since many of these features behaved very similarly, one parameter per channel was selected for the comparison. The parameters for tubulin are illustrated in figure 20. All five parameters seemed to correlate with each other. The fiber alignment and intensity parameters were preferred since they described the organization of the tubulin: increased intensity and decreased variation of the fiber alignment (Fiber alignment 1 feature) indicated the condensation of the tubulin fibers. The intensity of tubulin was chosen for the comparison since it was sensitive and gave response with each compound treatment. The response was also strong and therefore easy to detect.

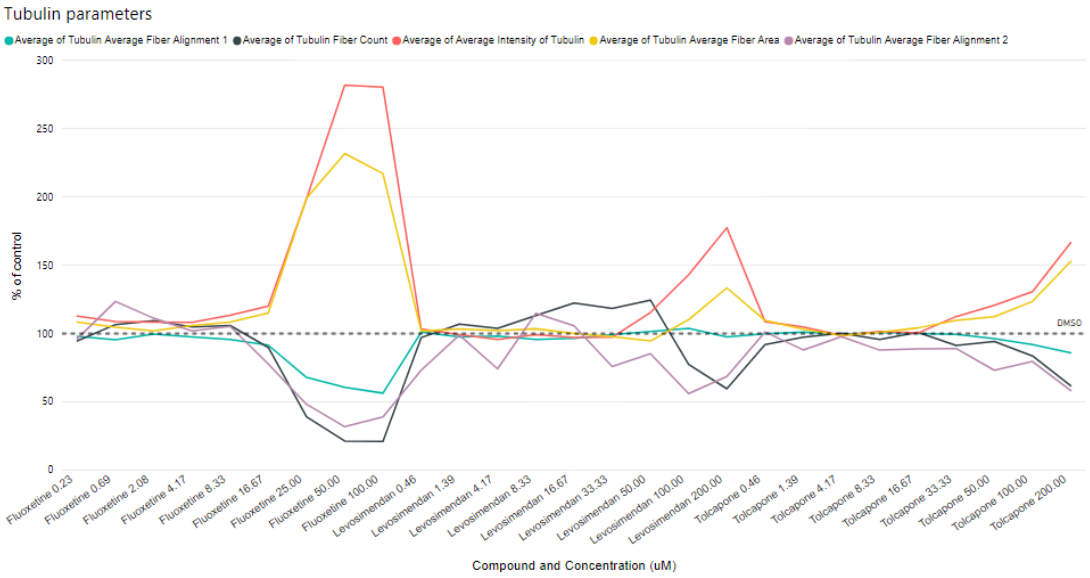

Figure 20. The measured tubulin parameters of the cells treated with different concentrations of fluoxetine, levosimendan or tolcapone at time point 24 h. It is seen that the parameters correlated with each other.

Similarly, the parameters for actin are shown in figure 21. The changes in all of the three parameters appeared to happen simultaneously. Intensity of actin was chosen for the comparison since it seemed to give a strong response and react sensitively e.g. to toxicity.

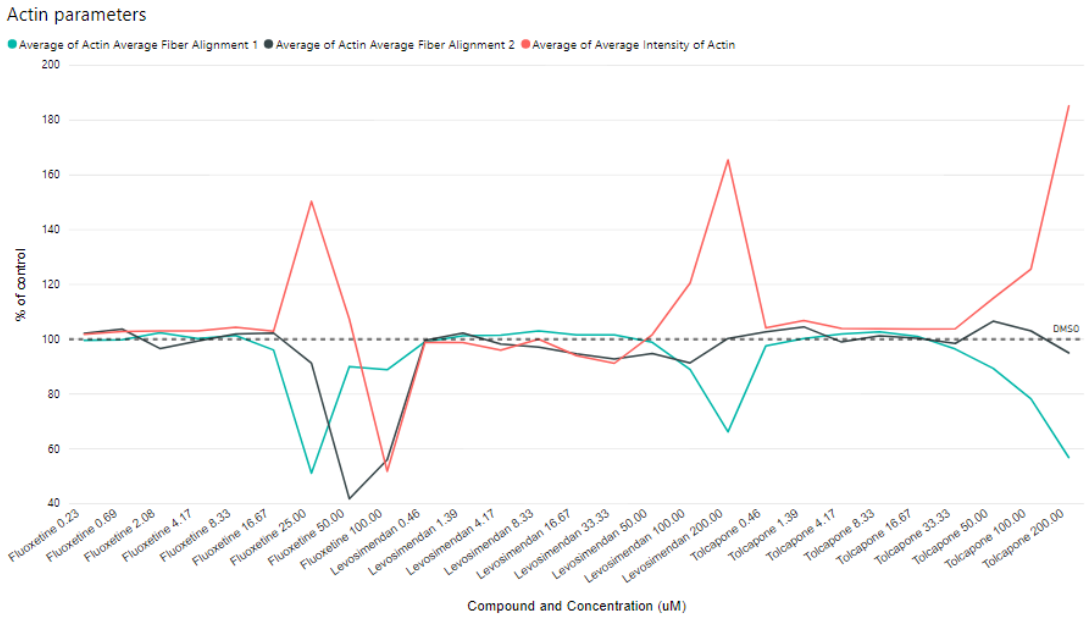

Figure 21. The measured actin parameters for the cells treated with fluoxetine, levosimendan or tolcapone at different concentrations. The time point was 24 h. It can be seen that all the parameters that gave responses reacted at the same concentrations.

Features, such as nucleus area and intensity, described the condensation of chromatins. These two parameters seemed to have negative association (figure 22). The area of the nucleus was chosen for the comparison since it is the more descriptive of the two parameters.

Figure 22. The measured nucleus parameters for cells treated with fluoxetine, levosimendan or tolcapone at different concentrations and at time point 24 h. It can be seen that the two parameters correlate with each other.

5.4 LECs of parameters

To investigate the order of the events and to estimate if the events occur because of the reduced ATP production, the LECs were determined for each selected parameter. The average intensity of nucleus and fiber alignment 1 features of tubulin and actin were also included in the LEC comparison to ensure the selection of the parameters described in previous chapter was well founded. The purpose was to find out which parameters reacted first to the compound treatment in order to evaluate the possible causality of the events. The determined LECs were also compared with the lowest concentrations causing mitochondrial toxicity (LEC of Seahorse oxygen consumption) to estimate whether ATP depletion is the cause of the other events. The concentrations for mitochondrial toxicity have been determined previously at Orion. LECs of different features at the time point 24 h are presented in table 9.

Table 9. The LECs of selected features at time point 24 h.

Lowest effective concentration (LEC), µM										
24h	Nucleus		pH3	γ-H2Ax	Tubulin		Actin			
Compound	Area	Average Intensity	Member Count	Average Intensity	Fiber Alignment 1	Average Intensity	Fiber Alignment 1	Average Intensity	Cell count	Seahorse oxygen consumption *
Troglitazone	> 100	> 100	> 100	100	> 100	> 100	50	50	> 100	1.56
Tolcapone	> 200	> 200	200	16.667	100	200	50	100	> 200	5
Nimesulide	> 200	> 200	> 200	> 200	> 200	> 200	200	> 200	> 200	6.25
Phenformin	> 200	> 200	> 200	0.463	> 200	> 200	200	> 200	> 200	50
Paclitaxel	0.019	0.056	0.019	0.019	0.019	0.019	0.019	0.019	0.056	-
Entacapone	100	> 200	> 200	200	100	> 200	> 200	> 200	200	100
Metformin	> 200	> 200	> 200	> 200	> 200	> 200	> 200	> 200	> 200	> 200
Nefazodone	50	50	> 50	25	50	25	12.5	12.5	12.5	6.25
Rotenone	0.007	> 1	> 1	0.083	0.5	> 1	1	0.167	0.007	<1
Buspirone	> 200	> 200	> 200	200	> 200	> 200	200	200	> 200	>40
2,4-dinitrophenol	> 200	> 200	> 200	> 200	> 200	> 200	200	> 200	200	30
Amiodarone	10	20	> 20	10	10	10	10	10	> 20	>5
Oligomycin	0.104	> 2.5	> 2.5	0.017	> 2.5	0.017	0.017	0.017	0.017	<1
Staurosporine	0.042	0.014	> 2	0.5	0.333	0.014	0.014	1	0.042	-
Levosimendan	> 200	> 200	> 200	> 200	> 200	> 200	100	> 200	50	25
Fluoxetine	25	25	> 100	25	25	16.667	25	25	50	25

* Determined previously at Orion

Seahorse assay has not been performed for paclitaxel and staurosporine and the concentration ranges have not been suitable for LEC determination for metformin, rotenone, buspirone, amiodarone and oligomycin. Mitochondrial toxicity of these compounds cannot thus be compared with cytoskeleton and DNA damage features but it can be seen that the concentrations are not divergent. Table 9 shows that mitochondrial toxicity is usually seen at lower concentrations than the other parameters. Exceptions are phenformin that seems to give γH2Ax response at its lowest concentration and fluoxetine that appears to affect tubulin before the mitochondria.

The order of the events differs considerably depending on the compound. Metformin treatment does not affect any of the measured features at all tested concentrations and nimesulide, buspirone and 2,4-dinitrophenol seem to have an effect only at the highest concentration. On the contrary, paclitaxel appears to affect all the features simultaneously at its lowest concentrations. To summarize the behaviour of different compounds and to examine the possible similarities, a hierarchical clustering based on the LECs and Euclidean distance was performed. Since the concentration series vary with different compounds, the rank of the LEC was used instead of actual concentration, meaning that the lowest concentration was given a value 1, the second lowest a value 2, etc. The clustering is represented in figure 23.

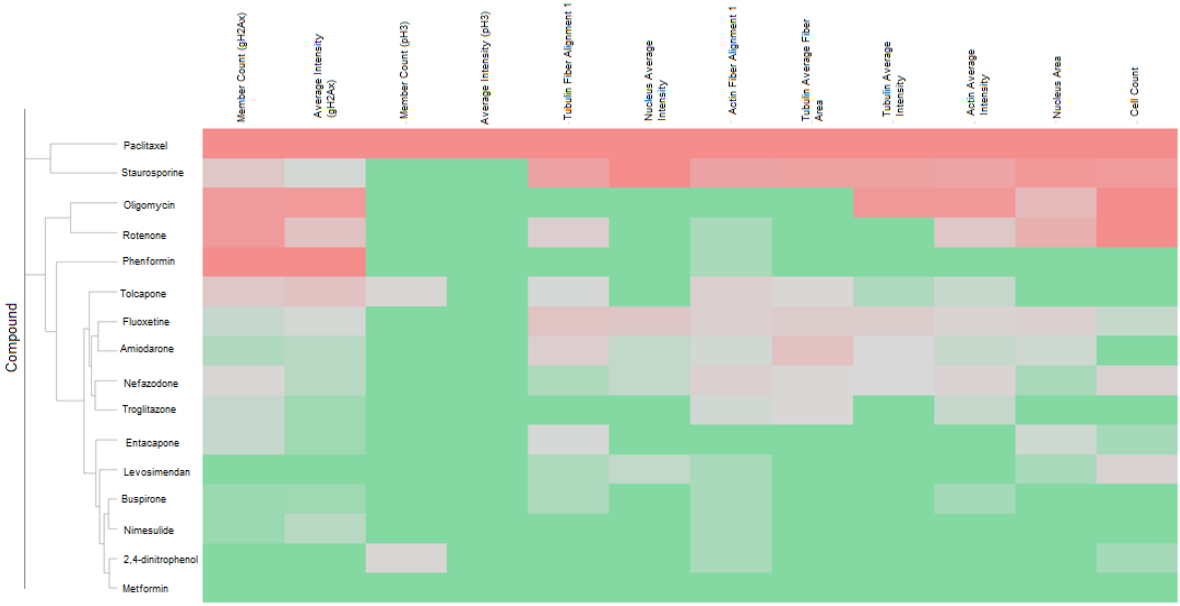

Figure 23. The clustering based on the ranking number of the LECs. The averages of both time points, 6 h and 24 h, were used in the clustering and it did not consider the direction of the response, i.e. if the LEC exceeded or went below the set limits. The order of the compounds depended on the similarity of the behavior of the compounds and it was affected by the strength of the response. The smallest ranking number is shown in dark red and the highest dark green.

The clustering separated paclitaxel and staurosporine from other compounds and they appeared to trigger the strongest response to the parameters. They were clustered next to oligomycin and rotenone and all of the four compounds appeared to affect especially the cell count, nucleus area and γH2Ax parameters. The weakest response was given by metformin but the compounds that also acted as negative control, buspirone and entacapone, were not among the weakest compounds. However, all of them were clustered together to a group that showed least effects.

Cytoskeleton was affected by paclitaxel and staurosporine but also by tolcapone, fluoxetine, amiodarone, nefazodone and troglitazone that were all at the same cluster. The mechanisms behind the toxicity of the compounds were not distinguished from the clustering, i.e. the compounds that disturb the ATP production the same way were not clustered exclusively together.

5.5 Toxicity of the compounds

The toxicity of the compounds was investigated by measuring the cell count and observing the possible decreasing dose response. If the cell count drops below 50%, it is a sign of a clear toxicity of the compound since it indicates that the cell proliferation has arrested and the cells have started dying immediately after the addition of the compound. The toxicity of the compounds was examined to evaluate if the concentration series have been optimal. The substantial decrease of the cell population due to the toxicity may cause an error to the results and, hence, it must be taken into consideration when interpreting the results. The cell counts for controls are presented in figure 24 and for each concentration of each compound in figure 25.

It can be seen from figure 25 that most of the compounds had a dose response in their cell count and the reduction was faster in 24 h time point than in 6 h. The cell count after the treatment by amiodarone, buspirone and metformin was not affected. Fluoxetine was strongly toxic in high concentrations as seen in 6 h and 24 h time points. The cell count of levosimendan, staurosporine and tolcapone was decreased to 50% in 24 h time point. The cells treated with oligomycin, paclitaxel, rotenone and staurosporine behaved very differently than the rest of the compounds. There was only a slight dose response and it seems that the decrease in the cell count stopped above 50% and remained constant despite the increasing concentration. Figure 24 shows that CCCP and MMS were also toxic at 24 h time point.

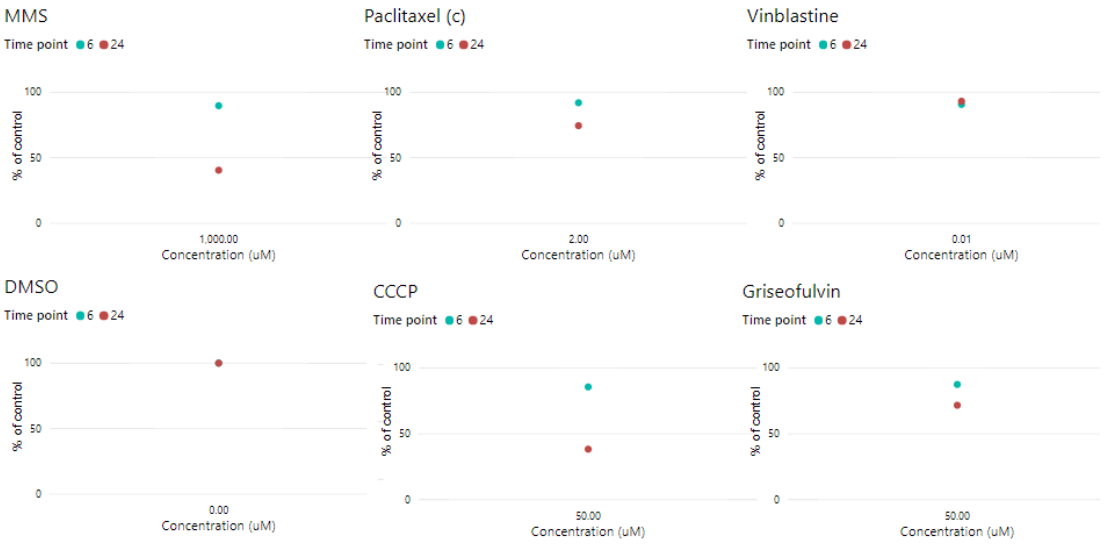

Figure 24. The cell counts of the controls as a percent of DMSO control. It is seen that the count of cells treated with positive controls was always lower than the count of untreated cells. MMS and CCCP were toxic to cells at time point 24 h since the cell count decreased below 50%.

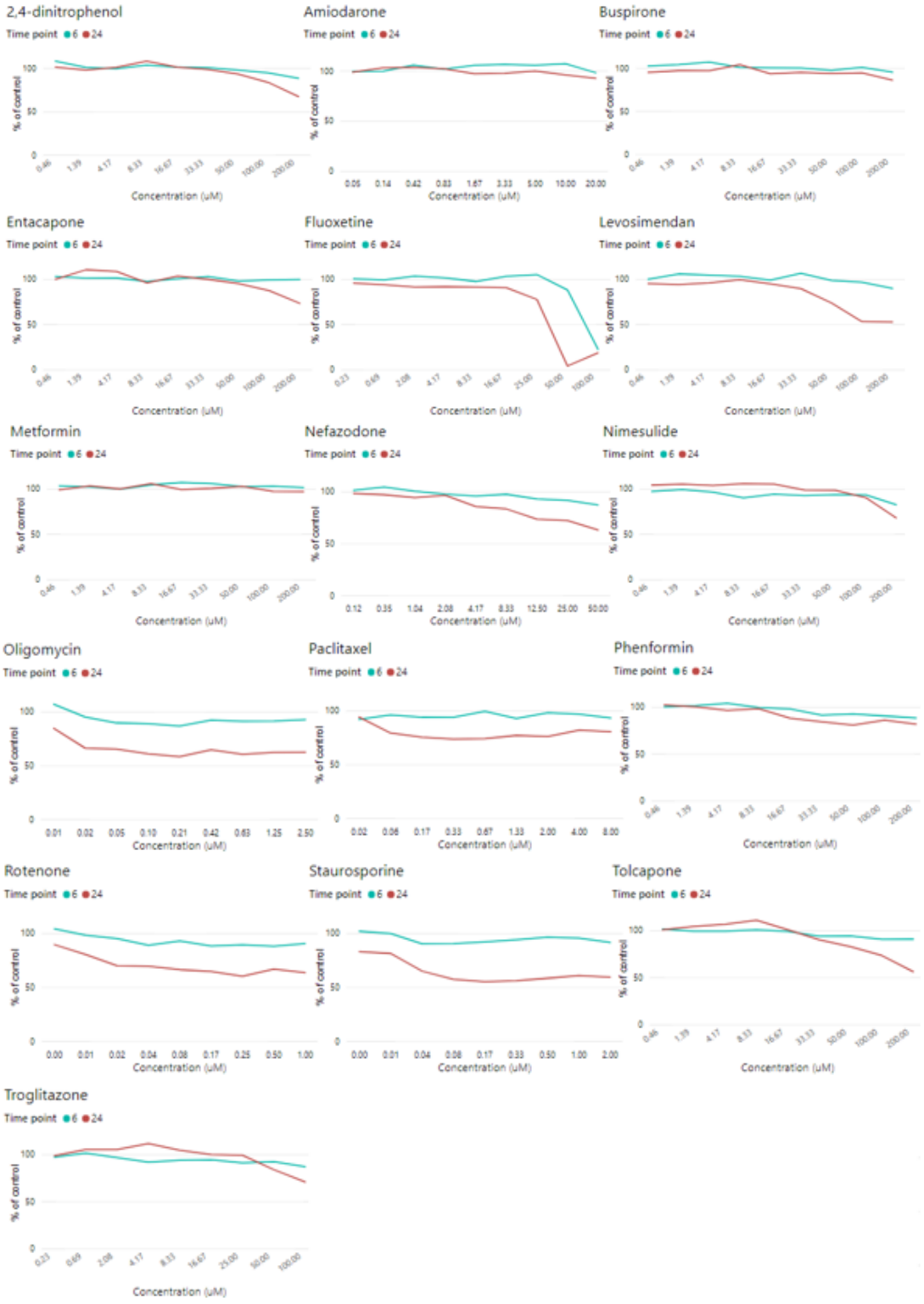

Figure 25. The cell counts after the treatment with the compounds. Fluoxetine, levosimendan, tolcapone and staurosporine showed toxicity at time point 24 h since the cell count decreased to or below 50%. Oligomycin, paclitaxel, rotenone and staurosporine appeared to have only a minor dose response in the cell count.

5.6 Responder analysis for pH3 and γH2Ax

The purpose of the responder analyses was to investigate if mitochondrial toxins cause increase of genotoxic markers. The amount of pH3 and γH2Ax positive cells was interpreted to be increased when it exceeded the average level of DMSO controls. The correlation between γH2Ax and pH3 was also examined. Altogether, the results of pH3 and γH2Ax responder analyses for each compound and time point are found in appendix A.

All the compounds, excluding metformin, seemed to increase the amount of γH2Ax responder cells at 24 h time point. Only paclitaxel, levosimendan and tolcapone treatments seemed to trigger the pH3 response but the quantity of pH3 responders was often decreased due to compound treatment. When pH3 and γH2Ax responses were compared, it was noticed that most of the compounds behaved similarly: the number of the γH2Ax responder cells was increased while the amount of pH3 positive cells was decreased with the increasing concentration. Figure 26 represents entacapone at time point 24 h as an example of this type of behaviour. The pH3 response of entacapone-treated cells was not triggered but the quantity of pH3 positive cells seemed to decrease dose dependently. The pH3 response was significantly different between entacapone-treated and DMSO-treated cells since concentration 33.33 µM ($p<0.01$). The amount of γH2Ax positive cells treated with entacapone increased dose dependently and differed significantly from DMSO level since concentration 100 µM ($p<0.05$). The significance levels of the presented concentrations are shown in figure 26.

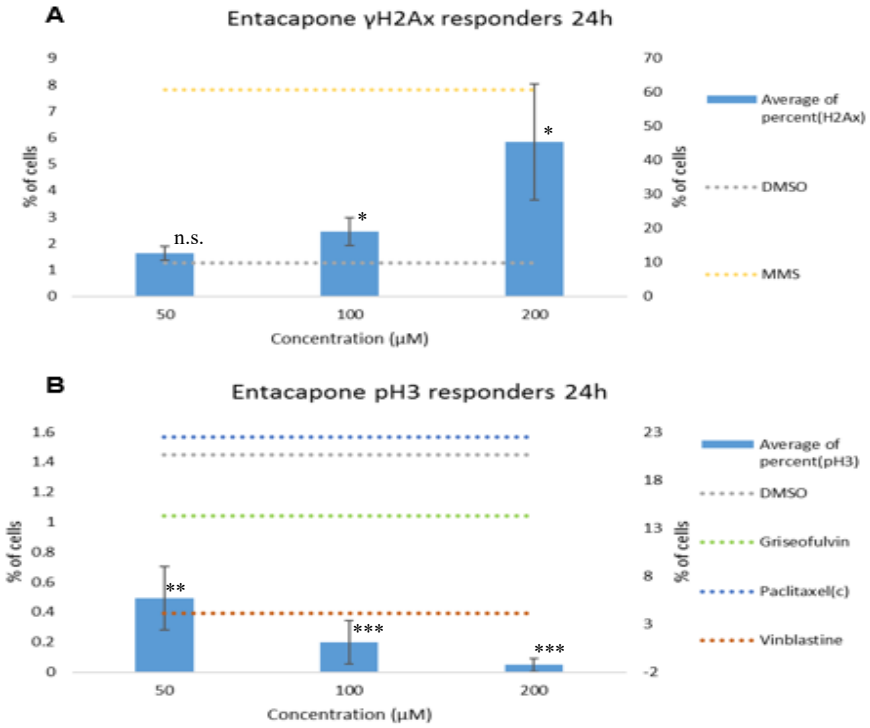

*Figure 26. The γH2Ax and pH3 responders of the three highest concentrations of entacapone. The responders of entacapone and DMSO are shown on primary y-axis and the positive controls on the secondary y-axis. The significances of differences to DMSO are shown in asterisks: (p>0.05 n.s., p≤0.05 *, p≤0.01 **, p≤0.001 ***) The error bars demonstrate the standard error. A) the amount of γH2Ax positive cell after entacapone treatment increased dose dependently. B) There was a decreasing dose response in the pH3 marker of entacapone-treated cells. The pH3 response of entacapone did not exceed the DMSO level at any concentration and the difference to DMSO was significant since concentration 33.33 µM.*

The results of levosimendan- and tolcapone-treated cells in time points 6 h and 24 h, respectively, were deviant since both the amount of γH2Ax and pH3 positive cells appeared to increase with the increasing concentration. The four highest concentrations of levosimendan at time point 6 h are shown in figure 27. It can be seen that the number of pH3 positive cells is increasing until it is reduced at concentration 200 µM. The pH3 response of levosimendan was significantly different from DMSO control since concentration 33.33 µM ($p<0.01$). The γH2Ax response differed significantly between DMSO control and levosimendan-treatment only at concentration 200 µM ($p<0.05$).

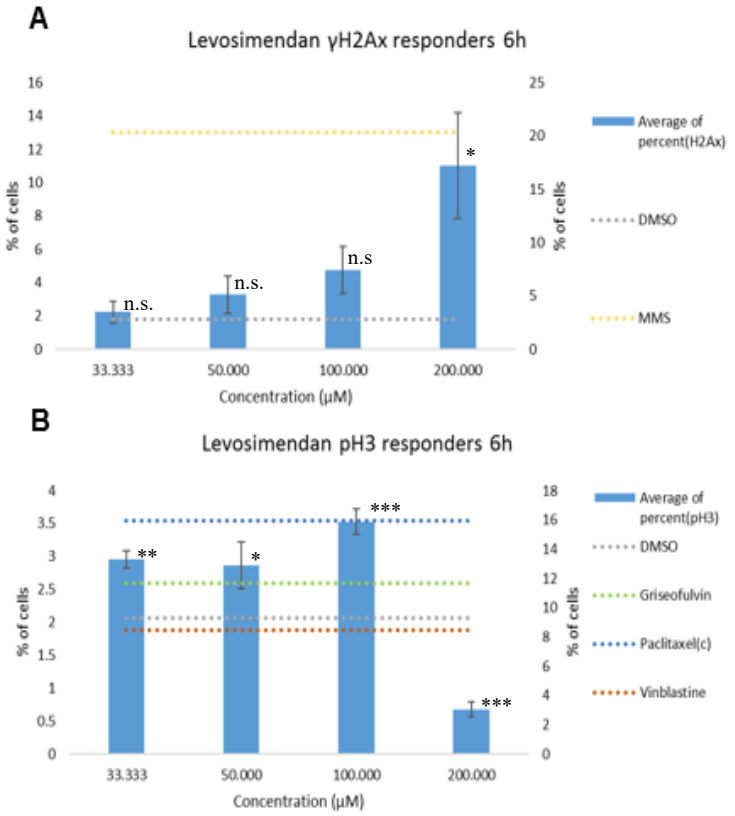

*Figure 27. The γH2Ax and pH3 responders at four highest concentrations of levosimendan and DMSO are shown on the primary y-axis and the positive controls on the secondary y-axis. The significances of differences to DMSO are shown as asterisks (p>0.05 n.s., p≤0.05 *, p≤0.01 **, p≤0.001 ***). The error bars refer to standard error. A) the quantity of γH2Ax positive cells increased dose dependently. B) There was an increase for pH3 marker until the collapse at concentration 200 µM.*

Paclitaxel-treatment was distinguishable in responder analyses since it increased the amount of both γH2Ax and pH3 positive cells substantially. The differences between DMSO level and γH2Ax and pH3 responses after paclitaxel treatment since the lowest concentration (0.019 µM) were statistically extremely significant ($p<0.001$). The responders at the four lowest concentrations of paclitaxel at time point 24 h are illustrated in figure 29.

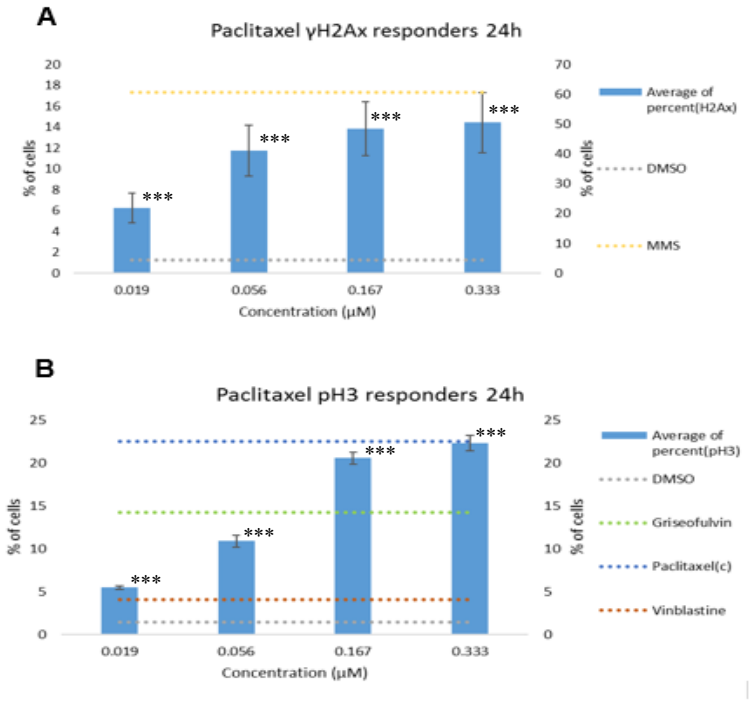

*Figure 29. The γH2Ax and pH3 responders at the four lowest concentrations of paclitaxel at time point 24 h. Paclitaxel and DMSO are show on primary y-axis and the positive controls on secondary y-axis. . The significances of differences to DMSO are shown as asterisks (p≤0.001 ***). The error bars demonstrate the standard error. A) the number of γH2Ax positive cells after paclitaxel treatment increased dose dependently and the difference to DMSO level was statistically significant already at the lowest concentration (0.019 µM). B) The increase of pH3 positive cells was statistically significant already at the lowest concentration (0.019 µM) of paclitaxel. The increase was dose dependent.*

5.7 Nucleus area and responder analyses

The nucleus area of the cells was compared with the γH2Ax and pH3 responder data to investigate the mechanism behind the changes of pH3 and γH2Ax responses. The purpose was to observe possible correlations between these parameters. The illustrations of this data comparison altogether can be found in appendix B.

Compounds, such as amiodarone, buspirone, fluoxetine, staurosporine and nefazodone appeared to decrease the nucleus area dose dependently. These compounds also showed dose response in γH2Ax and thus it seemed that the nucleus area and γH2Ax response had negative correlation. pH3 response did not seem to correlate with nucleus area. Amiodarone at time point 24 h is illustrated in figure 30 as an example. The nucleus area of amiodarone-treated cells differed from DMSO level at all presented concentrations while the γH2Ax response was different between

amiodarone and DMSO since concentration 10 µM. The changes between concentrations 10 µM and 20 µM was significant in nucleus area ($p<0.01$) and γH2Ax response ($p<0.05$).

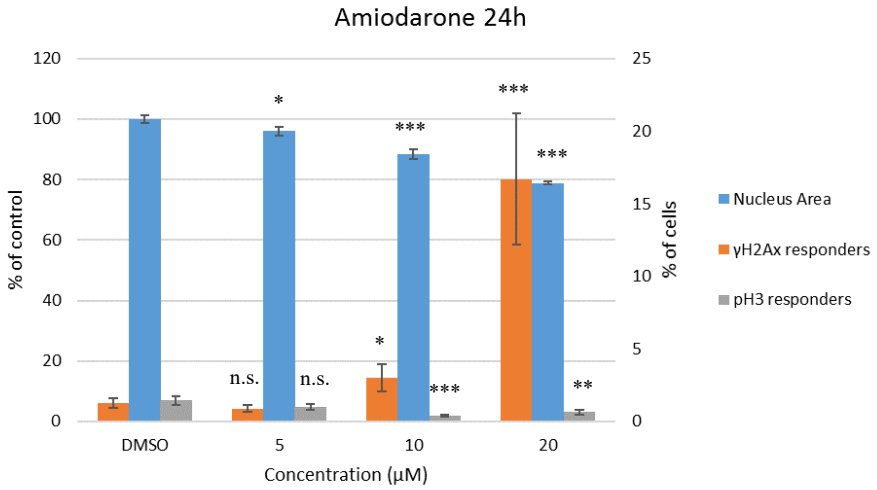

*Figure 30. The nucleus area, γH2Ax and pH3 responders of the cells treated with amiodarone at the three highest concentrations and with DMSO. The nucleus area is shown on the primary y-axis and the responders on secondary y-axis. The significances of differences to DMSO are shown as asterisks (p>0.05 n.s., p≤0.05 *, p≤0.01 **, p≤0.001 ***). The error bars demonstrate the standard error. The nucleus area decreased and the number of γH2Ax positive cells increased with the increasing concentration. There was no dose response in pH3. The change between concentrations 10 µM and 20 µM was very significant in nucleus area and significant in γH2Ax response.*

Compounds such as 2,4-dinitrophenol, entacapone, nimesulide, levosimendan and tolcapone, which are all uncouplers, appeared to increase both nucleus area and the amount of γH2Ax positive cells dose dependently. pH3 response did not appear to correlate with the nucleus area. Nucleus area and γH2Ax and pH3 responses of nimesulide-treated cells are illustrated in figure 31 as an example. The nucleus area and γH2Ax response of nimesulide-treated cells were significantly different to DMSO level at concentration 200 µM ($p<0.001$ and $p<0.05$, respectively). There was no statistically significant difference between pH3 responses of nimesulide-treated cells and DMSO level.

The rest of the compounds did not seem to cause increasing or decreasing trend in nucleus area. Nucleus area was elevated in the cells treated with oligomycin and rotenone, while paclitaxel-treated cells had reduced nuclei.

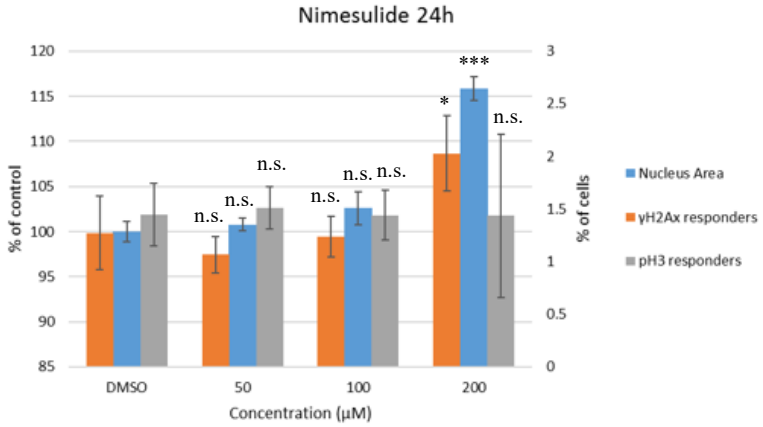

*Figure 31. The nucleus area, γH2Ax and pH3 responses of DMSO-treated cells and cells treated with nimesulide at three highest concentrations at time point 24 h. Nucleus area is shown on primary y-axis and responders on secondary y-axis. The significances of differences to DMSO are shown as asterisks (p>0.05 n.s., p≤0.05 *, p≤0.01 **, p≤0.001 ***). The error bars demonstrate the standard error. The nucleus area and the number of γH2Ax positive cells increased with the increasing nimesulide concentration but differed from DMSO level only at the highest concentration. The amount of pH3 responders decreased with increasing nimesulide concentration but the reduction was not statistically significant.*

5.8 Cytoskeleton and responder analyses

The actin and tubulin intensity was compared with γH2Ax and pH3 responder data to examine if the changes in the dynamics of cytoskeleton predicted or correlated with the genotoxic markers. The purpose was to estimate whether the ATP depletion might lead to DNA damage via changed dynamics of cytoskeleton. Altogether, the illustrations of this data are found in appendix C.

The compounds seemed to cause similar reactions to both actin and tubulin, excluding paclitaxel and staurosporine that appeared to affect tubulin more strongly than actin. Most of the compounds seemed to cause increase of tubulin and actin intensity together with triggered γH2Ax response at higher concentrations. However, which of the events occurred first, depended on the compound. The strength of the response of tubulin, actin and γH2Ax also appeared to have a possible association. The intensity of actin and tubulin and pH3 response did not have a visible association, with the exception of the compounds that caused negative correlation between γH2Ax and pH3 responses and paclitaxel. Figure 32 represents 2,4-dinitrophenol as an example. It shows that actin and tubulin intensity behaved identically and began to increase at the concentration 100 µM. The actin and tubulin intensity differed

significantly between DMSO level and 2,4-dinitrophenol-treatment at concentrations 100 µM ($p<0.01$) and 200 µM ($p<0.001$). The increase of tubulin and actin intensities between these concentrations was also statistically significant ($p<0.01$). The increase of γH2Ax positive cells followed behind and began at concentration 200 µM which differed from DMSO level very significantly ($p<0.01$). The change in the γH2Ax response after 2,4-dinitrophenol-treatment was also significant between concentrations 100 µM and 200 µM ($p<0.05$).

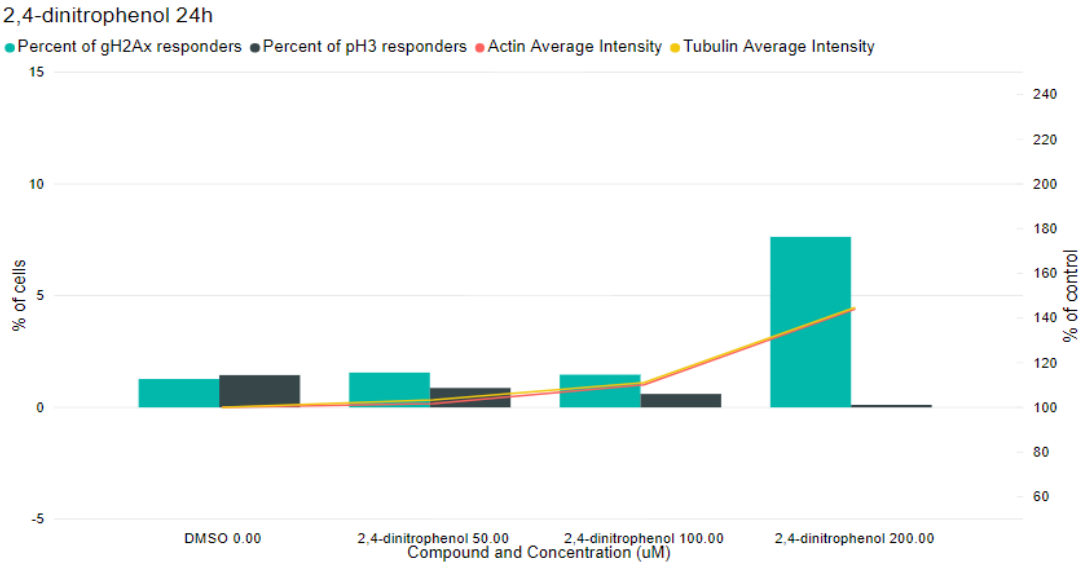

Figure 32. Tubulin and actin intensity and γH2Ax and pH3 responses at the three highest concentration of 2,4-dinitrophenol and DMSO at time point 24 h. The responder analyses are shown on the primary y-axis and the intensities on the secondary y-axis. The pH3 response of 2,4-dinitrophenol decreased dose dependently and differed from pH3 response of DMSO significantly since concentration 100 µM ($p<0.01$). γH2Ax response of 2,4-dinitrophenol began to increase and differed significantly from DMSO at concentration 200 µM ($p<0.01$). Tubulin and actin intensities behaved almost identically and they differed significantly between 2,4-dinitrophenol and DMSO since concentration 100 µM ($p<0.01$). The increase of actin and tubulin intensities began one concentration before γH2Ax response.

Entacapone, nimesulide and phenformin treatments did not appear to cause a similar association between actin and tubulin intensities and γH2Ax response. For example, entacapone increased the number of γH2Ax positive cells dose dependently. However, the actin and tubulin intensities did not increase but seemed to fluctuate below the DMSO level. As explained in chapter 5.6, γH2Ax response of entacapone and DMSO differed significantly at concentrations 100 µM and 200 µM. The tubulin and actin intensities did not increase significantly in these concentrations. The actin and tubulin intensities and responder analyses of entacapone are illustrated in figure 33.

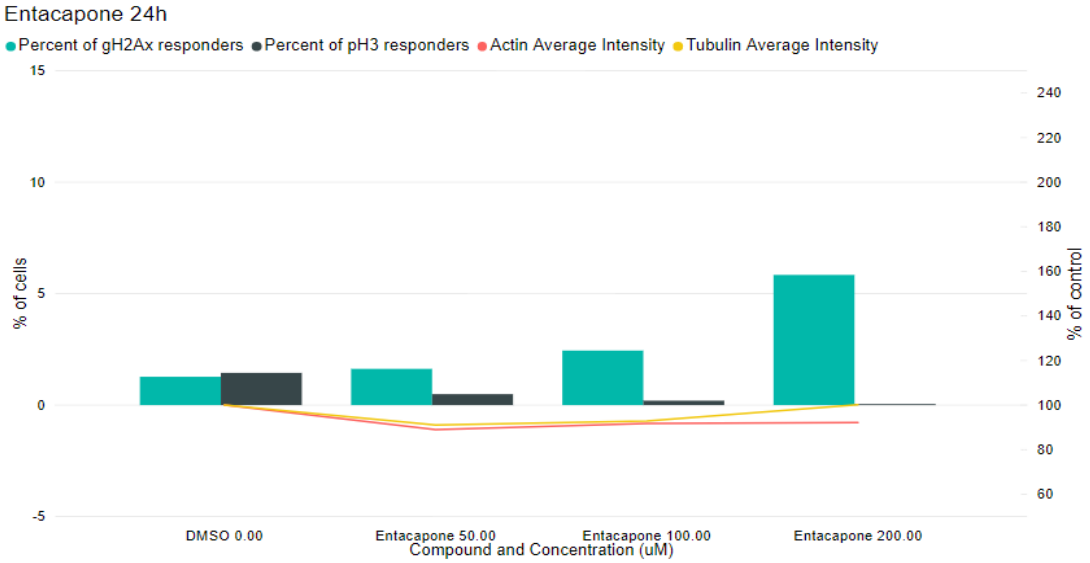

Figure 33. Tubulin and actin intensity and γH2Ax and pH3 responses after the treatment with entacapone at the three highest concentrations and DMSO at time point 24 h. The responder analyses are shown on the primary y-axis and the intensities on the secondary y-axis. The γH2Ax responses were significantly different from the DMSO level at concentrations 100 µM and 200 µM. The increase of tubulin and actin intensities were not significant (p>0.05). The p-values for γH2Ax and pH3 are presented in figure 26.

5.9 Analysis by Advanced cell classifier (ACC)

The data acquired from the HCA image analysis was analysed by ACC to investigate if certain types of cells were predominant after the compound treatment. Table 10 shows the distribution of the cells at time point 24 h for the top concentrations of the compounds. Since the top concentrations of staurosporine, fluoxetine, levosimendan and tolcapone lowered the cell count, as described in chapter 5.5, their highest non-toxic concentration was chosen for the presentation.

Table 10. The classification of the cells by ACC at time point 24 h. The percentage of each class is shown for the given concentration. The red color refers to highest percentages and blue to lowest, except for the classes interphase cells and mitotic cells where the red demonstrates the lowest and blue the highest percentage.

Compound	Concentration (µM)	Interphase cells (%)	Mitotic cells (%)	Rounded cells (%)	Stretched cells (%)	Damaged cells (%)	Unclassified (%)
2,4-dinitrophenol	200	76.4	8.3	0.4	11.2	0.9	2.7
amiodarone	20	38.0	21.9	13.9	19.2	2.7	4.2
Buspirone	200	82.0	11.2	0.1	4.2	0.2	2.2
Entacapone	200	91.9	3.0	0.0	0.5	0.6	4.0
Fluoxetine	25	67.0	16.7	5.0	7.6	1.8	1.8
Levosimendan	50	85.6	10.1	0.0	1.0	0.6	2.7
Metformin	200	90.5	5.2	0.0	0.1	0.6	3.5
Nefazodone	50	18.5	14.5	8.7	25.8	21.6	10.8
Nimesulide	200	80.8	3.1	1.1	12.7	0.3	2.0
Oligomycin	2.5	88.6	2.1	0.0	7.3	0.2	1.9
Paclitaxel	8	58.9	28.5	1.5	4.8	3.0	3.3
Phenformin	200	81.4	5.7	1.0	10.0	0.2	1.7
Rotenone	1	75.8	12.5	0.9	5.9	1.5	3.5
Staurosporine	0.042	91.4	4.0	0.0	0.0	0.2	4.4
Tolcapone	100	71.7	5.3	3.4	15.7	1.5	2.4
Troglitazone	100	83.7	4.4	1.1	7.4	0.4	2.9
Paclitaxel (c)	2	52.9	30.3	3.1	4.4	3.1	6.3
CCCP	50	4.3	17.7	41.5	21.7	7.7	7.0
MMS	1000	25.7	6.1	18.1	27.4	17.8	4.9
Vinblastine	0.01	81.6	12.8	0.5	1.6	0.7	2.7
Griseofulvin	50	61.3	23.7	3.0	4.4	3.0	4.6
DMSO	0	90.0	6.4	0.1	0.4	0.4	2.7

The table 10 shows that the percentages in each class appeared to vary evidently. Excluding the cells treated with amiodarone, nefazodone, CCCP and MMS, most of the cells seemed to be in interphase. The cells treated with tubulin stabilizers paclitaxel and griseofulvin had the highest percentage of mitotic cells. CCCP and MMS seemed to affect the cell shape since they caused both the rounding and stretching of the cells. According to this analysis, nefazodone and MMS caused distinctly more damage to the cells than the other compounds.

5.10 Comparing HCA data with flow cytometry data

Flow cytometry DNA damage assay was performed with both HepG2/C3A and TK6 cells. DNA damage assays are conventionally performed by flow cytometry with TK6 cells at Orion, and the purpose was to compare TK6 data with HepG2/C3A flow cytometry data. The flow cytometry DNA damage assay with HepG2/C3A cells was performed to have a comparison to γH2Ax and pH3 data gained from HCA. Even though the effects of a given concentrations cannot be compared between TK6 and

HepG2/C3A cells due to the differences of the two cell lines, it was possible to observe the similarities of the reactions to the compounds. Since γH2Ax and pH3 responses were the common parameters of FC and HCA assays, only those were compared. In FC assay, the responses were calculated as folds and no responder analysis was conducted.

The FC and HCA data of entacapone is illustrated in figure 34. It is seen that the number of γH2Ax positive cells increased dose dependently in both cell lines and assays. The increase started at lower concentration in TK6 cells than in HepG2/C3A cells. pH3 response had also similarities in both cell lines and assays. The number of pH3 positive cells fluctuated at lower concentrations and decreased at higher concentrations in TK6 cells and in HepG2/C3A cells of HCA assay. pH3 positive HepG2/C3A cells did not have similar visible decrease in FC assay but otherwise their fluctuation resembled that of TK6 cells. The pH3 response was lost at lower concentration in TK6 cells than in HepG2/C3A cells.

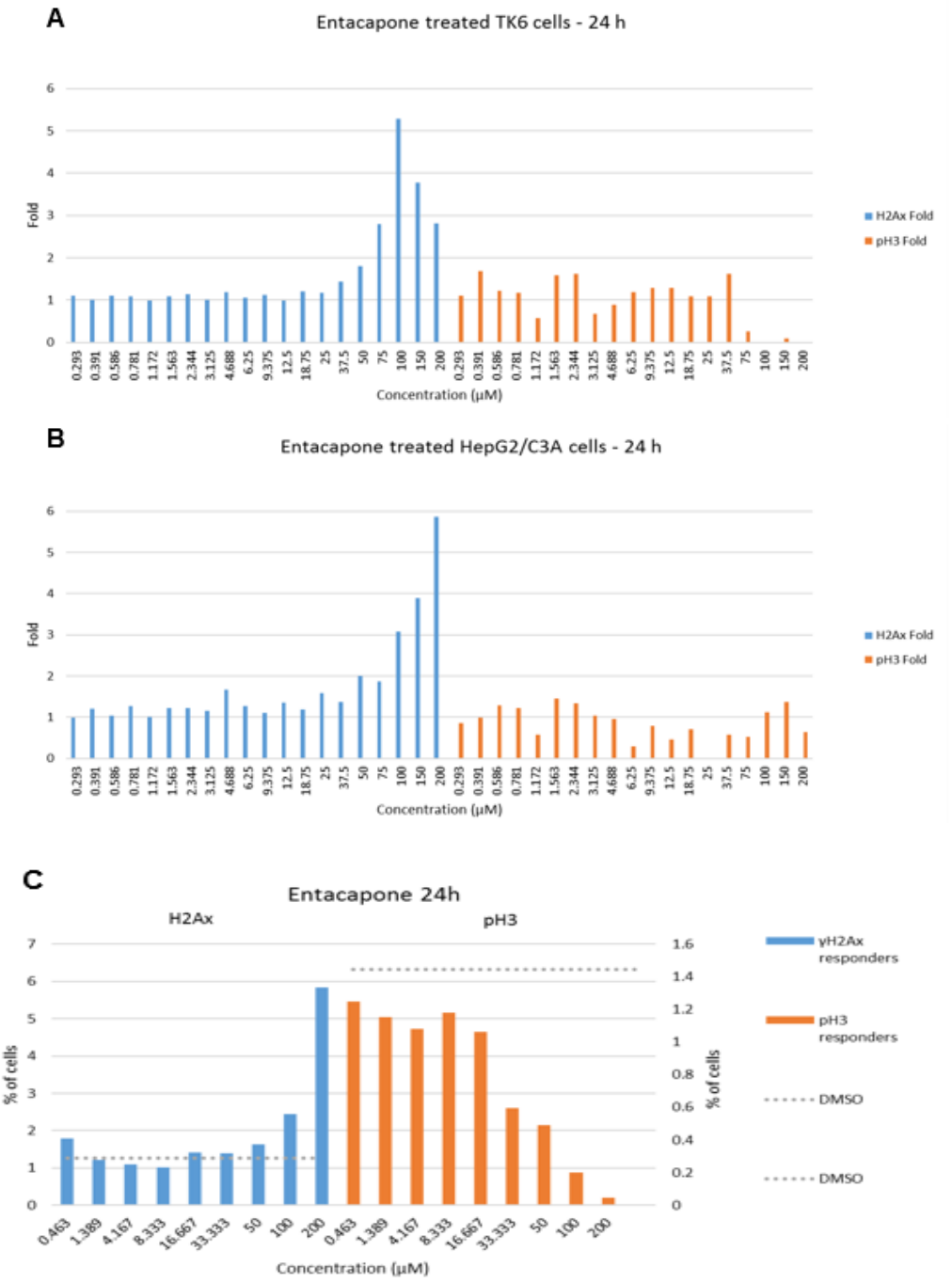

Figure 34. A) γH2Ax and pH3 folds of entacapone-treated TK6 cells determined by FC. γH2Ax fold increased dose dependently while pH3 fold fluctuated. Both of the folds decreased at highest concentrations. B) FC data of γH2Ax and pH3 folds of entacapone-treated HepG2/C3A cells. γH2Ax fold behaved similarly than in TK6 cells but the increase began at higher concentration. pH3 fold fluctuated similarly than in TK6 cells but the response was not lost at high concentrations. C) γH2Ax and pH3 responses of entacapone-treated HepG2/C3A cells determined by HCA. The number of γH2Ax positive cells increased dose dependently. The amount of pH3 positive cells fluctuated at lower concentrations but began to decrease dose dependently above a concentration of 33.333 µM.

6. Discussion

6.1 Evaluating the toxicity of the compounds

Before interpreting the other results, the toxicity of the compounds had to be investigated to evaluate both the optimality of the concentration series used in the assays and the possibility of an error caused by the reduced cell population. The cell count after the compound treatment was examined to evaluate the toxicity of the compounds. It was noticed that some compounds, such as amiodarone, metformin and buspirone, did not affect the cell count. This may have been due to the too low top concentrations of these compounds. This had to be taken into consideration when observing the behaviour of other parameters in these compounds since it is possible that some of the effects are not visible when the concentration is too low. Oligomycin, staurosporine and rotenone had a cell count lowering effect at the lowest concentration of the series at time point 24 h. This indicates that the lowest concentration of these compounds was not low enough. This might cause error when estimating the order of the events since some of the effects may have been visible only at the lower concentrations of the toxins. Fluoxetine, levosimendan and tolcapone reduced the cell count near to or below 50%. This had to be taken into consideration when interpreting the other results since the possibility of an error increases when the cell population caused by the toxicity of the compounds reduces considerably.

It was noticed that oligomycin, staurosporine, rotenone and paclitaxel did not cause dose dependent decrease in cell count but the cell count seemed to stabilize into constant level. This was expected from paclitaxel that is known to arrest the mitosis during metaphase (L. Yang et al., 2010). The cells did not proliferate but the toxic effect of paclitaxel was not strong enough to induce cell death. In addition to mitochondrial effect, staurosporine is known to inhibit the Cdk1, which is a component of the cell cycle checkpoint regulation (Vermeulen et al., 2003). This mechanism may explain the arrest of cell proliferation seen in the cell count data of staurosporine. As known complex inhibitors (Heinz et al., 2017; Jonckheere et al., 2012), rotenone and oligomycin arrested the cell cycle possibly due to the ATP depletion they cause in the

cell. Upon inefficient oxidative phosphorylation, the cells do not have enough energy for the proliferation and they may exit the cell cycle to the G_0 resting phase.

6.2 The order of the events and the similarities of the compounds

In this research, in addition to cell count, several parameters were determined to assess the effect of the compounds on the cells. Tubulin and actin require ATP to function and, hence, the possible changes in their dynamics after treatment with mitochondrial toxins were evaluated. The purpose of this research was to find out if mitochondrial toxins induce DNA damage and, thus, the DNA damage markers, pH3 and γH2Ax, were examined.

The LECs of the compounds for each chosen parameter were determined to investigate the order of the events caused by the compound treatment. The purpose was to investigate whether ATP depletion might cause increased number of pH3 and γH2Ax positive cells and if the effect might be due to the changed dynamics of cytoskeleton. Clustering was conducted based on the LECs to find similarities between the behaviour of different compounds. The LECs were compared with the lowest concentrations causing mitochondrial toxicity and it was noticed that, except for phenformin and fluoxetine, the mitochondrial toxicity was seen at lower concentrations than the other parameters. This supports the hypothesis of the thesis that the DNA damage and alterations in cytoskeleton dynamics would be caused by the mitochondrial dysfunction. However, the determination of the toxic concentrations to mitochondria was conducted in the absence of glucose whereas the other parameters were measured to cells grown in glucose medium. The presence of glucose enables glycolysis that compensates the insufficient function of oxidative phosphorylation. It is possible that without glycolysis the LECs for the HCA parameters would have been lower.

The order of the events varied depending on the compound. To support the hypothesis, the LECs for tubulin and actin parameters should have been lower than for γH2Ax and pH3 parameters but higher than for mitochondrial toxicity. Troglitazone, nefazodone and staurosporine were the only compounds that gave this type of result. Many LECs were determined to be higher than the top concentration tested in this research. This also confirms that the concentration series were not optimal for all

compounds as was suggested in chapter 6.1. The limits for LEC determination (Mean of DMSO ± 3SD) may have also been too exclusive. Some parameters might also have naturally larger deviation than others and therefore the threshold of LECs is higher for those parameters. This may cause error when comparing the different parameters and observing the order of the events.

The clustering analysis separated paclitaxel and staurosporine from the rest of the compounds. This was predictable since, as described in previous chapter (6.1), staurosporine and paclitaxel have direct effects on cell cycle and may arrest the cycle completely. Oligomycin and rotenone were clustered together, next to staurosporine. This supports the mechanism suggested in previous chapter (6.1) that the ATP depletion caused by them would arrest the cell cycle and hence, oligomycin and rotenone would cluster close to staurosporine and paclitaxel. However, unlike paclitaxel and staurosporine, oligomycin and rotenone did not seem to affect tubulin or actin dynamics. This difference can possibly be explained by the different mechanisms of these toxins. Paclitaxel is a tubulin stabilizer and may arrest the cell cycle during metaphase (L. Yang et al., 2010). Hence, it is expected that paclitaxel increases the proportion of polymerized tubulin which is prevalent in metaphase. Staurosporine inhibits Cdk1 which participates cell cycle regulation in restriction point (Vermeulen et al., 2003). Thus, it can be assumed that the cell cycle arrest would take place in the beginning of the cell cycle and the depolymerized tubulin would be predominant. Energy shortage, which may be the reason for the possible cell cycle arrest caused by rotenone and oligomycin, does not arrest the cell cycle as specifically in certain phase as tubulin stabilization or Cdk1 inhibition. Thus, the cell cycle of an individual cell may be arrested at any checkpoint and the arrest is not seen in tubulin dynamics of the rotenone or oligomycin treated cell population.

It would have been expected that compounds with similar mechanisms had clustered closer together. The suboptimal concentration series may have caused error to the clustering analysis. Also, since the clustering used averages from both time points and the number of events at 6 h was clearly lower than at 24 h, it is possible that some of the effects were not seen in it.

6.3 The correlation of pH3 and γH2Ax responses

One part of the research question was whether mitochondrial toxins cause DNA damage. This was investigated by observing the increase of mitotic marker, pH3 and DNA double strand break marker, γH2Ax. The developed responder analyses seemed to be functional since the positive controls caused the strongest responses as was expected. However, since the cells were categorized binary as positive or negative at both responder analyses, substantial reduction in cell count causes error in percentage. This was taken into consideration when interpreting the results. The comparison of γH2Ax and pH3 responses had to be treated with caution since the two markers were applied to the different plates. Hence, the cell population is not identical even though the treatment of the cells has been similar.

It was noticed that most of the compounds increased the number of γH2Ax positive cells and decreased the amount of pH3 positive cells dose dependently. This indicates that these compounds did affect the DNA damage markers. The negative correlation of pH3 and γH2Ax was expected since normally functioning cells should not enter mitosis if there are DNA double strand breaks in chromosomes. This expected result indicates that the mitochondrial toxins did not cause defects in cell cycle checkpoint system. This suggests that despite the ATP depletion caused by the mitochondrial toxins, the energy production of the cells was adequate to maintain the cell cycle regulation. Since the responder analysis for γH2Ax was developed to exclude the DNA double strand breaks that are caused by the topoisomerase II during DNA replication in interphase, the increase of γH2Ax responder cells suggests that the compounds induced the formation of DNA double strand breaks rather than arrested the cell cycle during interphase. However, if the thresholds for the γH2Ax responder analysis have been suboptimal, it is possible that the triggered γH2Ax response was due to the predominance of interphase cells. The increased γH2Ax response may also indicate that the DNA repair system was interfered due to the ATP shortage and did not work sufficiently.

Levosimendan at time point 6 h and tolcapone at time point 24 h increased both the number of pH3 and γH2Ax positive cells dose dependently. The behaviour of tolcapone can possibly be explained by the reduced cell count since the pH3 response was elevated only at top concentration, which was determined as toxic based on the cell count data. Levosimendan was not toxic at time point 6 h and pH3 response was

significantly increased at several concentrations. However, the increase of γH2Ax response was significant only at the top concentration where pH3 response was dropped. Thus, the γH2Ax and pH3 responses were not elevated simultaneously. Since none of the compounds, excluding paclitaxel, increased the amount of pH3 responder cells dose dependently, it is probable that the induction of γH2Ax responses was not due to stabilization or destabilization of tubulin. This means also that it is improbable that the energy shortage would lead to DNA damage because there would not be enough ATP for tubulin to depolymerize. Tubulin requires ATP for depolymerization as was explained in chapter 2.3 (Spurck & Pickett-Heaps, 1987). Paclitaxel is expected to trigger pH3 and γH2Ax responses simultaneously since as a tubulin stabilizer it disturbs the segregation of sister chromatids and may not only delay or arrest the cell cycle during mitosis but also tear the chromatids, which leads to DNA damage (Field et al., 2013).

6.4 The mechanisms behind the pH3 and γH2Ax responses

The results of γH2Ax and pH3 responder analyses were compared with nucleus area and tubulin and actin intensity to investigate the possible mechanisms behind the significant changes in DNA damage markers. The increase in the nucleus area indicates the decondensation of the chromatin, which may be caused by the DNA strand breaks. Nucleus area may also be larger after the DNA replication since the amount of chromatin is doubled. The decrease of the nucleus area refers to condensation of the chromatins, which is a sign of either mitosis or apoptosis. Amiodarone, buspirone, fluoxetine, staurosporine and nefazodone that are all complex inhibitors, decreased nucleus area and increased the number of γH2Ax positive cells dose dependently. This negative association indicates that the γH2Ax is caused by the cytotoxic effect since the cells are probably dead. The reduced nucleus area due to mitosis should have been observed also as an induction of pH3 response, which was not seen.

Entacapone, 2,4-dinitrophenol, nimesulide, levosimendan and tolcapone that are all uncouplers, increased both the nucleus area and the amount of γH2Ax responder cells. The positive association indicates that the increased quantity of γH2Ax positive cells was not a consequence of cell death but due to some other mechanism.

Simultaneous increase in nucleus area and in γH2Ax marker would be expected also when the cell cycle is arrested during interphase after the DNA replication. It is possible that the γH2Ax responder analysis has not been exclusive enough to limit all the naturally caused DNA double strand breaks and the uncouplers would cause triggered γH2Ax response due to the interphase arrest caused by the ATP shortage. However, the cell counts of uncouplers did not indicate a cell cycle arrest. It is rational that the complex inhibitors induced cell death whereas uncouplers did not appear to do that, since complex inhibition in mitochondria prevents the ATP production completely while uncoupling merely reduces it.

The increase of tubulin and actin intensities indicates the condensation, i.e. polymerization, of the microtubules and microfilaments, respectively. Especially the polymerization of tubulin suggests that the cells are in mitosis. As was described in chapter 2.3, actin polymerization and tubulin depolymerization requires ATP and, thus, ATP depletion might result in tubulin stabilization or actin disruption (Heng & Koh, 2010; Spurck & Pickett-Heaps, 1987). Most of the compounds appeared to affect both tubulin and actin and there seemed to be positive association between cytoskeleton intensities and triggered γH2Ax response. However, the causal connection between cytoskeleton markers and γH2Ax response could not be verified, since it seemed that all the events started at the same concentration. The number of pH3 positive cells was not increased and hence the increase in tubulin intensity was probably not due to stabilization of tubulin in mitosis. The increasing number of γH2Ax positive cells can also be caused by the cell cycle arrest in S phase that could occur due to energy shortage. However, if the cells do not enter mitosis, it would be expected that the tubulin intensity would not increase as it did.

The connection between cytoskeleton and DNA damage has been previously studied. Since actin participates in DNA repair system, it should have a correlation with γH2Ax. This correlation has been confirmed by several studies that have shown that the inhibition of actin polymerization results in DNA damage and that DNA damage induces the actin polymerization (Andrin et al., 2012; Belin et al., 2015; Shin et al., 2011). Also, tubulin dynamics and DNA damage has been associated with each other but based on studies by Porter & Lee (2001) and Schofield & Bernard (2013) DNA damage seems to induce the tubulin polymerization rather than vice versa. The previous studies would suggest that the increase of tubulin and actin intensity

simultaneously with triggered γH2Ax response that was seen in this research would be a consequence of DNA damage rather than because of ATP depletion.

Compounds such as entacapone, phenformin and nimesulide showed either negative association or no association at all between γH2Ax marker and cytoskeleton intensities. This does not support the suggestion that the polymerization of actin and tubulin was due to DNA damage but rather that the γH2Ax response and changes in cytoskeleton dynamics would be independent events caused by the ATP depletion or cytotoxicity. However, these two suggestions are not exclusive since the mechanism behind the disruption in cytoskeleton dynamics and DNA damage may vary depending on the compound.

Since the tested compounds included only mitochondrial toxins, it is difficult to estimate if the changes in cytoskeleton dynamics were due to ATP depletion or cytotoxic effect. Previous studies have suggested that ATP depletion would increase actin aggregation but decrease actin polymerization (Atkinson et al., 2004; Bacallao et al., 1994; Ozawa et al., 2015). The intensity of the actin marker is probably not a suitable parameter to estimate whether actin is aggregated or polymerized since both aggregation and polymerization would increase the intensity compared to globular actin. The association between tubulin and ATP depletion has not been as unanimous. Bacallao et al. (1994) did not find any difference in the behaviour of tubulin after ATP depletion while Rand et al. (2014) suggested that ATP depletion would stabilize microtubules. Hence, it is possible that ATP depletion could result in increased tubulin intensity. However, further investigations are needed to estimate whether ATP depletion is responsible for the changes in cytoskeleton dynamics and for triggered γH2Ax response.

6.5 Analysis with ACC and FC

The purpose of analysing the cells with ACC was to gain additional information about the phenotype and cell cycle of the cells after each treatment. It was also examined whether ACC would be a suitable tool to analyse HCA data in future. The original purpose was to identify the cells in interphase and different phases of mitosis to examine if some compounds delay specific stage of the cell cycle and estimate

whether this might be due to insufficient energy supply. It was noticed that the HCA image analysis was not suitable for this since ACC could not distinguish the different phases of mitosis from each other even though the number of cells used for training of the model should have been adequate. By optimizing the image analysis conducted with HCA, it might be possible to accomplish better classification. Also, the number of classified cells was quite large and the classification of fewer cells at a time might give better results. Despite that the plates with pH3 marker was not used in ACC analysis, ACC was able to recognize mitotic cells since the highest percentages of those were seen after treatment with paclitaxel and griseofulvin, as expected. Most of the cells, despite the compound treatment, appeared to be normal-shaped interphase cells. This might suggest that compounds increased the γH2Ax response due to cell cycle arrest during interphase.

ACC was also able to recognize the differences between normal, rounded and stretched cells. Based on the cell images, MMS and CCCP caused the rounding and stretching of the cells and this was also seen in ACC data. The validity of the classification was 75.5%, which indicates that almost 25% of the cells were classified incorrectly. Hence, the ACC data should be interpreted with caution. However, the validity is quite high since the HCA image analysis was not developed or optimized specifically for ACC analysis. Thus, even though the image analysis requires optimization to reach better validity, it appears that ACC may be a useful tool for interpreting HCA data.

FC was used to collect parallel data to compare with HCA data. The purpose was also to investigate the similarity of the DNA damage responses seen in these two assays and to consider if HCA could be used for genotoxic screening. The FC assay for HepG2/C3A cells needs optimizing since the detachment of those cells from the wells and from each other varied greatly. This led to the irregular cell count and affected the fold of pH3 and γH2Ax and reliable data was not acquired of all of the compounds. Thus, it was not possible to conduct a comprehensive comparison between TK6 and HepG2/C3A FC data and between HepG2/C3A FC and HCA data.

However, it was observed from the available data that γH2Ax and pH3 responses were similar in both assays and cell lines. The changes in responses began on average at one concentration lower in TK6 cells than in HepG2/C3A cells. This was

probably due to faster proliferation time of TK6 cells. TK6 cells duplicate 1.8 times per day whereas HepG2/C3A cells duplicate once. Since the elevation of both γH2Ax and pH3 responses were observed similarly in both assays, it is possible that DNA damage assays could be conducted by HCA.

IV CONCLUSIONS

The aim of the study was to investigate if mitochondrial dysfunction caused by the mitochondrial toxins may lead to false positive results in DNA damage assays. The purpose was to examine if the ATP depletion caused by the insufficient energy production would interfere with the proper functioning of the cell and lead to DNA damage responses indirectly. Even though an indirect DNA damage response is an actual response, it is not considered as a determining factor of genotoxicity. The focus was on investigating if the ATP depletion caused the possible DNA damage via changes in cytoskeleton dynamics.

All the examined compounds, excluding metformin, triggered γH2Ax response at least at time point 24 h, which indicates that they would induce DNA damage. However, when investigating the possible mechanisms of the increased number of γH2Ax positive cells, it was observed that nucleus area often correlated negatively with the increase. This indicates that the triggered γH2Ax response was a consequence of cell death caused by the cytotoxicity. Many of the uncouplers increased the quantity of γH2Ax responder cells and nucleus area simultaneously. This may have been an indication of a cell cycle arrest after S phase or of some other mechanism than cell death that caused the DNA damage. Paclitaxel was the only compound that increased the number of pH3 positive cells. Tolcapone and levosimendan seemed to cause elevation in pH3 response but the increase was interpreted as an artefact caused by the cell count reduction.

Excluding entacapone and metformin, the compounds influenced tubulin and actin. The induction of tubulin and actin polymerization seemed to correlate with the increase of γH2Ax positive cells. The causality of these two, however, was not verified. In case of compounds such as nimesulide and phenformin, there did not seem to be an association between changed cytoskeleton dynamics and γH2Ax response.

Based on this research the mitochondrial toxins seemed to induce DNA damage but probably mostly due to induced cell death and cell cycle arrest in the S-phase. The toxins also affected the dynamics of cytoskeleton but the causality of changed

dynamics and DNA damage could not be verified. The lack of inducing effect on pH3 responders indicates that excluding paclitaxel, none of the examined compounds induced DNA damage via interference of mitosis.

In the future experiments, some issues should be considered. The DNA damage markers, pH3 and γH2Ax should be applied to the same plates to ensure that the responses are characteristic to a specific compound. The selection of examined compounds could also be more extensive and include cytotoxic compounds that do not affect the mitochondria. This would give more information of which responses are due to the cytotoxic effect in general and what is caused by the energy deprivation. The responses caused by the energy depletion would probably be stronger if the conducted research would be repeated with the cells cultivated in galactose medium instead of glucose, since glycolysis would not compensate the interference of oxidative phosphorylation. Addition of apoptosis marker would also give an unambiguous answer whether some responses are caused by the cell death. If the concentration series were more frequent, the order of the events might become more visible. This might enable the evaluation of possible causality between cytoskeleton and γH2Ax. However, to ensure that the top concentration is high enough and the lowest concentration low enough, the concentration range needs to be wide. The increase in the quantity of concentrations per series might require changing the assay from 96-well format to 384-well format. The optimization of the concentration series and the top concentration of each compound is important if the HCA assay developed in this study would be transferred into screening assay. In screening assay, the concentration series need to be fixed.

To conclude, it seems that based on this study the misleading positives in DNA damage assays can be caused by mitochondrial toxins and possibly due to energy depletion. However, whether this effect was mediated by the changed dynamics of tubulin or actin cannot be concluded and requires further investigation.

REFERENCES

Abraham, V. C., Taylor, D. L., & Haskins, J. R. (2004). High content screening applied to large-scale cell biology. *Trends Biotechnol, 22*(1), 15-22. doi:10.1016/j.tibtech.2003.10.012

Abraham, V. C., Towne, D. L., Waring, J. F., Warrior, U., & Burns, D. J. (2008). Application of a high-content multiparameter cytotoxicity assay to prioritize compounds based on toxicity potential in humans. *J Biomol Screen, 13*(6), 527-537. doi:10.1177/1087057108318428

Abrahams, J. P., Buchanan, S. K., Van Raaij, M. J., Fearnley, I. M., Leslie, A. G., & Walker, J. E. (1996). The structure of bovine F1-ATPase complexed with the peptide antibiotic efrapeptin. *Proc Natl Acad Sci U S A, 93*(18), 9420-9424.

Alberts, B., Johnson, A., Lewis, J., Morgan, D., Raff, M., Roberts, K., & Walter, P. (2015a). Cell Chemistry and Bioenergetics. In *Molecular Biology of the Cell* (6 ed., pp. 43-108): Garland Science, Taylor & Francis Group.

Alberts, B., Johnson, A., Lewis, J., Morgan, D., Raff, M., Roberts, K., & Walter, P. (2015b). The cell cycle. In *Molecular Biology of the Cell* (6 ed., pp. 963-1019): Garland Science, Taylor & Francis Group.

Alberts, B., Johnson, A., Lewis, J., Morgan, D., Raff, M., Roberts, K., & Walter, P. (2015c). The cytoskeleton. In *Molecular Biology of the Cell* (6 ed., pp. 889-960): Garland Science, Taylor & Francis Group.

Alberts, B., Johnson, A., Lewis, J., Morgan, D., Raff, M., Roberts, K., & Walter, P. (2015d). Energy conversion: mitochondria and chloroplasts. In *Molecular Biology of the Cell* (6 ed., pp. 753-812): Garland Science, Taylor & Francis Group.

Alvarez-Barrientos, A., Arroyo, J., Canton, R., Nombela, C., & Sanchez-Perez, M. (2000). Applications of flow cytometry to clinical microbiology. *Clin Microbiol Rev, 13*(2), 167-195.

Amacher, D. E. (2005). Drug-associated mitochondrial toxicity and its detection. *Curr Med Chem, 12*(16), 1829-1839.

Andrin, C., McDonald, D., Attwood, K. M., Rodrigue, A., Ghosh, S., Mirzayans, R., Masson, J. Y., Dellaire, G., & Hendzel, M. J. (2012). A requirement for polymerized actin in DNA double-strand break repair. *Nucleus, 3*(4), 384-395. doi:10.4161/nucl.21055

Atkinson, S. J., Hosford, M. A., & Molitoris, B. A. (2004). Mechanism of actin polymerization in cellular ATP depletion. *J Biol Chem, 279*(7), 5194-5199. doi:10.1074/jbc.M306973200

Bacallao, R., Garfinkel, A., Monke, S., Zampighi, G., & Mandel, L. J. (1994). ATP depletion: a novel method to study junctional properties in epithelial tissues. I. Rearrangement of the actin cytoskeleton. *J Cell Sci, 107 (Pt 12)*, 3301-3313.

Barnum, K. J., & O'Connell, M. J. (2014). Cell cycle regulation by checkpoints. *Methods Mol Biol, 1170*, 29-40. doi:10.1007/978-1-4939-0888-2_2

Bates, D., & Eastman, A. (2017). Microtubule destabilising agents: far more than just antimitotic anticancer drugs. *Br J Clin Pharmacol, 83*(2), 255-268. doi:10.1111/bcp.13126

Belin, B. J., Lee, T., & Mullins, R. D. (2015). DNA damage induces nuclear actin filament assembly by Formin -2 and Spire-(1/2) that promotes efficient DNA repair. [corrected]. *Elife, 4*, e07735. doi:10.7554/eLife.07735

Benigni, R., & Bossa, C. (2011). Alternative strategies for carcinogenicity assessment: an efficient and simplified approach based on in vitro mutagenicity and cell transformation assays. *Mutagenesis, 26*(3), 455-460. doi:10.1093/mutage/ger004

Berg, J. M., Tymoczko, J. L., & Stryer, L. (2002a). The citric acid cycle. *Biochemistry.* 5. Retrieved from https://www.ncbi.nlm.nih.gov/books/NBK21163/, 10.3.2018

Berg, J. M., Tymoczko, J. L., & Stryer, L. (2002b). The citric acid cycle oxidizes two-carbon units. *Biochemistry.* 5. Retrieved from https://www.ncbi.nlm.nih.gov/books/NBK22427/#A2398, 20.4.2018

Berg, J. M., Tymoczko, J. L., & Stryer, L. (2002c). Glycolysis in an energy-conversion pathway in many organisms. *Biochemistry.* 5. Retrieved from https://www.ncbi.nlm.nih.gov/books/NBK22593/, 4.3.2018

Blagosklonny, M. V., & Pardee, A. B. (2002). The restriction point of the cell cycle. *Cell Cycle, 1*(2), 103-110.

Bluemel, J. (2012). Toxicity testing in the 21st century: challenges and perspectives. *Journal of Drug Metabolism & Toxicology, 3*(5).

Brand, M. D. (2000). Uncoupling to survive? The role of mitochondrial inefficiency in ageing. *Exp Gerontol, 35*(6-7), 811-820.

Brinkman, K., ter Hofstede, H. J., Burger, D. M., Smeitink, J. A., & Koopmans, P. P. (1998). Adverse effects of reverse transcriptase inhibitors: mitochondrial toxicity as common pathway. *AIDS, 12*(14), 1735-1744.

Brooker, A. S., & Berkowitz, K. M. (2014). The roles of cohesins in mitosis, meiosis, and human health and disease. *Methods Mol Biol, 1170*, 229-266. doi:10.1007/978-1-4939-0888-2_11

Buchser, W., Collins, M., Garyantes, T., Guha, R., Haney, S., Lemmon, V., Li, Z., & Trask, O. J. (2004). Assay Development Guidelines for Image-Based High Content Screening, High Content Analysis and High Content Imaging. In G. S. Sittampalam, N. P. Coussens, K. Brimacombe, A. Grossman, M. Arkin, D. Auld, C. Austin, J. Baell, B. Bejcek, T. D. Y. Chung, J. L. Dahlin, V. Devanaryan, T. L. Foley, M. Glicksman, M. D. Hall, J. V. Hass, J. Inglese, P. W. Iversen, S. D. Kahl, S. C. Kales, M. Lal-Nag, Z. Li, J. McGee, O. McManus, T. Riss, O. J. Trask, Jr., J. R. Weidner, M. Xia, & X. Xu (Eds.), *Assay Guidance Manual*. Bethesda (MD).

Buttgereit, F., & Brand, M. D. (1995). A hierarchy of ATP-consuming processes in mammalian cells. *Biochem J, 312 (Pt 1)*, 163-167.

Cleveland, D. W., Mao, Y., & Sullivan, K. F. (2003). Centromeres and kinetochores: from epigenetics to mitotic checkpoint signaling. *Cell, 112*(4), 407-421.

Corvi, R., & Madia, F. (2017). In vitro genotoxicity testing-Can the performance be enhanced? *Food Chem Toxicol, 106*(Pt B), 600-608. doi:10.1016/j.fct.2016.08.024

Dallas, C. E., & Evans, D. L. (1990). Flow cytometry in toxicity analysis. *Nature, 345*, 557. doi:10.1038/345557a0

de Oliveira, M. R. (2016). Fluoxetine and the mitochondria: A review of the toxicological aspects. *Toxicol Lett, 258*, 185-191. doi:10.1016/j.toxlet.2016.07.001

Degli Esposti, M. (1998). Inhibitors of NADH-ubiquinone reductase: an overview. *Biochim Biophys Acta, 1364*(2), 222-235.

Devenish, R. J., Prescott, M., Boyle, G. M., & Nagley, P. (2000). The oligomycin axis of mitochondrial ATP synthase: OSCP and the proton channel. *J Bioenerg Biomembr, 32*(5), 507-515.

Díaz, M., Herrero, M., García, L. A., & Quirós, C. (2010). Application of flow cytometry to industrial microbial bioprocesses. *Biochemical Engineering Journal, 48*(3), 385-407. doi:https://doi.org/10.1016/j.bej.2009.07.013

Donaldson, J. G. (2015). Immunofluorescence Staining. *Curr Protoc Cell Biol, 69*, 4 3 1-7. doi:10.1002/0471143030.cb0403s69

Duan, S., Hajek, P., Lin, C., Shin, S. K., Attardi, G., & Chomyn, A. (2003). Mitochondrial outer membrane permeability change and hypersensitivity to digitonin early in staurosporine-induced apoptosis. *J Biol Chem, 278*(2), 1346-1353. doi:10.1074/jbc.M209269200

Dykens, J. A., Jamieson, J., Marroquin, L., Nadanaciva, S., Billis, P. A., & Will, Y. (2008a). Biguanide-induced mitochondrial dysfunction yields increased lactate production and cytotoxicity of aerobically-poised HepG2 cells and human hepatocytes in vitro. *Toxicol Appl Pharmacol, 233*(2), 203-210. doi:10.1016/j.taap.2008.08.013

Dykens, J. A., Jamieson, J. D., Marroquin, L. D., Nadanaciva, S., Xu, J. J., Dunn, M. C., Smith, A. R., & Will, Y. (2008b). In vitro assessment of mitochondrial dysfunction and cytotoxicity of nefazodone, trazodone, and buspirone. *Toxicol Sci, 103*(2), 335-345. doi:10.1093/toxsci/kfn056

Dykens, J. A., & Will, Y. (2007). The significance of mitochondrial toxicity testing in drug development. *Drug Discov Today, 12*(17-18), 777-785. doi:10.1016/j.drudis.2007.07.013

Edwards, B. S., Young, S. M., Saunders, M. J., Bologa, C., Oprea, T. I., Ye, R. D., Prossnitz, E. R., Graves, S. W., & Sklar, L. A. (2007). High-throughput flow cytometry for drug discovery. *Expert Opin Drug Discov, 2*(5), 685-696. doi:10.1517/17460441.2.5.685

Enomoto, T., Tanuma, S., & Yamada, M. A. (1981). ATP requirement for the processes of DNA replication in isolated HeLa cell nuclei. *J Biochem, 89*(3), 801-807.

Esser, L., Quinn, B., Li, Y. F., Zhang, M., Elberry, M., Yu, L., Yu, C. A., & Xia, D. (2004). Crystallographic studies of quinol oxidation site inhibitors: a modified classification of inhibitors for the cytochrome bc(1) complex. *J Mol Biol, 341*(1), 281-302. doi:10.1016/j.jmb.2004.05.065

Estornell, E. (2000). Mitochondrial complex I: new insights from inhibitor assays. *Protoplasma, 213*(1), 11-17. doi:10.1007/bf01280500

Eto, K., Tsubamoto, Y., Terauchi, Y., Sugiyama, T., Kishimoto, T., Takahashi, N., Yamauchi, N., Kubota, N., Murayama, S., Aizawa, T., Akanuma, Y., Aizawa, S., Kasai, H., Yazaki, Y., & Kadowaki, T. (1999). Role of NADH shuttle system in glucose-induced activation of mitochondrial metabolism and insulin secretion. *Science, 283*(5404), 981-985.

Ewesuedo, R. B., & Ratain, M. J. (1997). Topoisomerase I Inhibitors. *Oncologist, 2*(6), 359-364.

Faccenda, D., & Campanella, M. (2012). Molecular Regulation of the Mitochondrial F(1)F(o)-ATPsynthase: Physiological and Pathological Significance of the Inhibitory Factor 1 (IF(1)). *Int J Cell Biol, 2012*, 367934. doi:10.1155/2012/367934

Fanale, D., Bronte, G., Passiglia, F., Calo, V., Castiglia, M., Di Piazza, F., Barraco, N., Cangemi, A., Catarella, M. T., Insalaco, L., Listi, A., Maragliano, R., Massihnia, D., Perez, A., Toia, F., Cicero, G., & Bazan, V. (2015). Stabilizing versus destabilizing the microtubules: a double-edge sword for an effective cancer treatment option? *Anal Cell Pathol (Amst), 2015*, 690916. doi:10.1155/2015/690916

Field, J. J., Diaz, J. F., & Miller, J. H. (2013). The binding sites of microtubule-stabilizing agents. *Chem Biol, 20*(3), 301-315. doi:10.1016/j.chembiol.2013.01.014

Finger, F. P., & White, J. G. (2002). Fusion and fission: membrane trafficking in animal cytokinesis. *Cell, 108*(6), 727-730.

Fowler, P., Smith, K., Young, J., Jeffrey, L., Kirkland, D., Pfuhler, S., & Carmichael, P. (2012a). Reduction of misleading ("false") positive results in mammalian cell genotoxicity assays. I. Choice of cell type. *Mutat Res, 742*(1-2), 11-25. doi:10.1016/j.mrgentox.2011.10.014

Fowler, P., Smith, R., Smith, K., Young, J., Jeffrey, L., Kirkland, D., Pfuhler, S., & Carmichael, P. (2012b). Reduction of misleading ("false") positive results in mammalian cell genotoxicity assays. II. Importance of accurate toxicity measurement. *Mutat Res, 747*(1), 104-117. doi:10.1016/j.mrgentox.2012.04.013

Freudenberg, H., & Mager, J. (1971). Studies on the mechanism of the inhibition of protein synthesis induced by intracellular ATP depletion. *Biochim Biophys Acta, 232*(3), 537-555.

Frey, T. G., & Mannella, C. A. (2000). The internal structure of mitochondria. *Trends Biochem Sci, 25*(7), 319-324.

Fritschy, J. M., & Härtig, W. (2001). Immunofluorescence. *Encyclopedia of Life Sciences.* Retrieved from https://onlinelibrary.wiley.com/doi/pdf/10.1038/npg.els.0001174, 4.3.2018

Fromenty, B., & Pessayre, D. (1997). Impaired mitochondrial function in microvesicular steatosis. Effects of drugs, ethanol, hormones and cytokines. *J Hepatol, 26 Suppl 2*, 43-53.

Ganote, C. E., & Armstrong, S. C. (2003). Effects of CCCP-induced mitochondrial uncoupling and cyclosporin A on cell volume, cell injury and preconditioning protection of isolated rabbit cardiomyocytes. *J Mol Cell Cardiol, 35*(7), 749-759.

Glotzer, M. (2005). The molecular requirements for cytokinesis. *Science, 307*(5716), 1735-1739. doi:10.1126/science.1096896

Gorbsky, G. J. (2015). The spindle checkpoint and chromosome segregation in meiosis. *FEBS J, 282*(13), 2471-2487. doi:10.1111/febs.13166

Grady, W. M., & Ulrich, C. M. (2007). DNA alkylation and DNA methylation: cooperating mechanisms driving the formation of colorectal adenomas and adenocarcinomas? *Gut, 56*(3), 318-320. doi:10.1136/gut.2006.106849

Greb, C. (2012). Fluorescent dyes. Retrieved from https://www.leica-microsystems.com/science-lab/fluorescent-dyes/, 2.4.2018

Grossman, L. I., Wildman, D. E., Schmidt, T. R., & Goodman, M. (2004). Accelerated evolution of the electron transport chain in anthropoid primates. *Trends Genet, 20*(11), 578-585. doi:10.1016/j.tig.2004.09.002

Grundlingh, J., Dargan, P. I., El-Zanfaly, M., & Wood, D. M. (2011). 2,4-dinitrophenol (DNP): a weight loss agent with significant acute toxicity and risk of death. *J Med Toxicol, 7*(3), 205-212. doi:10.1007/s13181-011-0162-6

Grunig, D., Felser, A., Bouitbir, J., & Krahenbuhl, S. (2017). The catechol-O-methyltransferase inhibitors tolcapone and entacapone uncouple and inhibit the mitochondrial respiratory chain in HepaRG cells. *Toxicol In Vitro, 42*, 337-347. doi:10.1016/j.tiv.2017.05.013

Guenebaut, V., Schlitt, A., Weiss, H., Leonard, K., & Friedrich, T. (1998). Consistent structure between bacterial and mitochondrial NADH:ubiquinone oxidoreductase (complex I). *J Mol Biol, 276*(1), 105-112. doi:10.1006/jmbi.1997.1518

Guengerich, F. P. (2011). Mechanisms of drug toxicity and relevance to pharmaceutical development. *Drug Metab Pharmacokinet, 26*(1), 3-14.

Hagerhall, C. (1997). Succinate: quinone oxidoreductases. Variations on a conserved theme. *Biochim Biophys Acta, 1320*(2), 107-141.

Hagstrom, K. A., & Meyer, B. J. (2003). Condensin and cohesin: more than chromosome compactor and glue. *Nat Rev Genet, 4*(7), 520-534. doi:10.1038/nrg1110

Halestrap, A. P. (2009). What is the mitochondrial permeability transition pore? *J Mol Cell Cardiol, 46*(6), 821-831. doi:10.1016/j.yjmcc.2009.02.021

Hande, K. R. (2008). Topoisomerase II inhibitors. *Update on Cancer Therapeutics, 3*(1), 13-26. doi:https://doi.org/10.1016/j.uct.2008.02.001

Harris, M. H., & Thompson, C. B. (2000). The role of the Bcl-2 family in the regulation of outer mitochondrial membrane permeability. *Cell Death Differ, 7*(12), 1182-1191. doi:10.1038/sj.cdd.4400781

Haug, E., Sand, O., Sjaastad, Ø. V., & Toverud, K. C. (2009). ATP ja solujen energia-aineenvaihdunta. In *Ihmisen Fysiologia* (4 ed., pp. 46-53): WSOY.

Heinz, S., Freyberger, A., Lawrenz, B., Schladt, L., Schmuck, G., & Ellinger-Ziegelbauer, H. (2017). Mechanistic Investigations of the Mitochondrial Complex I Inhibitor Rotenone in the Context of Pharmacological and Safety Evaluation. *Sci Rep, 7*, 45465. doi:10.1038/srep45465

Hendzel, M. J., Wei, Y., Mancini, M. A., Van Hooser, A., Ranalli, T., Brinkley, B. R., Bazett-Jones, D. P., & Allis, C. D. (1997). Mitosis-specific phosphorylation of histone H3 initiates primarily within pericentromeric heterochromatin during G2 and spreads in an ordered fashion coincident with mitotic chromosome condensation. *Chromosoma, 106*(6), 348-360.

Heng, Y. W., & Koh, C. G. (2010). Actin cytoskeleton dynamics and the cell division cycle. *Int J Biochem Cell Biol, 42*(10), 1622-1633. doi:10.1016/j.biocel.2010.04.007

Hirano, T. (2012). Condensins: universal organizers of chromosomes with diverse functions. *Genes Dev, 26*(15), 1659-1678. doi:10.1101/gad.194746.112

Hirst, J. (2009). Towards the molecular mechanism of respiratory complex I. *Biochem J, 425*(2), 327-339. doi:10.1042/BJ20091382

Hoff, F. (2015). How to prepare your specimen for immunofluorescence microscopy. Retrieved from http://www.mcb5068.wustl.edu/MCB/DiscussionSection/Technique%20References/Immunofluorescence%20Microscopy.pdf, 19.9.2017

Honda, H. M., & Ping, P. (2006). Mitochondrial permeability transition in cardiac cell injury and death. *Cardiovasc Drugs Ther, 20*(6), 425-432. doi:10.1007/s10557-006-0642-0

Houtgraaf, J. H., Versmissen, J., & van der Giessen, W. J. (2006). A concise review of DNA damage checkpoints and repair in mammalian cells. *Cardiovasc Revasc Med, 7*(3), 165-172. doi:10.1016/j.carrev.2006.02.002

Huttemann, M., Lee, I., Samavati, L., Yu, H., & Doan, J. W. (2007). Regulation of mitochondrial oxidative phosphorylation through cell signaling. *Biochim Biophys Acta, 1773*(12), 1701-1720.

ICHS2(R1). (2011). Guidance on genotoxicity testing and data interpretation for pharmaceuticals intended for human use. Step 4. Retrieved from http://www.ich.org/fileadmin/Public_Web_Site/ICH_Products/Guidelines/Safety/S2_R1/Step4/S2R1_Step4.pdf, 4.4.2018

Jonckheere, A. I., Smeitink, J. A., & Rodenburg, R. J. (2012). Mitochondrial ATP synthase: architecture, function and pathology. *J Inherit Metab Dis, 35*(2), 211-225. doi:10.1007/s10545-011-9382-9

Kadenbach, B. (2003). Intrinsic and extrinsic uncoupling of oxidative phosphorylation. *Biochimica et Biophysica Acta (BBA) - Bioenergetics, 1604*(2), 77-94. doi:https://doi.org/10.1016/S0005-2728(03)00027-6

Kaufmann, W. K. (2007). Initiating the uninitiated: replication of damaged DNA and carcinogenesis. *Cell Cycle, 6*(12), 1460-1467.

Khoury, L., Zalko, D., & Audebert, M. (2016). Complementarity of phosphorylated histones H2AX and H3 quantification in different cell lines for genotoxicity screening. *Arch Toxicol, 90*(8), 1983-1995. doi:10.1007/s00204-015-1599-1

Kirkland, D., Pfuhler, S., Tweats, D., Aardema, M., Corvi, R., Darroudi, F., Elhajouji, A., Glatt, H., Hastwell, P., Hayashi, M., Kasper, P., Kirchner, S., Lynch, A., Marzin, D., Maurici, D., Meunier, J. R., Muller, L., Nohynek, G., Parry, J., Parry, E., Thybaud, V., Tice, R., van Benthem, J., Vanparys, P., & White, P. (2007). How to reduce false positive results when undertaking in vitro genotoxicity testing and thus avoid unnecessary follow-up animal tests: Report of an ECVAM Workshop. *Mutat Res, 628*(1), 31-55. doi:10.1016/j.mrgentox.2006.11.008

Kondo, N., Takahashi, A., Ono, K., & Ohnishi, T. (2010). DNA damage induced by alkylating agents and repair pathways. *J Nucleic Acids, 2010*, 543531. doi:10.4061/2010/543531

Krahenbuhl, S. (2001). Mitochondria: important target for drug toxicity? *J Hepatol, 34*(2), 334-336.

Krauss, S. (2001). Mitochondria: structure and role in respiration. *Encyclopedia of Life Sciences.* Retrieved from https://web.archive.org/web/20121021071651/http://www.med.ufro.cl/clases_apuntes/cs_preclinicas/mg-fisica-medica/sub-modulo-1/Mitochondria.pdf, 22.2.2018

Krutzik, P. O., & Nolan, G. P. (2006). Fluorescent cell barcoding in flow cytometry allows high-throughput drug screening and signaling profiling. *Nat Methods, 3*(5), 361-368. doi:10.1038/nmeth872

Kueh, H. Y., & Mitchison, T. J. (2009). Structural plasticity in actin and tubulin polymer dynamics. *Science, 325*(5943), 960-963. doi:10.1126/science.1168823

Kuo, L. J., & Yang, L. X. (2008). Gamma-H2AX - a novel biomarker for DNA double-strand breaks. *In Vivo, 22*(3), 305-309.

Labbe, G., Pessayre, D., & Fromenty, B. (2008). Drug-induced liver injury through mitochondrial dysfunction: mechanisms and detection during preclinical safety studies. *Fundam Clin Pharmacol, 22*(4), 335-353. doi:10.1111/j.1472-8206.2008.00608.x

Lans, H., Marteijn, J. A., & Vermeulen, W. (2012). ATP-dependent chromatin remodeling in the DNA-damage response. *Epigenetics Chromatin, 5*, 4. doi:10.1186/1756-8935-5-4

Lara-Gonzalez, P., Westhorpe, F. G., & Taylor, S. S. (2012). The spindle assembly checkpoint. *Curr Biol, 22*(22), R966-980. doi:10.1016/j.cub.2012.10.006

Lee, S., Kim, S., Sun, X., Lee, J. H., & Cho, H. (2007). Cell cycle-dependent mitochondrial biogenesis and dynamics in mammalian cells. *Biochem Biophys Res Commun, 357*(1), 111-117. doi:10.1016/j.bbrc.2007.03.091

Liu, B., Yip, R., & Zhou, Z. (2012). Chromatin remodeling, DNA damage repair and aging. *Curr Genomics, 13*(7), 533-547. doi:10.2174/138920212803251373

Lodish, H., Berk, A., Zipursky, L., Matsudaira, P., Baltimore, D., & Darnell, J. (2000). Electron transport and oxidative phosphorylation. *Molecular Cell Biology*. 4. Retrieved from https://www.ncbi.nlm.nih.gov/books/NBK21528/, 10.3.2018

Longo, D. M., Yang, Y., Watkins, P. B., Howell, B. A., & Siler, S. Q. (2016). Elucidating Differences in the Hepatotoxic Potential of Tolcapone and Entacapone With DILIsym((R)), a Mechanistic Model of Drug-Induced Liver Injury. *CPT Pharmacometrics Syst Pharmacol, 5*(1), 31-39. doi:10.1002/psp4.12053

Lukas, J., Lukas, C., & Bartek, J. (2004). Mammalian cell cycle checkpoints: signalling pathways and their organization in space and time. *DNA Repair (Amst), 3*(8-9), 997-1007. doi:10.1016/j.dnarep.2004.03.006

Lundin, C., North, M., Erixon, K., Walters, K., Jenssen, D., Goldman, A. S., & Helleday, T. (2005). Methyl methanesulfonate (MMS) produces heat-labile DNA damage but no detectable in vivo DNA double-strand breaks. *Nucleic Acids Res, 33*(12), 3799-3811. doi:10.1093/nar/gki681

Ma, X., Jin, M., Cai, Y., Xia, H., Long, K., Liu, J., Yu, Q., & Yuan, J. (2011). Mitochondrial electron transport chain complex III is required for antimycin A to inhibit autophagy. *Chem Biol, 18*(11), 1474-1481. doi:10.1016/j.chembiol.2011.08.009

MacAskill, A. F., & Kittler, J. T. (2010). Control of mitochondrial transport and localization in neurons. *Trends Cell Biol, 20*(2), 102-112. doi:10.1016/j.tcb.2009.11.002

Masubuchi, Y., Kano, S., & Horie, T. (2006). Mitochondrial permeability transition as a potential determinant of hepatotoxicity of antidiabetic thiazolidinediones. *Toxicology, 222*(3), 233-239. doi:10.1016/j.tox.2006.02.017

McFarland, D., & Harkins, K. R. (2010). Flow cytometry in preclinical toxicology/safety assessment. In V. Litwin & P. Marder (Eds.), *Flow Cytometry in Drug Discovery and Development* (pp. 123-150): John Wiley & Sons, Inc. .

McManus, K. J., & Hendzel, M. J. (2005). ATM-dependent DNA damage-independent mitotic phosphorylation of H2AX in normally growing mammalian cells. *Mol Biol Cell, 16*(10), 5013-5025. doi:10.1091/mbc.E05-01-0065

Meyer, J. N., Hartman, J. H., & Mello, D. F. (2018). Mitochondrial Toxicity. *Toxicol Sci, 162*(1), 15-23. doi:10.1093/toxsci/kfy008

Mikhailov, A., Shinohara, M., & Rieder, C. L. (2004). Topoisomerase II and histone deacetylase inhibitors delay the G2/M transition by triggering the p38 MAPK checkpoint pathway. *J Cell Biol, 166*(4), 517-526. doi:10.1083/jcb.200405167

Mingatto, F. E., Rodrigues, T., Pigoso, A. A., Uyemura, S. A., Curti, C., & Santos, A. C. (2002). The critical role of mitochondrial energetic impairment in the toxicity of nimesulide to hepatocytes. *J Pharmacol Exp Ther, 303*(2), 601-607. doi:10.1124/jpet.102.038620

Miniowitz-Shemtov, S., Eytan, E., Ganoth, D., Sitry-Shevah, D., Dumin, E., & Hershko, A. (2012). Role of phosphorylation of Cdc20 in p31(comet)-stimulated disassembly of the mitotic checkpoint complex. *Proc Natl Acad Sci U S A, 109*(21), 8056-8060. doi:10.1073/pnas.1204081109

Miniowitz-Shemtov, S., Teichner, A., Sitry-Shevah, D., & Hershko, A. (2010). ATP is required for the release of the anaphase-promoting complex/cyclosome from inhibition by the mitotic checkpoint. *Proc Natl Acad Sci U S A, 107*(12), 5351-5356. doi:10.1073/pnas.1001875107

Miyadera, H., Shiomi, K., Ui, H., Yamaguchi, Y., Masuma, R., Tomoda, H., Miyoshi, H., Osanai, A., Kita, K., & Omura, S. (2003). Atpenins, potent and specific inhibitors of mitochondrial complex II (succinate-ubiquinone oxidoreductase). *Proc Natl Acad Sci U S A, 100*(2), 473-477. doi:10.1073/pnas.0237315100

Modica-Napolitano, J. S., Kulawiec, M., & Singh, K. K. (2007). Mitochondria and human cancer. *Curr Mol Med, 7*(1), 121-131.

Molinari, M. (2000). Cell cycle checkpoints and their inactivation in human cancer. *Cell Prolif, 33*(5), 261-274.

Murai, M., & Miyoshi, H. (2016). Current topics on inhibitors of respiratory complex I. *Biochim Biophys Acta, 1857*(7), 884-891. doi:10.1016/j.bbabio.2015.11.009

Nadanaciva, S., Dykens, J. A., Bernal, A., Capaldi, R. A., & Will, Y. (2007). Mitochondrial impairment by PPAR agonists and statins identified via immunocaptured OXPHOS complex activities and respiration. *Toxicol Appl Pharmacol, 223*(3), 277-287. doi:10.1016/j.taap.2007.06.003

Nakaseko, Y., & Yanagida, M. (2001). Cell biology. Cytoskeleton in the cell cycle. *Nature, 412*(6844), 291-292. doi:10.1038/35085684

Neustadt, J., & Pieczenik, S. R. (2008). Medication-induced mitochondrial damage and disease. *Mol Nutr Food Res, 52*(7), 780-788. doi:10.1002/mnfr.200700075

Nicolette, J. (2012). Genetic toxicology testing. In A. S. Faqi (Ed.), *A Comprehensive Guide to Toxicology in Preclinical Drug Development* (pp. 141-166): Elsevier Science & Technology.

O'Brien, P. J., Irwin, W., Diaz, D., Howard-Cofield, E., Krejsa, C. M., Slaughter, M. R., Gao, B., Kaludercic, N., Angeline, A., Bernardi, P., Brain, P., & Hougham, C. (2006). High concordance of drug-induced human hepatotoxicity with in vitro cytotoxicity measured in a novel cell-based model using high content screening. *Arch Toxicol, 80*(9), 580-604. doi:10.1007/s00204-006-0091-3

O'Connor, C. (2008). Cell Division: Stages of Mitosis. *Nature Education*. Retrieved from https://web.archive.org/web/20151114201118/http://www.nature.com/scitable/topicpage/mitosis-and-cell-division-205#, 4.3.2018

OECD. (2015). Guidance document on revisions to OECD genetic toxicology test guidelines. Retrieved from https://www.oecd.org/chemicalsafety/testing/Genetic%20Toxicology%20Guidance%20Document%20Aug%2031%202015.pdf, 5.4.2018

Oki, T., Nishimura, K., Kitaura, J., Togami, K., Maehara, A., Izawa, K., Sakaue-Sawano, A., Niida, A., Miyano, S., Aburatani, H., Kiyonari, H., Miyawaki, A., & Kitamura, T. (2014). A novel cell-cycle-indicator, mVenus-p27K-, identifies quiescent cells and visualizes G0-G1 transition. *Sci Rep, 4*, 4012. doi:10.1038/srep04012

Osellame, L. D., Blacker, T. S., & Duchen, M. R. (2012). Cellular and molecular mechanisms of mitochondrial function. *Best Pract Res Clin Endocrinol Metab, 26*(6), 711-723. doi:10.1016/j.beem.2012.05.003

Ozawa, S., Ueda, S., Imamura, H., Mori, K., Asanuma, K., Yanagita, M., & Nakagawa, T. (2015). Glycolysis, but not Mitochondria, responsible for intracellular ATP distribution in cortical area of podocytes. *Sci Rep, 5*, 18575. doi:10.1038/srep18575

Parasuraman, S. (2011). Toxicological screening. *J Pharmacol Pharmacother, 2*(2), 74-79. doi:10.4103/0976-500X.81895

Parry, J. M., Parry, E., Phrakonkham, P., & Corvi, R. (2010). Analysis of published data for top concentration considerations in mammalian cell genotoxicity testing. *Mutagenesis, 25*(6), 531-538. doi:10.1093/mutage/geq046

Pedreira, C. E., Costa, E. S., Lecrevisse, Q., van Dongen, J. J., Orfao, A., & EuroFlow, C. (2013). Overview of clinical flow cytometry data analysis: recent advances and future challenges. *Trends Biotechnol, 31*(7), 415-425. doi:10.1016/j.tibtech.2013.04.008

Peyressatre, M., Prevel, C., Pellerano, M., & Morris, M. C. (2015). Targeting cyclin-dependent kinases in human cancers: from small molecules to Peptide inhibitors. *Cancers (Basel), 7*(1), 179-237. doi:10.3390/cancers7010179

Phillips, D. H., & Arlt, V. M. (2009). Genotoxicity: damage to DNA and its consequences. *EXS, 99*, 87-110.

Piccinini, F., Balassa, T., Szkalisity, A., Molnar, C., Paavolainen, L., Kujala, K., Buzas, K., Sarazova, M., Pietiainen, V., Kutay, U., Smith, K., & Horvath, P. (2017). Advanced Cell Classifier: User-Friendly Machine-Learning-Based Software for Discovering Phenotypes in High-Content Imaging Data. *Cell Systems, 4*(6), 651-655.e655. doi:https://doi.org/10.1016/j.cels.2017.05.012

Podhorecka, M., Skladanowski, A., & Bozko, P. (2010). H2AX Phosphorylation: Its Role in DNA Damage Response and Cancer Therapy. *J Nucleic Acids, 2010*. doi:10.4061/2010/920161

Polymenis, M., & Aramayo, R. (2015). Translate to divide: control of the cell cycle by protein synthesis. *Microb Cell, 2*(4), 94-104. doi:10.15698/mic2015.04.198

Pontes, M. H., Sevostyanova, A., & Groisman, E. A. (2015). When Too Much ATP Is Bad for Protein Synthesis. *J Mol Biol, 427*(16), 2586-2594. doi:10.1016/j.jmb.2015.06.021

Poot, M., Epe, B., & Hoehn, H. (1992). Cell cycle effects of the DNA topoisomerase inhibitors camptothecin and m-AMSA in lymphoblastoid cell lines from patients with Fanconi anemia. *Mutat Res, 270*(2), 185-189.

Porter, L. A., & Lee, J. M. (2001). alpha-, beta-, and gamma-Tubulin polymerization in response to DNA damage. *Exp Cell Res, 270*(2), 151-158. doi:10.1006/excr.2001.5322

Rand, S., Lawrence, K., & Danowski, B. (2014). A possible role for adenosine monophosphate-activated protein kinase in regulating tubulin acetylation (739.10). *The FASEB Journal, 28*(1_supplement), 739.710. doi:10.1096/fasebj.28.1_supplement.739.10

Reddy, S. K., Rape, M., Margansky, W. A., & Kirschner, M. W. (2007). Ubiquitination by the anaphase-promoting complex drives spindle checkpoint inactivation. *Nature, 446*(7138), 921-925. doi:10.1038/nature05734

Salazar-Roa, M., & Malumbres, M. (2017). Fueling the Cell Division Cycle. *Trends Cell Biol, 27*(1), 69-81. doi:10.1016/j.tcb.2016.08.009

Saltsman, K. (2005). Cellular reproduction: multiplication by division. In *Inside the Cell* (pp. 46-59): U.S. Department of Health and Human Services.

Saraste, M. (1999). Oxidative phosphorylation at the fin de siecle. *Science, 283*(5407), 1488-1493.

Sarti, P., Arese, M., Bacchi, A., Barone, M. C., Forte, E., Mastronicola, D., Brunori, M., & Giuffre, A. (2003). Nitric oxide and mitochondrial complex IV. *IUBMB Life, 55*(10-11), 605-611. doi:10.1080/15216540310001628726

Schofield, A., & Bernard, O. (2013). Tubulin polymerization promoting protein 1 (TPPP1): A DNA-damage induced microtubule regulatory gene. *Commun Integr Biol, 6*(6), e26316. doi:10.4161/cib.26316

Scholey, J. M., Civelekoglu-Scholey, G., & Brust-Mascher, I. (2016). Anaphase B. *Biology (Basel), 5*(4). doi:10.3390/biology5040051

Sept, D. (2007). Microtubule polymerization: one step at a time. *Curr Biol, 17*(17), R764-766. doi:10.1016/j.cub.2007.07.002

Serviddio, G., Bellanti, F., Giudetti, A. M., Gnoni, G. V., Capitanio, N., Tamborra, R., Romano, A. D., Quinto, M., Blonda, M., Vendemiale, G., & Altomare, E. (2011). Mitochondrial oxidative stress and respiratory chain dysfunction account for liver toxicity during amiodarone but not dronedarone administration. *Free Radic Biol Med, 51*(12), 2234-2242. doi:10.1016/j.freeradbiomed.2011.09.004

Shapiro, G. I., & Harper, J. W. (1999). Anticancer drug targets: cell cycle and checkpoint control. *J Clin Invest, 104*(12), 1645-1653. doi:10.1172/JCI9054

Shin, I. J., Ahn, Y. T., Kim, Y., Kim, J. M., & An, W. G. (2011). Actin disruption agents induce phosphorylation of histone H2AX in human breast adenocarcinoma MCF-7 cells. *Oncol Rep, 25*(5), 1313-1319. doi:10.3892/or.2011.1214

Shukla, S. J., Huang, R., Austin, C. P., & Xia, M. (2010). The future of toxicity testing: a focus on in vitro methods using a quantitative high-throughput screening platform. *Drug Discov Today, 15*(23-24), 997-1007. doi:10.1016/j.drudis.2010.07.007

Sled, V. D., Rudnitzky, N. I., Hatefi, Y., & Ohnishi, T. (1994). Thermodynamic analysis of flavin in mitochondrial NADH:ubiquinone oxidoreductase (complex I). *Biochemistry, 33*(33), 10069-10075.

Spurck, T. P., & Pickett-Heaps, J. D. (1987). On the mechanism of anaphase A: evidence that ATP is needed for microtubule disassembly and not generation of polewards force. *J Cell Biol, 105*(4), 1691-1705.

Stark, G. R., & Taylor, W. R. (2006). Control of the G2/M transition. *Mol Biotechnol, 32*(3), 227-248. doi:10.1385/MB:32:3:227

Symersky, J., Osowski, D., Walters, D. E., & Mueller, D. M. (2012). Oligomycin frames a common drug-binding site in the ATP synthase. *Proc Natl Acad Sci U S A, 109*(35), 13961-13965. doi:10.1073/pnas.1207912109

Tang, X. J., Lancelle, S. A., & Hepler, P. K. (1989). Fluorescence microscopic localization of actin in pollen tubes: comparison of actin antibody and phalloidin staining. *Cell Motil Cytoskeleton, 12*(4), 216-224. doi:10.1002/cm.970120404

Tomitsuka, E., Goto, Y., Taniwaki, M., & Kita, K. (2003). Direct evidence for expression of type II flavoprotein subunit in human complex II (succinate-ubiquinone reductase). *Biochem Biophys Res Commun, 311*(3), 774-779.

Trask, O. J., Jr., & Johnston, P. A. (2015). Standardization of high content imaging and informatics. *Assay Drug Dev Technol, 13*(7), 341-346. doi:10.1089/adt.2015.29022.ojt

Trumpower, B. L. (1990). The protonmotive Q cycle. Energy transduction by coupling of proton translocation to electron transfer by the cytochrome bc1 complex. *J Biol Chem, 265*(20), 11409-11412.

Verbist, B. M., Verheyen, G. R., Vervoort, L., Crabbe, M., Beerens, D., Bosmans, C., Jaensch, S., Osselaer, S., Talloen, W., Van den Wyngaert, I., Van Hecke, G., Wuyts, D., Consortium, Q., Van Goethem, F., & Gohlmann, H. W. (2015). Integrating High-Dimensional Transcriptomics and Image Analysis Tools into Early Safety Screening: Proof of Concept for a New Early Drug Development Strategy. *Chem Res Toxicol, 28*(10), 1914-1925. doi:10.1021/acs.chemrestox.5b00103

Vermeulen, K., Van Bockstaele, D. R., & Berneman, Z. N. (2003). The cell cycle: a review of regulation, deregulation and therapeutic targets in cancer. *Cell Prolif, 36*(3), 131-149.

Wallace, K. B., & Starkov, A. A. (2000). Mitochondrial targets of drug toxicity. *Annu Rev Pharmacol Toxicol, 40*, 353-388. doi:10.1146/annurev.pharmtox.40.1.353

Wang, Y., Yu, Y., Li, G. B., Li, S. A., Wu, C., Gigant, B., Qin, W., Chen, H., Wu, Y., Chen, Q., & Yang, J. (2017). Mechanism of microtubule stabilization by taccalonolide AJ. *Nat Commun, 8*, 15787. doi:10.1038/ncomms15787

Weaver, B. A., & Cleveland, D. W. (2005). Decoding the links between mitosis, cancer, and chemotherapy: The mitotic checkpoint, adaptation, and cell death. *Cancer Cell, 8*(1), 7-12. doi:10.1016/j.ccr.2005.06.011

Webster, M., Witkin, K. L., & Cohen-Fix, O. (2009). Sizing up the nucleus: nuclear shape, size and nuclear-envelope assembly. *J Cell Sci, 122*(Pt 10), 1477-1486. doi:10.1242/jcs.037333

Whitebread, S., Hamon, J., Bojanic, D., & Urban, L. (2005). Keynote review: in vitro safety pharmacology profiling: an essential tool for successful drug development. *Drug Discov Today, 10*(21), 1421-1433. doi:10.1016/S1359-6446(05)03632-9

Wieser, W., & Krumschnabel, G. (2001). Hierarchies of ATP-consuming processes: direct compared with indirect measurements, and comparative aspects. *Biochem J, 355*(Pt 2), 389-395.

Yang, H., Ganguly, A., & Cabral, F. (2010). Inhibition of cell migration and cell division correlates with distinct effects of microtubule inhibiting drugs. *J Biol Chem, 285*(42), 32242-32250. doi:10.1074/jbc.M110.160820

Yang, L., Besschetnova, T. Y., Brooks, C. R., Shah, J. V., & Bonventre, J. V. (2010). Epithelial cell cycle arrest in G2/M mediates kidney fibrosis after injury. *Nat Med, 16*(5), 535-543, 531p following 143. doi:10.1038/nm.2144

Yao, G. (2014). Modelling mammalian cellular quiescence. *Interface Focus, 4*(3), 20130074. doi:10.1098/rsfs.2013.0074

Zacharaki, P., Stephanou, G., & Demopoulos, N. A. (2013). Comparison of the aneugenic properties of nocodazole, paclitaxel and griseofulvin in vitro. Centrosome defects and alterations in protein expression profiles. *J Appl Toxicol, 33*(9), 869-879. doi:10.1002/jat.2745

Zanella, F., Lorens, J. B., & Link, W. (2010). High content screening: seeing is believing. *Trends Biotechnol, 28*(5), 237-245. doi:10.1016/j.tibtech.2010.02.005

Zheng, J. (2012). Energy metabolism of cancer: Glycolysis versus oxidative phosphorylation (Review). *Oncol Lett, 4*(6), 1151-1157. doi:10.3892/ol.2012.928

Zheng, J., & Ramirez, V. D. (2000). Inhibition of mitochondrial proton F0F1-ATPase/ATP synthase by polyphenolic phytochemicals. *Br J Pharmacol, 130*(5), 1115-1123. doi:10.1038/sj.bjp.0703397

APPENDICES

Appendix A. The results of γH2Ax and pH3 responder analyses of each compound treatment at each concentration and at both time points, 6 h and 24 h. The responders caused by compound treatment and DMSO are shown on primary y-axis and the positive controls on the secondary y-axis. The error bars refer to the standard error of the three parallel plates.

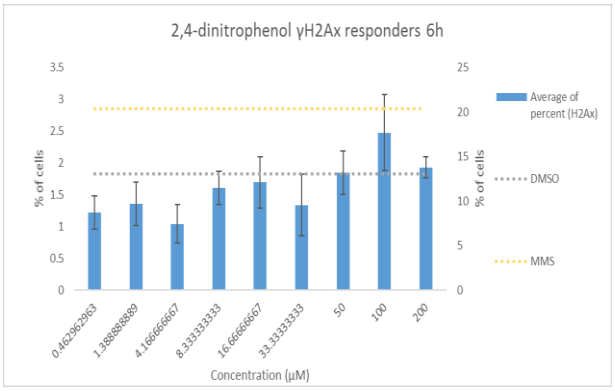

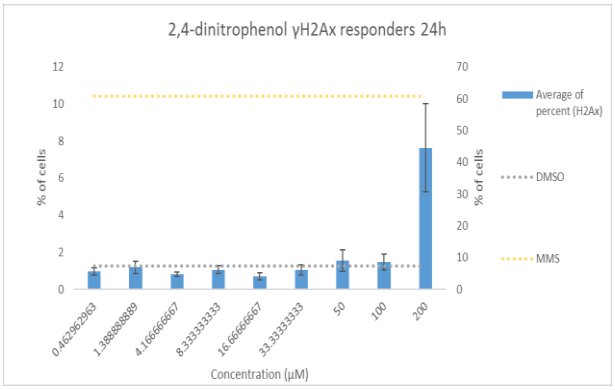

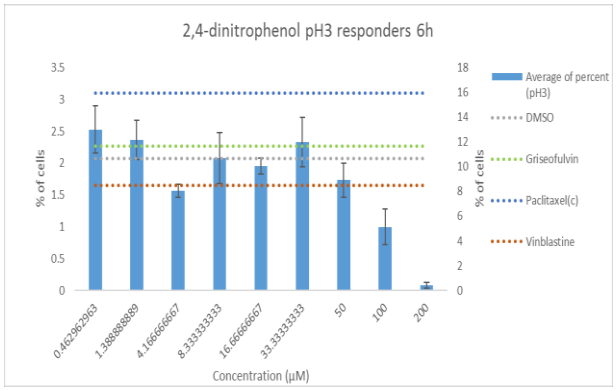

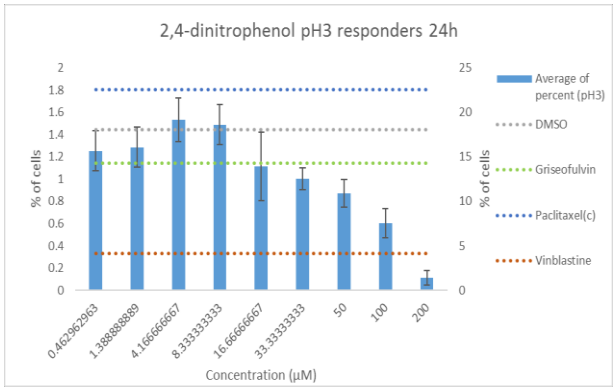

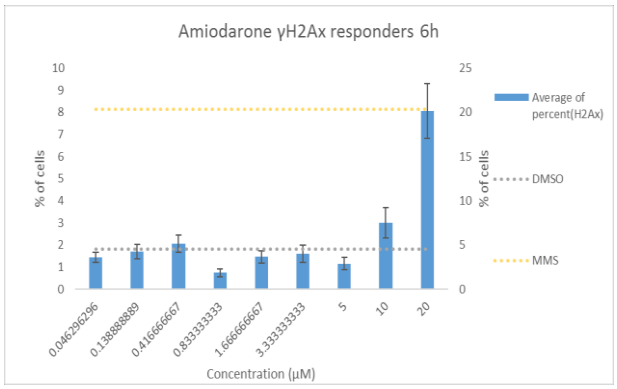

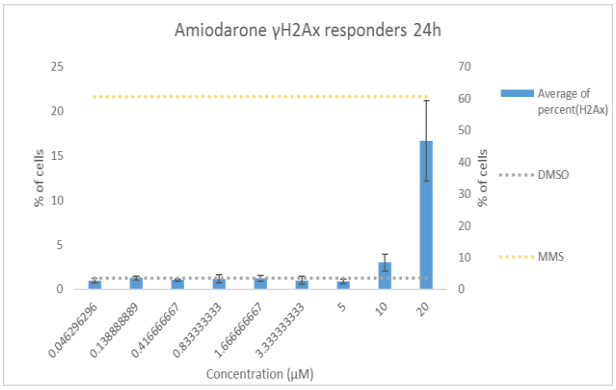

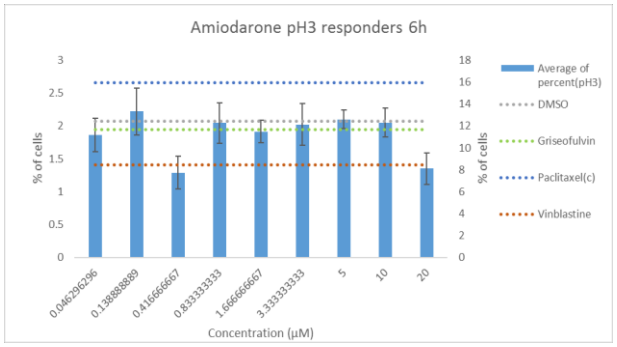
Amiodarone pH3 responders 6h
% of cells
Concentration (µM)
Average of percent(pH3)
DMSO
Griseofulvin
Paclitaxel(c)
Vinblastine

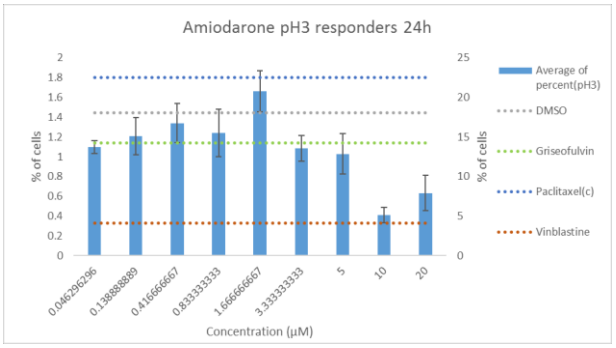
Amiodarone pH3 responders 24h
% of cells
Concentration (µM)
Average of percent(pH3)
DMSO
Griseofulvin
Paclitaxel(c)
Vinblastine

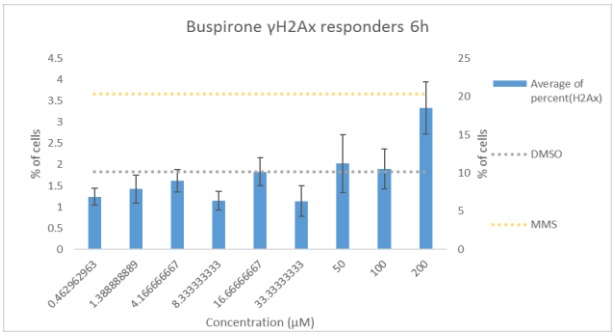
Buspirone γH2Ax responders 6h
% of cells
Concentration (µM)
Average of percent(H2Ax)
DMSO
MMS

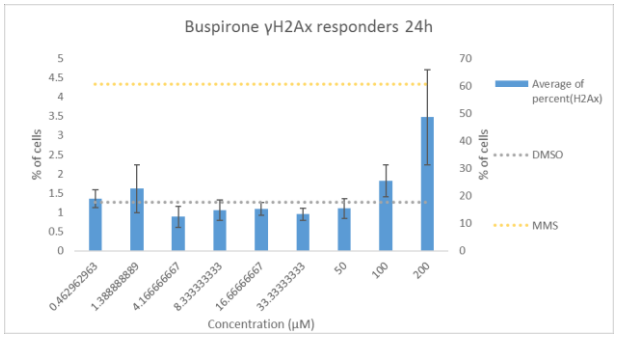
Buspirone γH2Ax responders 24h
% of cells
Concentration (µM)
Average of percent(H2Ax)
DMSO
MMS

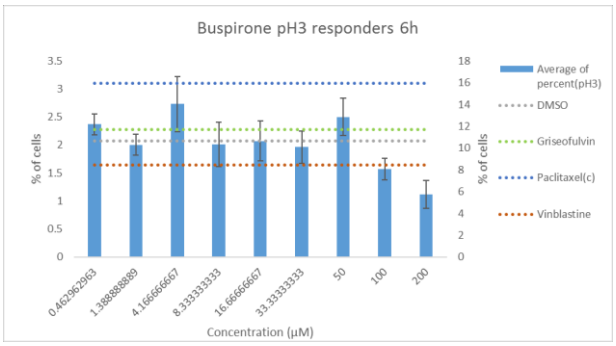
Buspirone pH3 responders 6h
% of cells
Concentration (µM)
Average of percent(pH3)
DMSO
Griseofulvin
Paclitaxel(c)
Vinblastine

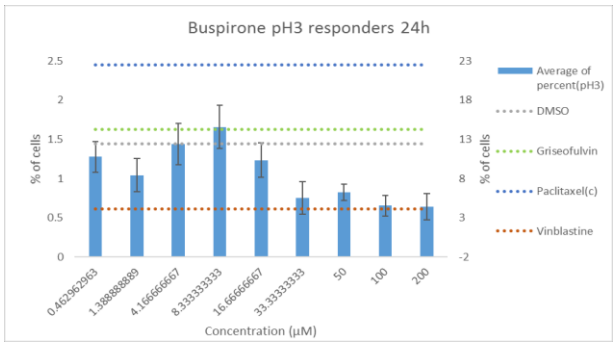
Buspirone pH3 responders 24h
% of cells
Concentration (µM)
Average of percent(pH3)
DMSO
Griseofulvin
Paclitaxel(c)
Vinblastine

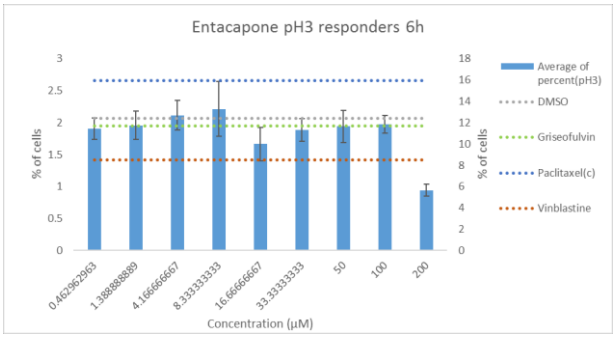
Entacapone pH3 responders 6h
% of cells
Concentration (µM)
Average of percent(pH3)
DMSO
Griseofulvin
Paclitaxel(c)
Vinblastine

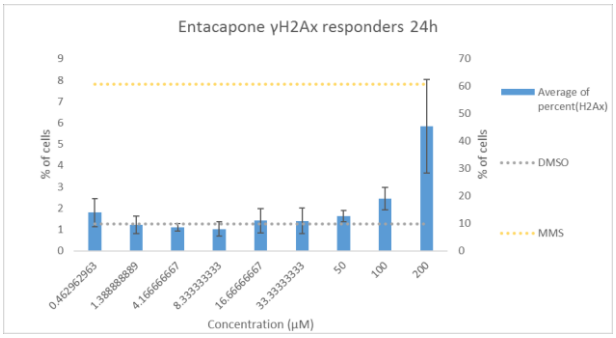
Entacapone γH2Ax responders 24h
% of cells
Concentration (µM)
Average of percent(H2Ax)
DMSO
MMS

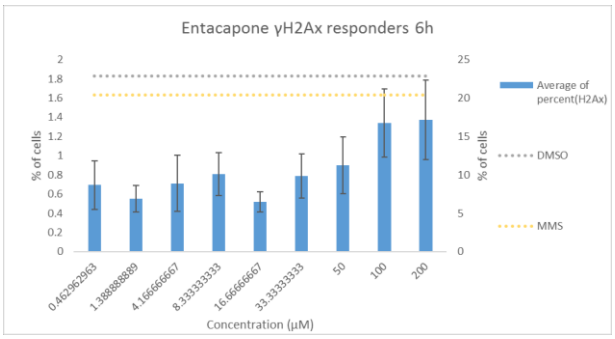
Entacapone γH2Ax responders 6h
% of cells
Concentration (µM)
Average of percent(H2Ax)
DMSO
MMS

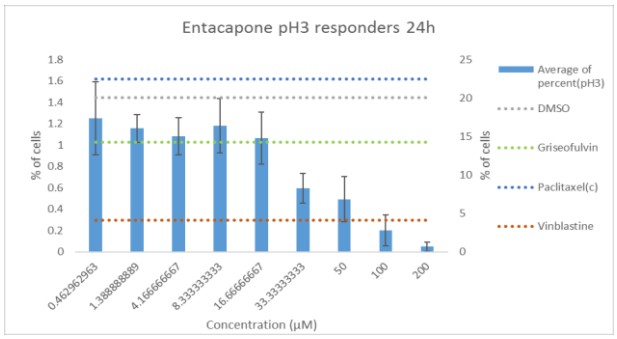
Entacapone pH3 responders 24h
% of cells
Concentration (µM)
Average of percent(pH3)
DMSO
Griseofulvin
Paclitaxel(c)
Vinblastine

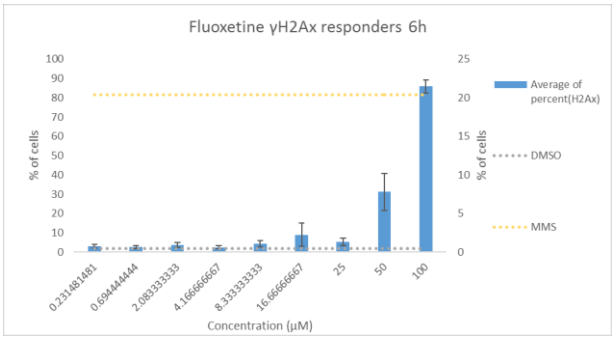
Fluoxetine γH2Ax responders 6h
% of cells
Concentration (μM)
Average of percent(H2Ax)
DMSO
MMS

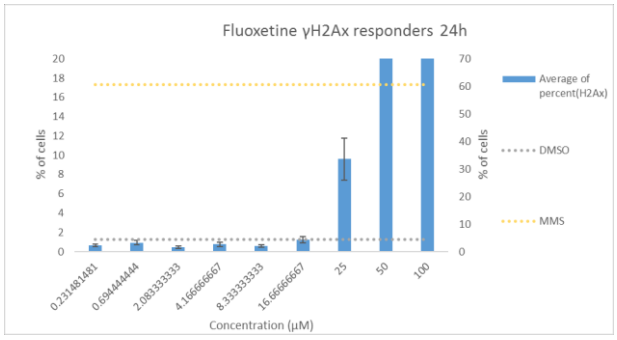
Fluoxetine γH2Ax responders 24h
% of cells
Concentration (μM)
Average of percent(H2Ax)
DMSO
MMS

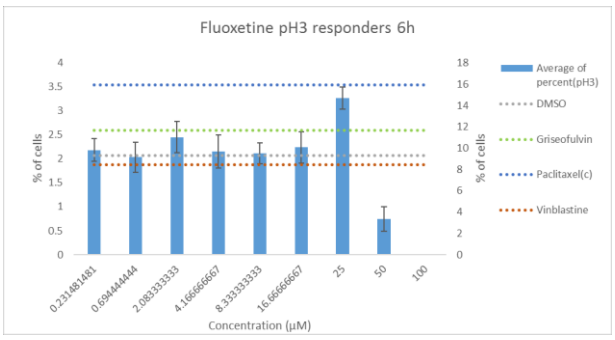
Fluoxetine pH3 responders 6h
% of cells
Concentration (μM)
Average of percent(pH3)
DMSO
Griseofulvin
Paclitaxel(c)
Vinblastine

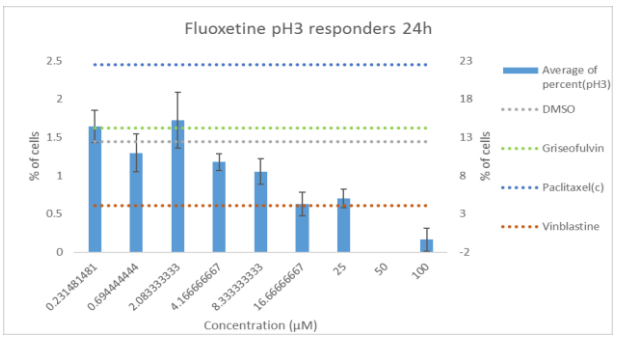
Fluoxetine pH3 responders 24h
% of cells
Concentration (μM)
Average of percent(pH3)
DMSO
Griseofulvin
Paclitaxel(c)
Vinblastine

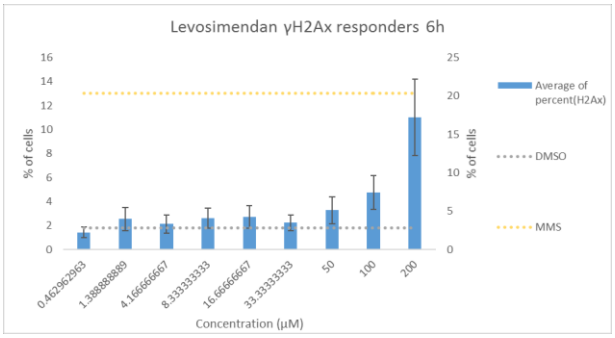
Levosimendan γH2Ax responders 6h
% of cells
Concentration (μM)
Average of percent(H2Ax)
DMSO
MMS

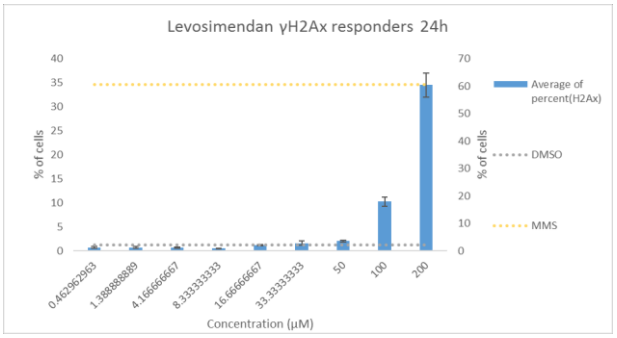
Levosimendan γH2Ax responders 24h
% of cells
Concentration (μM)
Average of percent(H2Ax)
DMSO
MMS

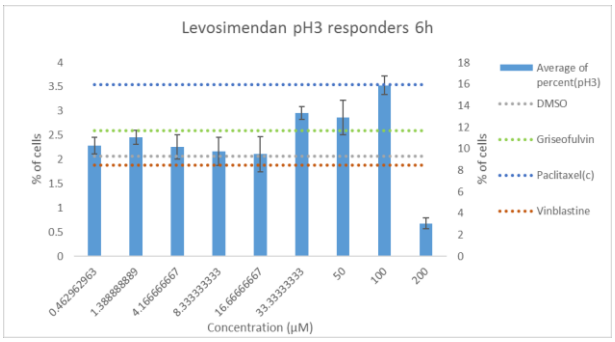
Levosimendan pH3 responders 6h
% of cells
Concentration (μM)
Average of percent(pH3)
DMSO
Griseofulvin
Paclitaxel(c)
Vinblastine

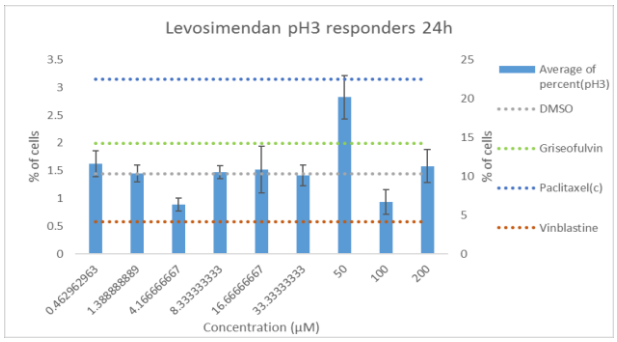
Levosimendan pH3 responders 24h
% of cells
Concentration (μM)
Average of percent(pH3)
DMSO
Griseofulvin
Paclitaxel(c)
Vinblastine

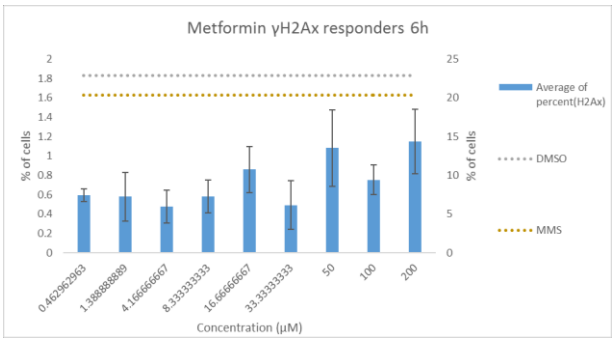
Metformin γH2Ax responders 6h
% of cells
Concentration (μM)
Average of percent(H2Ax)
DMSO
MMS

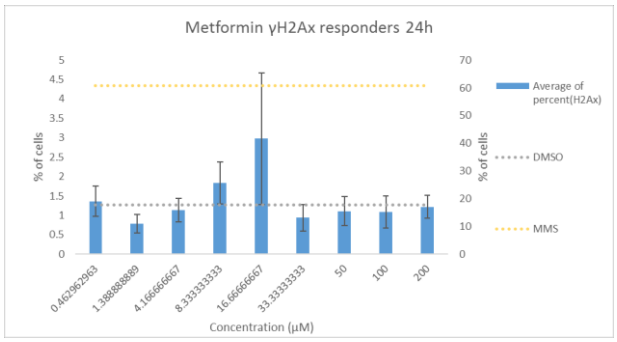
Metformin γH2Ax responders 24h
% of cells
Concentration (μM)
Average of percent(H2Ax)
DMSO
MMS

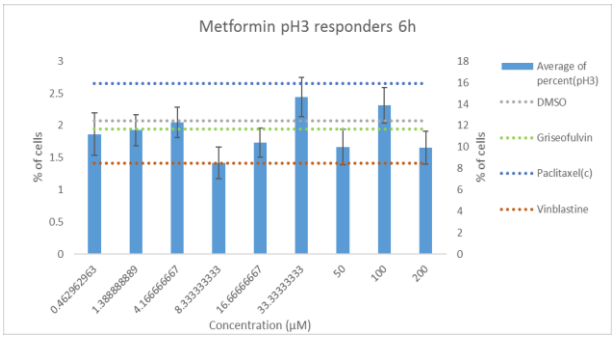
Metformin pH3 responders 6h
% of cells
% of cells
Concentration (µM)
0.462962963
1.388888889
4.166666667
8.333333333
16.66666667
33.33333333
50
100
200
Average of percent(pH3)
DMSO
Griseofulvin
Paclitaxel(c)
Vinblastine

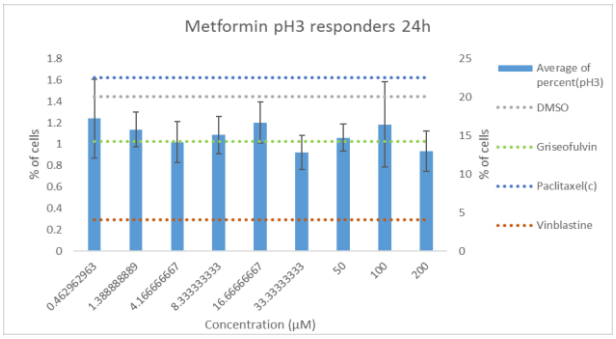
Metformin pH3 responders 24h
% of cells
% of cells
Concentration (µM)
0.462962963
1.388888889
4.166666667
8.333333333
16.66666667
33.33333333
50
100
200
Average of percent(pH3)
DMSO
Griseofulvin
Paclitaxel(c)
Vinblastine

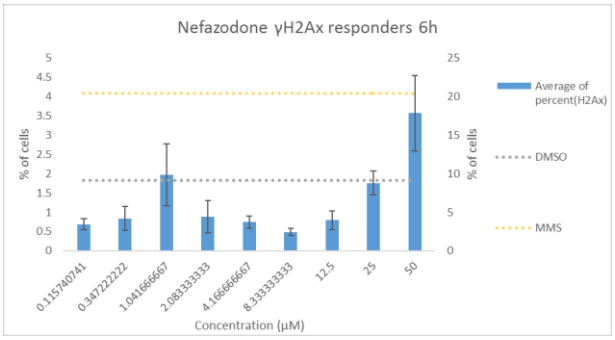
Nefazodone γH2Ax responders 6h
% of cells
% of cells
Concentration (µM)
0.115740741
0.347222222
1.041666667
2.083333333
4.166666667
8.333333333
12.5
25
50
Average of percent(H2Ax)
DMSO
MMS

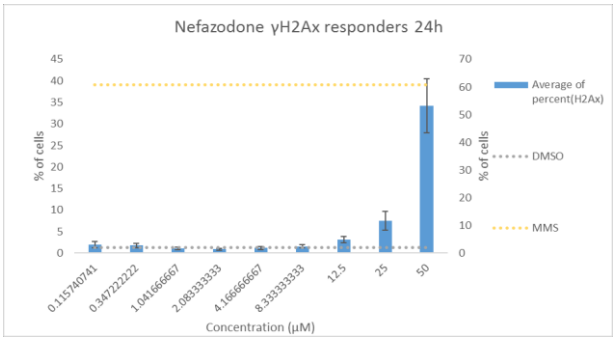
Nefazodone γH2Ax responders 24h
% of cells
% of cells
Concentration (µM)
0.115740741
0.347222222
1.041666667
2.083333333
4.166666667
8.333333333
12.5
25
50
Average of percent(H2Ax)
DMSO
MMS

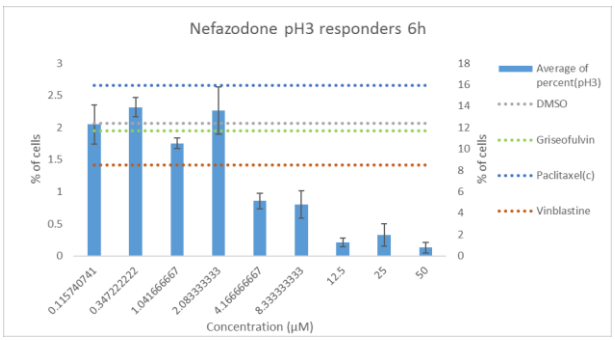
Nefazodone pH3 responders 6h
% of cells
% of cells
Concentration (µM)
0.115740741
0.347222222
1.041666667
2.083333333
4.166666667
8.333333333
12.5
25
50
Average of percent(pH3)
DMSO
Griseofulvin
Paclitaxel(c)
Vinblastine

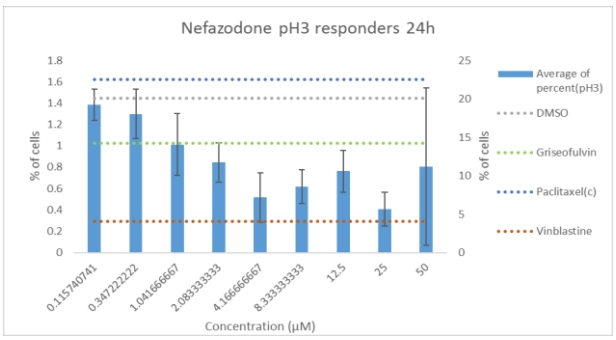
Nefazodone pH3 responders 24h
% of cells
% of cells
Concentration (µM)
0.115740741
0.347222222
1.041666667
2.083333333
4.166666667
8.333333333
12.5
25
50
Average of percent(pH3)
DMSO
Griseofulvin
Paclitaxel(c)
Vinblastine

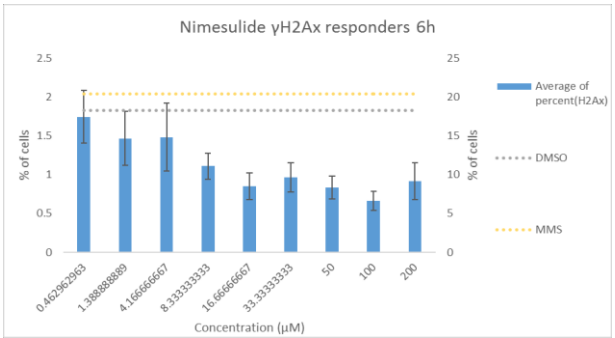
Nimesulide γH2Ax responders 6h
% of cells
% of cells
Concentration (µM)
0.462962963
1.388888889
4.166666667
8.333333333
16.66666667
33.33333333
50
100
200
Average of percent(H2Ax)
DMSO
MMS

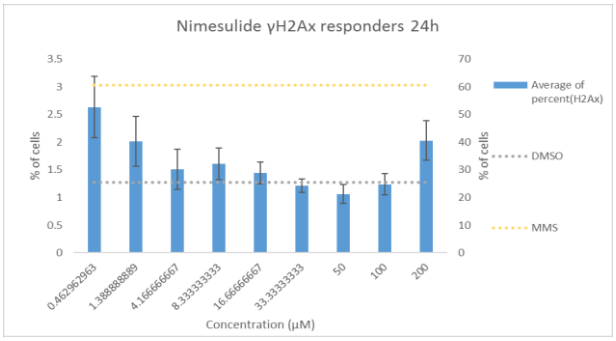
Nimesulide γH2Ax responders 24h
% of cells
% of cells
Concentration (µM)
0.462962963
1.388888889
4.166666667
8.333333333
16.66666667
33.33333333
50
100
200
Average of percent(H2Ax)
DMSO
MMS

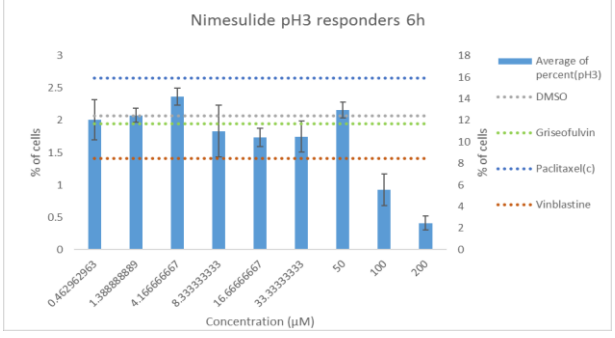
Nimesulide pH3 responders 6h
% of cells
% of cells
Concentration (µM)
0.462962963
1.388888889
4.166666667
8.333333333
16.66666667
33.33333333
50
100
200
Average of percent(pH3)
DMSO
Griseofulvin
Paclitaxel(c)
Vinblastine

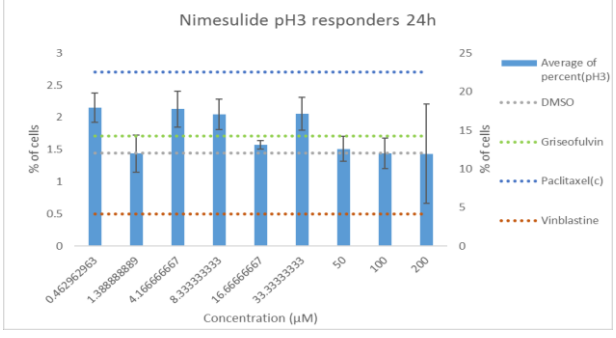
Nimesulide pH3 responders 24h
% of cells
% of cells
Concentration (µM)
0.462962963
1.388888889
4.166666667
8.333333333
16.66666667
33.33333333
50
100
200
Average of percent(pH3)
DMSO
Griseofulvin
Paclitaxel(c)
Vinblastine

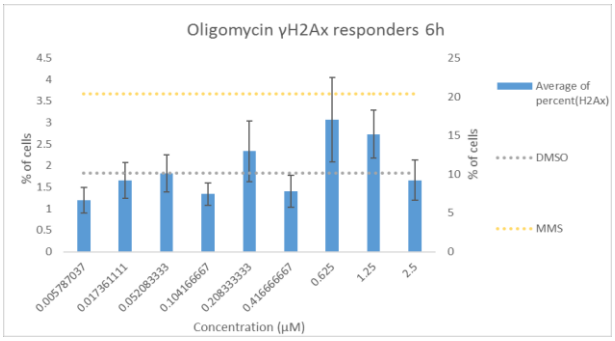
Oligomycin γH2Ax responders 6h
% of cells
Concentration (μM)
Average of percent(H2Ax)
DMSO
MMS

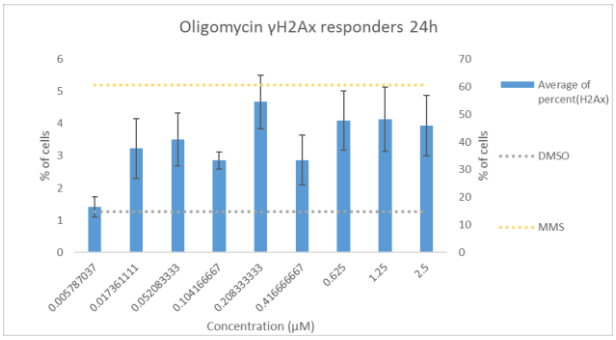
Oligomycin γH2Ax responders 24h
% of cells
Concentration (μM)
Average of percent(H2Ax)
DMSO
MMS

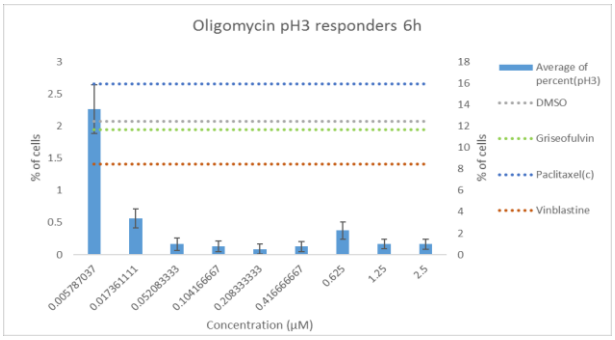
Oligomycin pH3 responders 6h
% of cells
Concentration (μM)
Average of percent(pH3)
DMSO
Griseofulvin
Paclitaxel(c)
Vinblastine

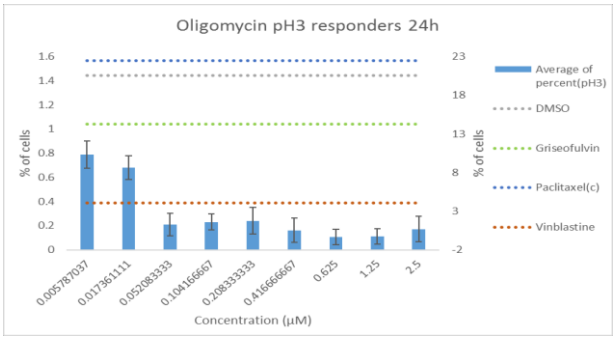
Oligomycin pH3 responders 24h
% of cells
Concentration (μM)
Average of percent(pH3)
DMSO
Griseofulvin
Paclitaxel(c)
Vinblastine

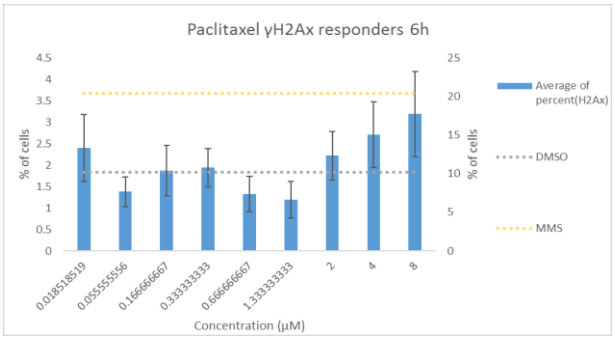
Paclitaxel γH2Ax responders 6h
% of cells
Concentration (μM)
Average of percent(H2Ax)
DMSO
MMS

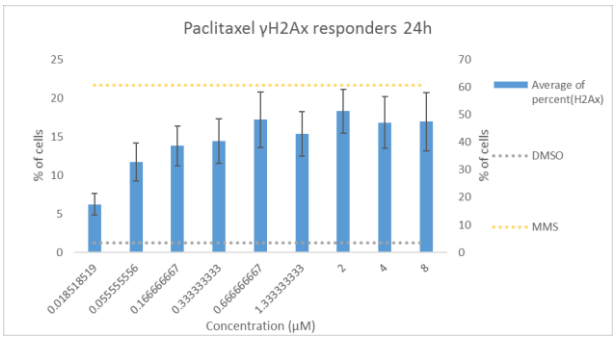
Paclitaxel γH2Ax responders 24h
% of cells
Concentration (μM)
Average of percent(H2Ax)
DMSO
MMS

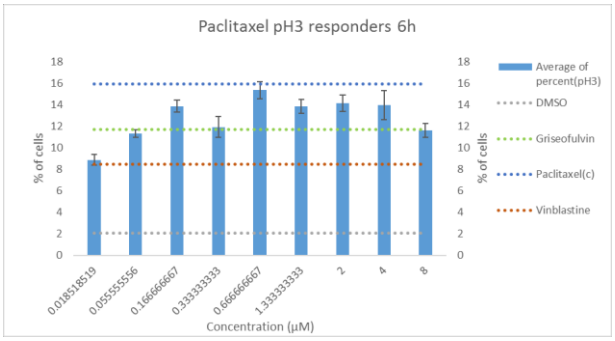
Paclitaxel pH3 responders 6h
% of cells
Concentration (μM)
Average of percent(pH3)
DMSO
Griseofulvin
Paclitaxel(c)
Vinblastine

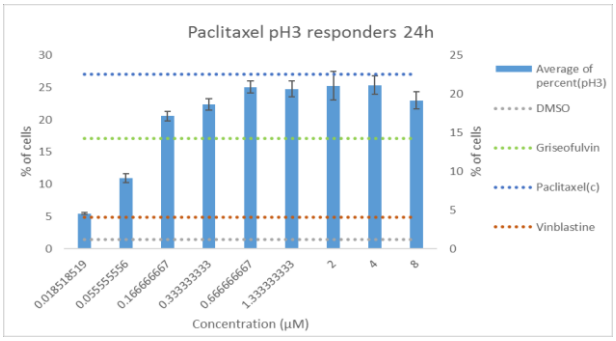
Paclitaxel pH3 responders 24h
% of cells
Concentration (μM)
Average of percent(pH3)
DMSO
Griseofulvin
Paclitaxel(c)
Vinblastine

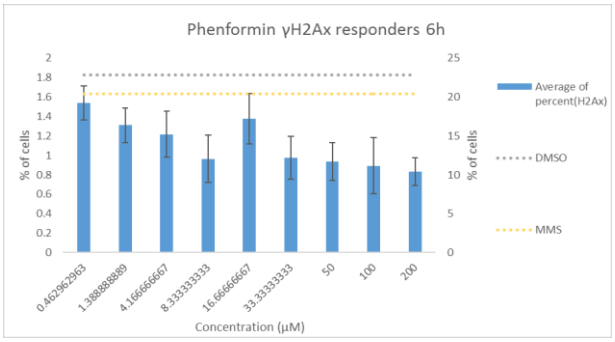
Phenformin γH2Ax responders 6h
% of cells
Concentration (μM)
Average of percent(H2Ax)
DMSO
MMS

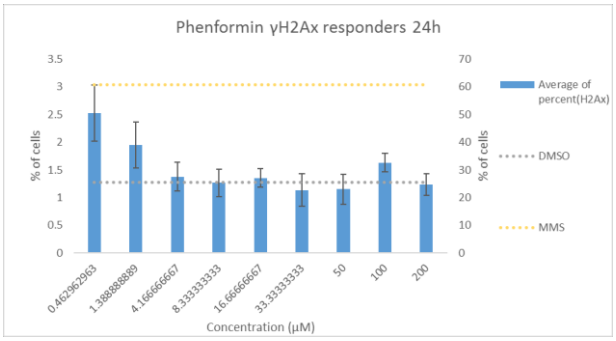
Phenformin γH2Ax responders 24h
% of cells
Concentration (μM)
Average of percent(H2Ax)
DMSO
MMS

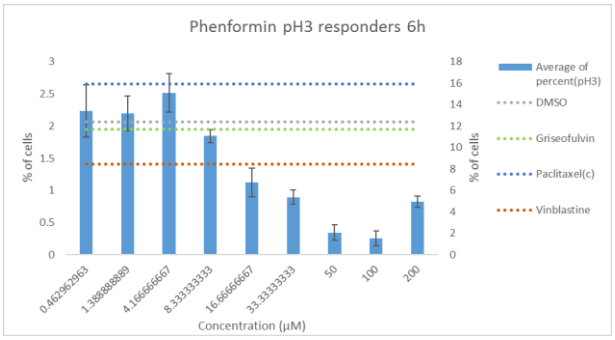
Phenformin pH3 responders 6h
% of cells
Concentration (µM)
Average of percent(pH3)
DMSO
Griseofulvin
Paclitaxel(c)
Vinblastine

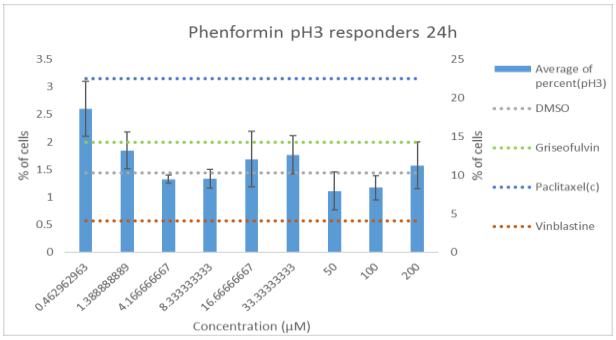
Phenformin pH3 responders 24h
% of cells
Concentration (µM)
Average of percent(pH3)
DMSO
Griseofulvin
Paclitaxel(c)
Vinblastine

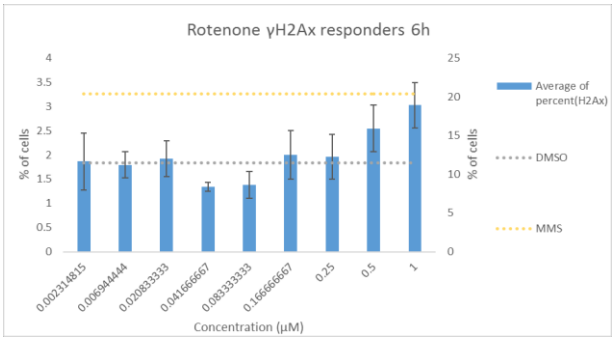
Rotenone γH2Ax responders 6h
% of cells
Concentration (µM)
Average of percent(H2Ax)
DMSO
MMS

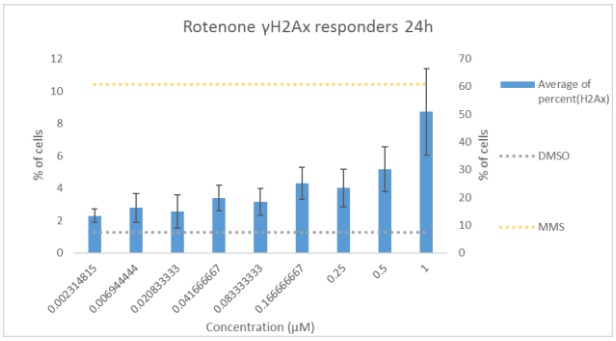
Rotenone γH2Ax responders 24h
% of cells
Concentration (µM)
Average of percent(H2Ax)
DMSO
MMS

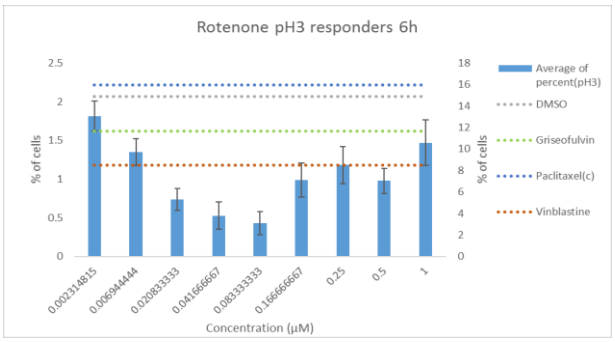
Rotenone pH3 responders 6h
% of cells
Concentration (µM)
Average of percent(pH3)
DMSO
Griseofulvin
Paclitaxel(c)
Vinblastine

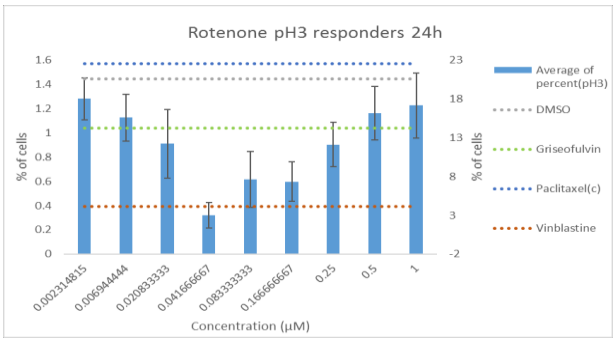
Rotenone pH3 responders 24h
% of cells
Concentration (µM)
Average of percent(pH3)
DMSO
Griseofulvin
Paclitaxel(c)
Vinblastine

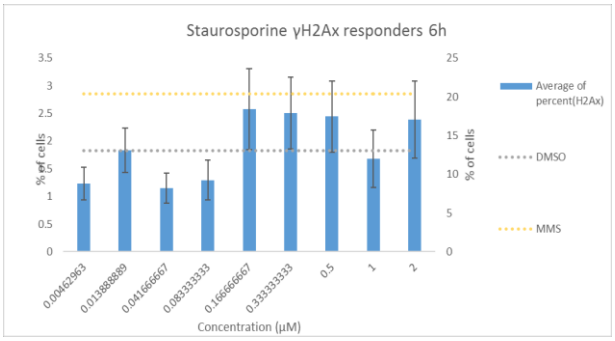
Staurosporine γH2Ax responders 6h
% of cells
Concentration (µM)
Average of percent(H2Ax)
DMSO
MMS

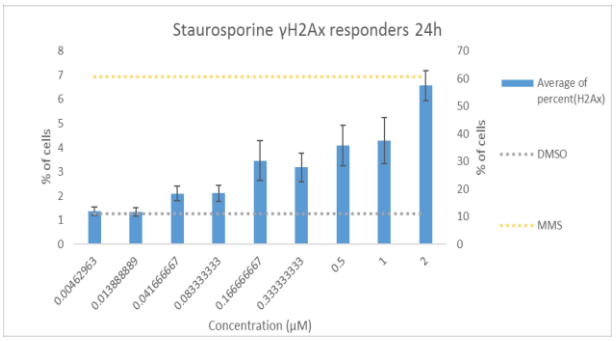
Staurosporine γH2Ax responders 24h
% of cells
Concentration (µM)
Average of percent(H2Ax)
DMSO
MMS

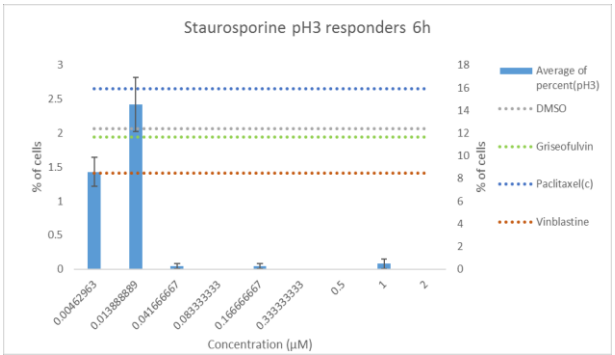
Staurosporine pH3 responders 6h
% of cells
Concentration (µM)
Average of percent(pH3)
DMSO
Griseofulvin
Paclitaxel(c)
Vinblastine

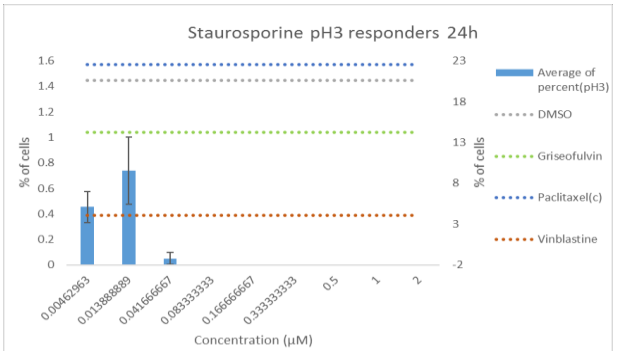
Staurosporine pH3 responders 24h
% of cells
Concentration (µM)
Average of percent(pH3)
DMSO
Griseofulvin
Paclitaxel(c)
Vinblastine

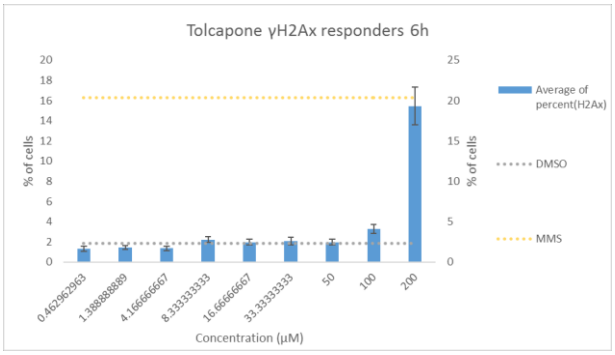
Tolcapone γH2Ax responders 6h
% of cells
Concentration (μM)
Average of percent(H2Ax)
DMSO
MMS

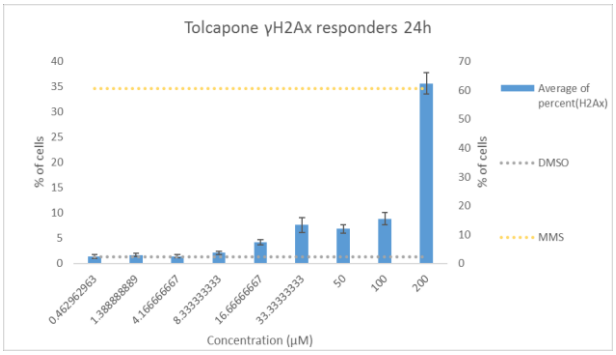
Tolcapone γH2Ax responders 24h
% of cells
Concentration (μM)
Average of percent(H2Ax)
DMSO
MMS

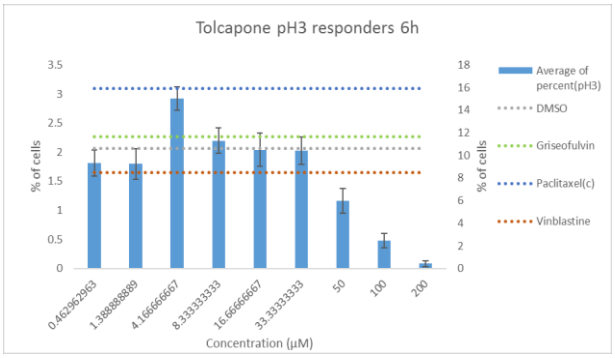
Tolcapone pH3 responders 6h
% of cells
Concentration (μM)
Average of percent(pH3)
DMSO
Griseofulvin
Paclitaxel(c)
Vinblastine

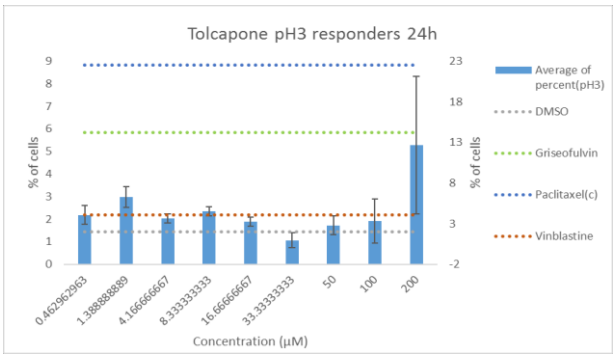
Tolcapone pH3 responders 24h
% of cells
Concentration (μM)
Average of percent(pH3)
DMSO
Griseofulvin
Paclitaxel(c)
Vinblastine

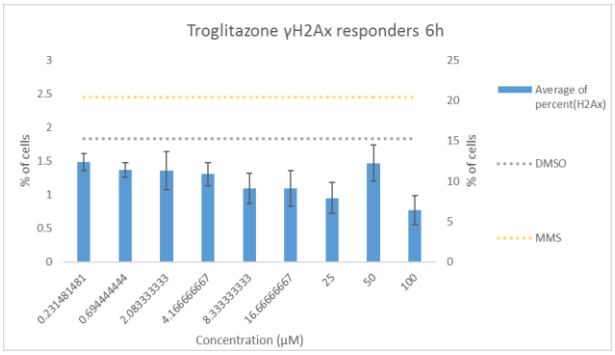
Troglitazone γH2Ax responders 6h
% of cells
Concentration (μM)
Average of percent(H2Ax)
DMSO
MMS

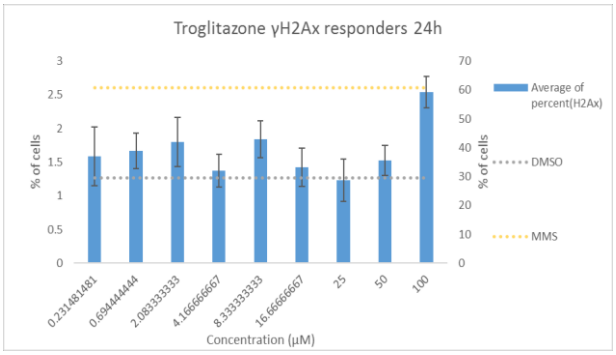
Troglitazone γH2Ax responders 24h
% of cells
Concentration (μM)
Average of percent(H2Ax)
DMSO
MMS

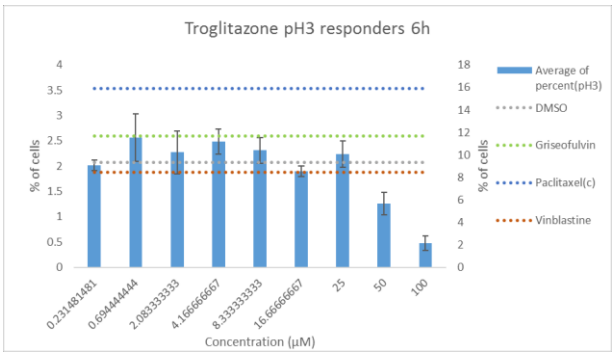
Troglitazone pH3 responders 6h
% of cells
Concentration (μM)
Average of percent(pH3)
DMSO
Griseofulvin
Paclitaxel(c)
Vinblastine

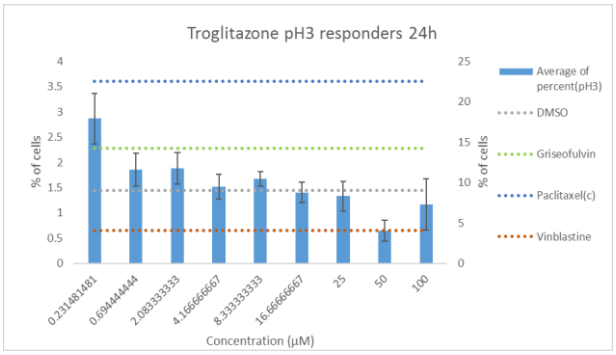
Troglitazone pH3 responders 24h
% of cells
Concentration (μM)
Average of percent(pH3)
DMSO
Griseofulvin
Paclitaxel(c)
Vinblastine

Appendix B. The comparison of γH2Ax and pH3 responses with the nucleus area of each compounds and controls at both time points, 6 h and 24 h. The responders caused by compound treatments and DMSO are shown on primary y-axis and the nucleus count on the secondary y-axis.

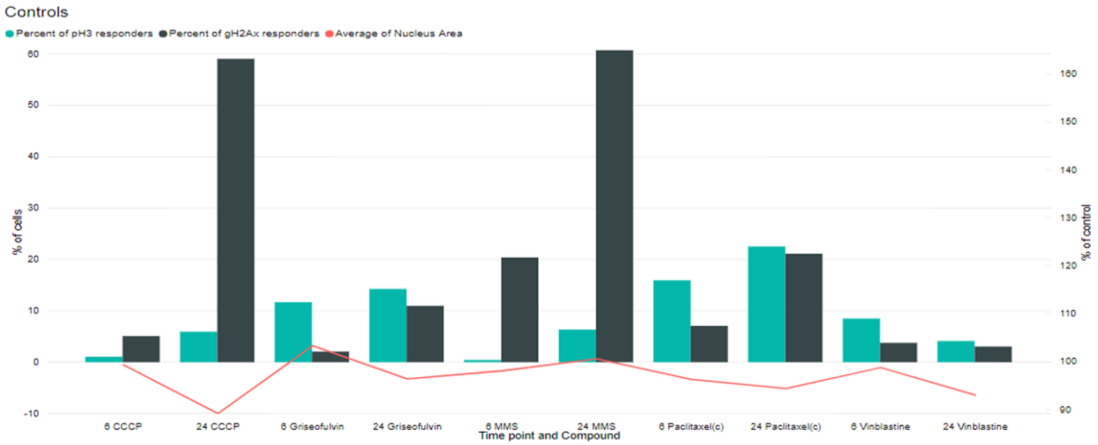

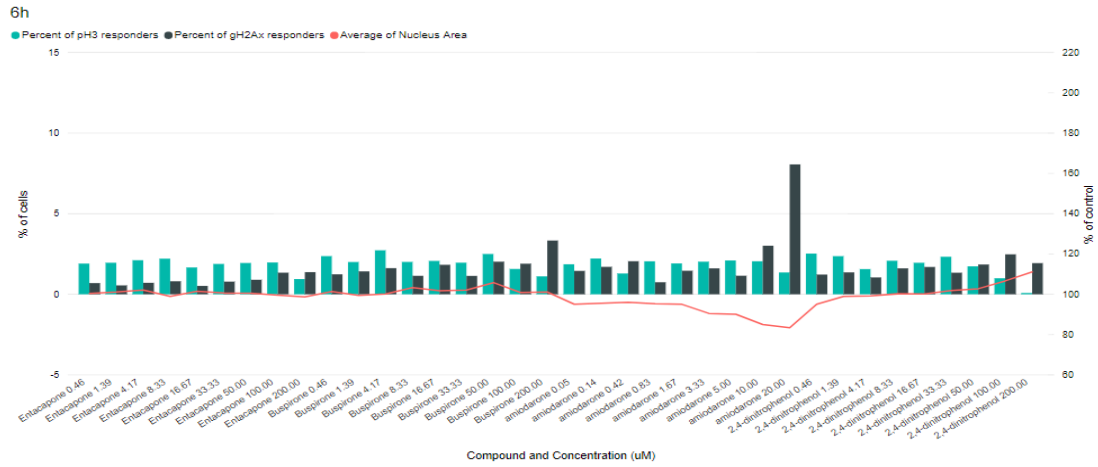

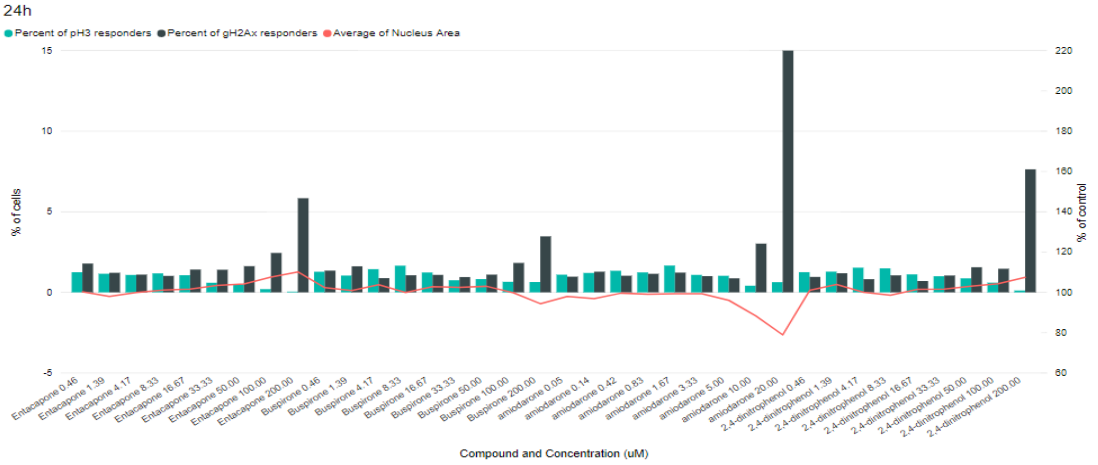

6h

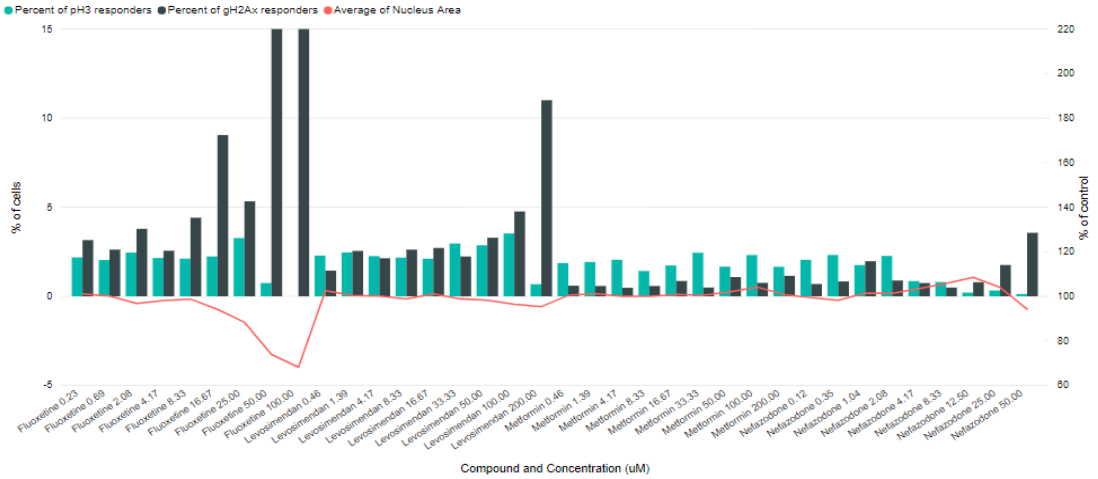
Percent of pH3 responders
Percent of gH2Ax responders
Average of Nucleus Area
% of cells
% of control
Fluoxetine 0.23
Fluoxetine 0.69
Fluoxetine 2.08
Fluoxetine 4.17
Fluoxetine 8.33
Fluoxetine 16.67
Fluoxetine 25.00
Fluoxetine 50.00
Fluoxetine 100.00
Levosimendan 0.46
Levosimendan 1.39
Levosimendan 4.17
Levosimendan 8.33
Levosimendan 16.67
Levosimendan 33.33
Levosimendan 50.00
Levosimendan 100.00
Levosimendan 200.00
Metformin 0.46
Metformin 1.39
Metformin 4.17
Metformin 8.33
Metformin 16.67
Metformin 33.33
Metformin 50.00
Metformin 100.00
Metformin 200.00
Nefazodone 0.12
Nefazodone 0.35
Nefazodone 1.04
Nefazodone 2.08
Nefazodone 4.17
Nefazodone 8.33
Nefazodone 12.50
Nefazodone 25.00
Nefazodone 50.00
Compound and Concentration (uM)

24h

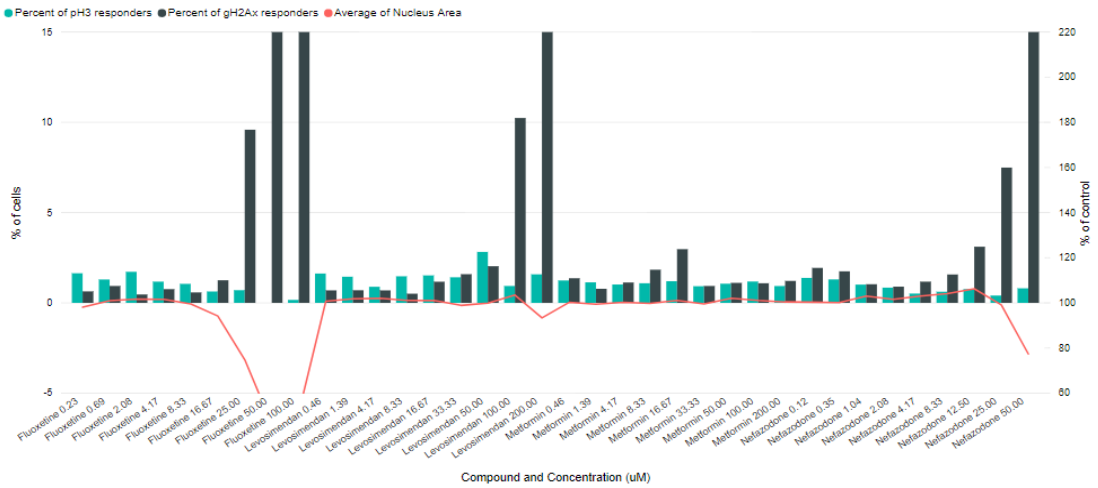
Percent of pH3 responders
Percent of gH2Ax responders
Average of Nucleus Area
% of cells
% of control
Fluoxetine 0.23
Fluoxetine 0.69
Fluoxetine 2.08
Fluoxetine 4.17
Fluoxetine 8.33
Fluoxetine 16.67
Fluoxetine 25.00
Fluoxetine 50.00
Fluoxetine 100.00
Levosimendan 0.46
Levosimendan 1.39
Levosimendan 4.17
Levosimendan 8.33
Levosimendan 16.67
Levosimendan 33.33
Levosimendan 50.00
Levosimendan 100.00
Levosimendan 200.00
Metformin 0.46
Metformin 1.39
Metformin 4.17
Metformin 8.33
Metformin 16.67
Metformin 33.33
Metformin 50.00
Metformin 100.00
Metformin 200.00
Nefazodone 0.12
Nefazodone 0.35
Nefazodone 1.04
Nefazodone 2.08
Nefazodone 4.17
Nefazodone 8.33
Nefazodone 12.50
Nefazodone 25.00
Nefazodone 50.00
Compound and Concentration (uM)

6h

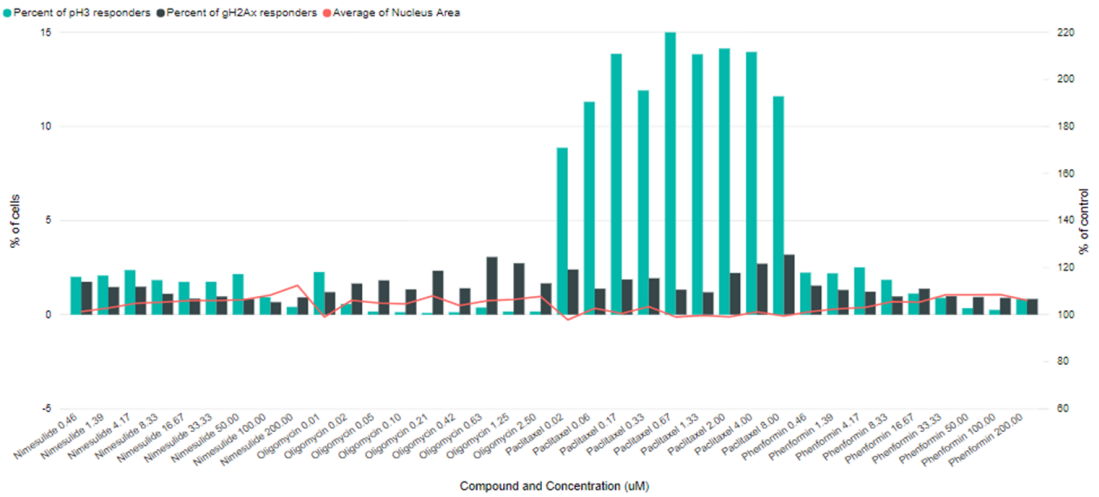
Percent of pH3 responders
Percent of gH2Ax responders
Average of Nucleus Area
% of cells
% of control
Nimesulide 0.46
Nimesulide 1.39
Nimesulide 4.17
Nimesulide 8.33
Nimesulide 16.67
Nimesulide 33.33
Nimesulide 50.00
Nimesulide 100.00
Nimesulide 200.00
Oligomycin 0.01
Oligomycin 0.02
Oligomycin 0.05
Oligomycin 0.10
Oligomycin 0.21
Oligomycin 0.42
Oligomycin 0.63
Oligomycin 1.25
Oligomycin 2.50
Paclitaxel 0.02
Paclitaxel 0.06
Paclitaxel 0.17
Paclitaxel 0.33
Paclitaxel 0.67
Paclitaxel 1.33
Paclitaxel 2.00
Paclitaxel 4.00
Paclitaxel 8.00
Phenformin 0.46
Phenformin 1.39
Phenformin 4.17
Phenformin 8.33
Phenformin 16.67
Phenformin 33.33
Phenformin 50.00
Phenformin 100.00
Phenformin 200.00
Compound and Concentration (uM)

24h

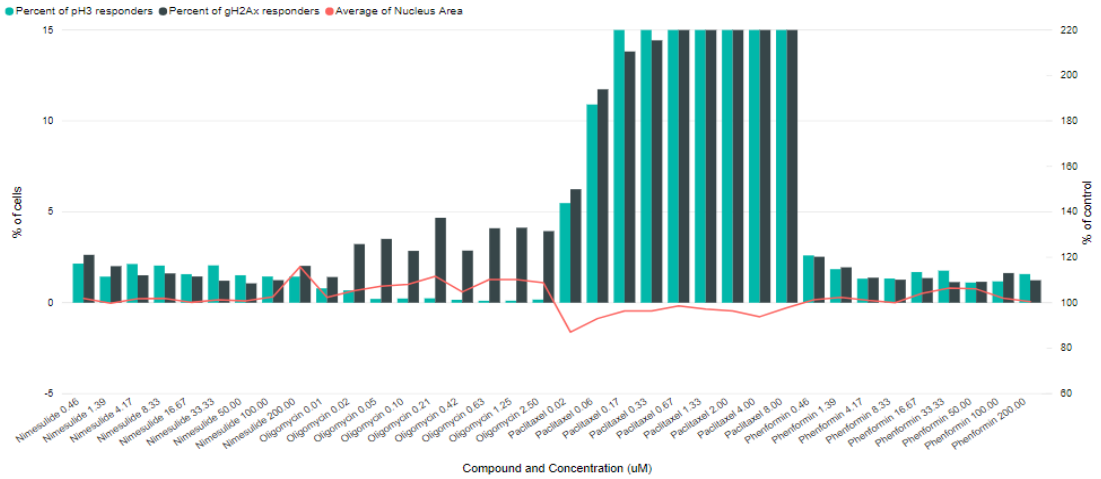
Percent of pH3 responders
Percent of gH2Ax responders
Average of Nucleus Area
% of cells
% of control
Nimesulide 0.46
Nimesulide 1.39
Nimesulide 4.17
Nimesulide 8.33
Nimesulide 16.67
Nimesulide 33.33
Nimesulide 50.00
Nimesulide 100.00
Nimesulide 200.00
Oligomycin 0.01
Oligomycin 0.02
Oligomycin 0.05
Oligomycin 0.10
Oligomycin 0.21
Oligomycin 0.42
Oligomycin 0.63
Oligomycin 1.25
Oligomycin 2.50
Paclitaxel 0.02
Paclitaxel 0.06
Paclitaxel 0.17
Paclitaxel 0.33
Paclitaxel 0.67
Paclitaxel 1.33
Paclitaxel 2.00
Paclitaxel 4.00
Paclitaxel 8.00
Phenformin 0.46
Phenformin 1.39
Phenformin 4.17
Phenformin 8.33
Phenformin 16.67
Phenformin 33.33
Phenformin 50.00
Phenformin 100.00
Phenformin 200.00
Compound and Concentration (uM)

6h

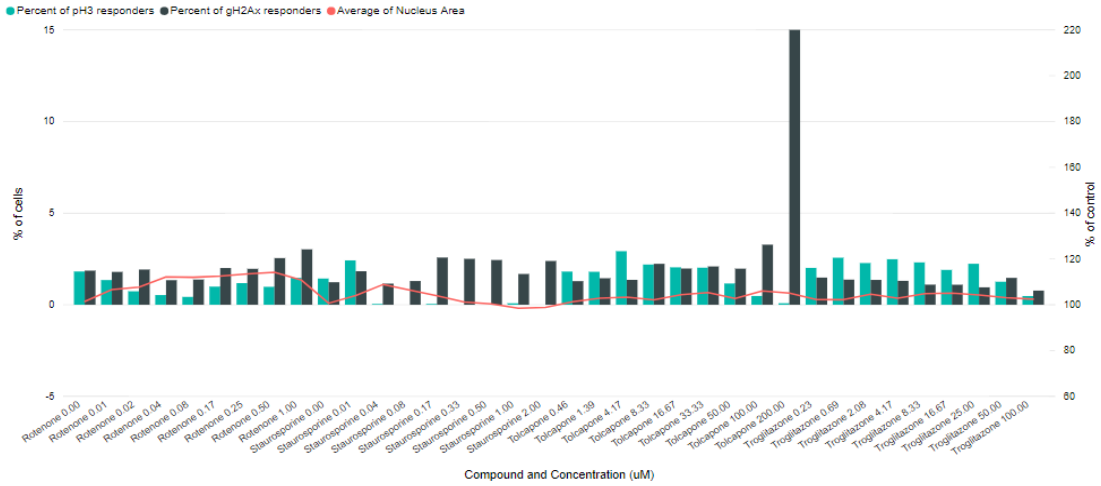
Percent of pH3 responders
Percent of gH2Ax responders
Average of Nucleus Area
% of cells
% of control
Rotenone 0.00
Rotenone 0.01
Rotenone 0.02
Rotenone 0.04
Rotenone 0.08
Rotenone 0.17
Rotenone 0.25
Rotenone 0.50
Rotenone 1.00
Staurosporine 0.00
Staurosporine 0.01
Staurosporine 0.04
Staurosporine 0.08
Staurosporine 0.17
Staurosporine 0.33
Staurosporine 0.50
Staurosporine 1.00
Staurosporine 2.00
Tolcapone 0.46
Tolcapone 1.39
Tolcapone 4.17
Tolcapone 8.33
Tolcapone 16.67
Tolcapone 33.33
Tolcapone 50.00
Tolcapone 100.00
Tolcapone 200.00
Troglitazone 0.23
Troglitazone 0.69
Troglitazone 2.08
Troglitazone 4.17
Troglitazone 8.33
Troglitazone 16.67
Troglitazone 25.00
Troglitazone 50.00
Troglitazone 100.00
Compound and Concentration (uM)

24h

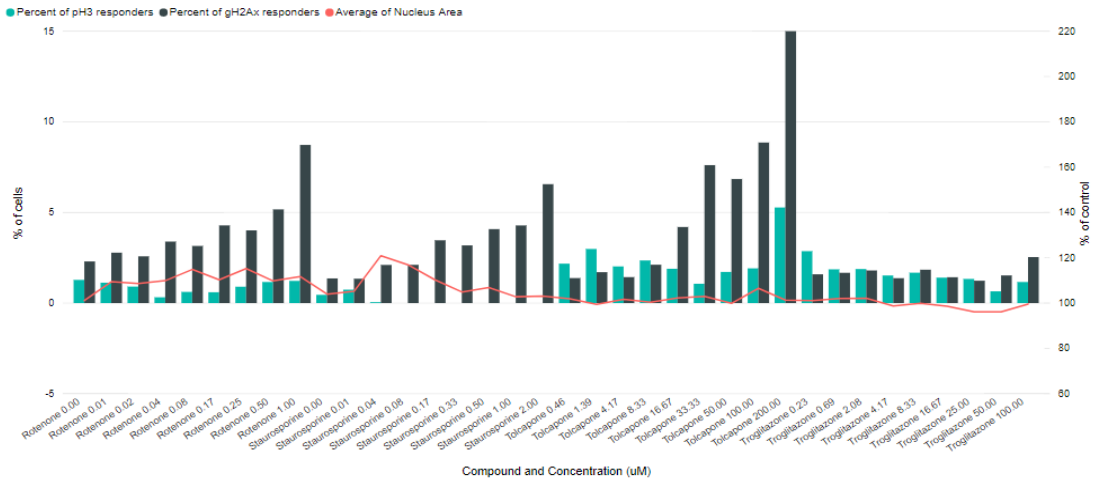
Percent of pH3 responders
Percent of gH2Ax responders
Average of Nucleus Area
% of cells
% of control
Rotenone 0.00
Rotenone 0.01
Rotenone 0.02
Rotenone 0.04
Rotenone 0.08
Rotenone 0.17
Rotenone 0.25
Rotenone 0.50
Rotenone 1.00
Staurosporine 0.00
Staurosporine 0.01
Staurosporine 0.04
Staurosporine 0.08
Staurosporine 0.17
Staurosporine 0.33
Staurosporine 0.50
Staurosporine 1.00
Staurosporine 2.00
Tolcapone 0.46
Tolcapone 1.39
Tolcapone 4.17
Tolcapone 8.33
Tolcapone 16.67
Tolcapone 33.33
Tolcapone 50.00
Tolcapone 100.00
Tolcapone 200.00
Troglitazone 0.23
Troglitazone 0.69
Troglitazone 2.08
Troglitazone 4.17
Troglitazone 8.33
Troglitazone 16.67
Troglitazone 25.00
Troglitazone 50.00
Troglitazone 100.00
Compound and Concentration (uM)

Appendix C. The comparison of γH2Ax and pH3 responses with the tubulin and actin intensities of each compounds and controls at both time points, 6 h and 24 h. The responders caused by compound treatments and DMSO are shown on primary y-axis and the tubulin and actin intensities on the secondary y-axis.

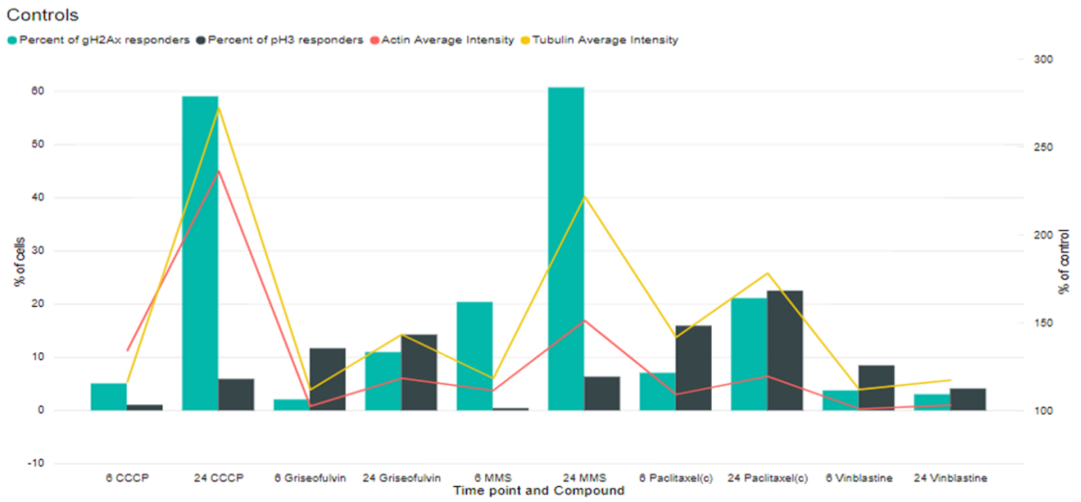

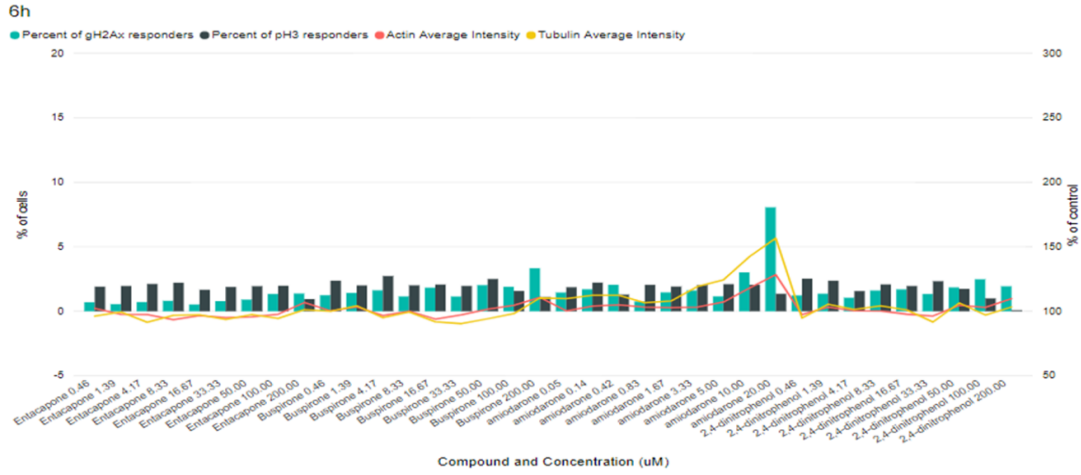

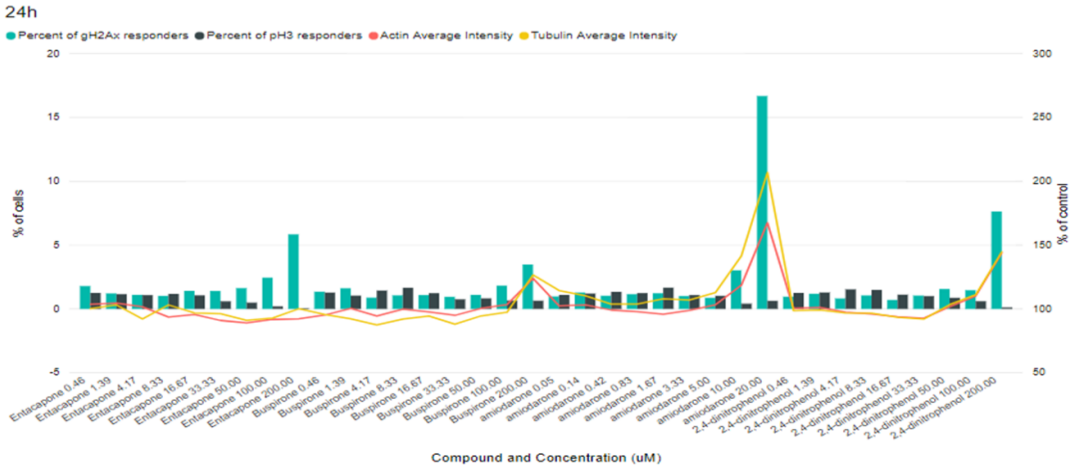

6h

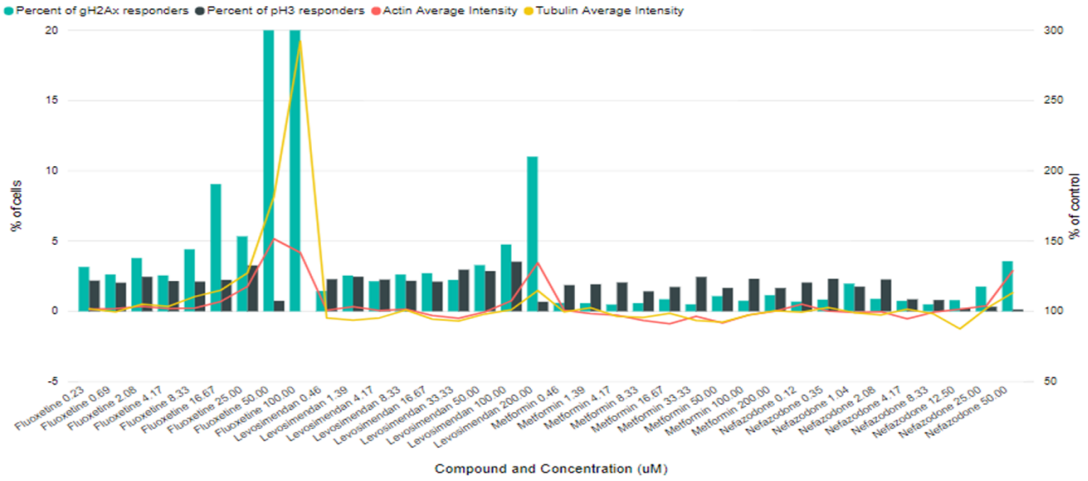
Percent of gH2Ax responders
Percent of pH3 responders
Actin Average Intensity
Tubulin Average Intensity
% of cells
% of control
Fluoxetine 0.23
Fluoxetine 0.69
Fluoxetine 2.08
Fluoxetine 4.17
Fluoxetine 8.33
Fluoxetine 16.67
Fluoxetine 25.00
Fluoxetine 50.00
Fluoxetine 100.00
Levosimendan 0.46
Levosimendan 1.39
Levosimendan 4.17
Levosimendan 8.33
Levosimendan 16.67
Levosimendan 33.33
Levosimendan 50.00
Levosimendan 100.00
Levosimendan 200.00
Metformin 0.46
Metformin 1.39
Metformin 4.17
Metformin 8.33
Metformin 16.67
Metformin 33.33
Metformin 50.00
Metformin 100.00
Metformin 200.00
Nefazodone 0.12
Nefazodone 0.35
Nefazodone 1.04
Nefazodone 2.08
Nefazodone 4.17
Nefazodone 8.33
Nefazodone 12.50
Nefazodone 25.00
Nefazodone 50.00
Compound and Concentration (uM)

24h

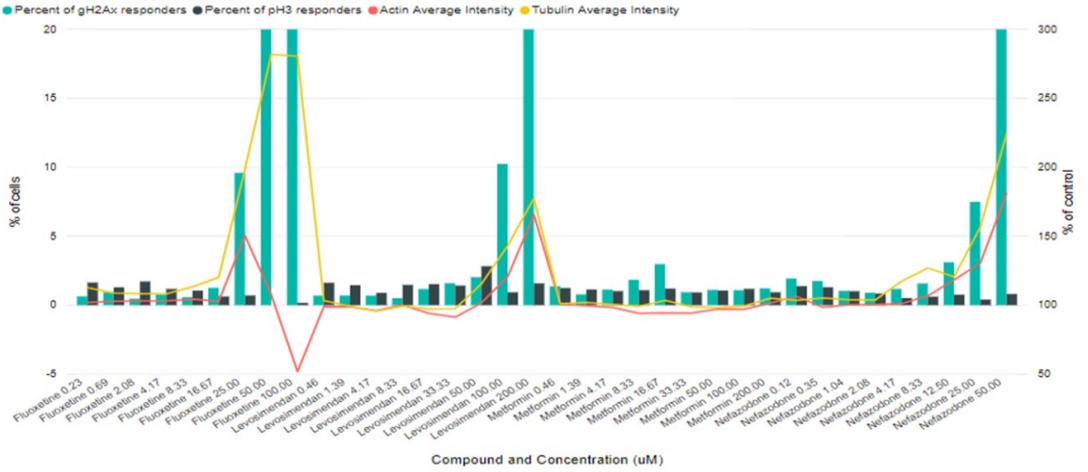
Percent of gH2Ax responders
Percent of pH3 responders
Actin Average Intensity
Tubulin Average Intensity
% of cells
% of control
Compound and Concentration (uM)

6h

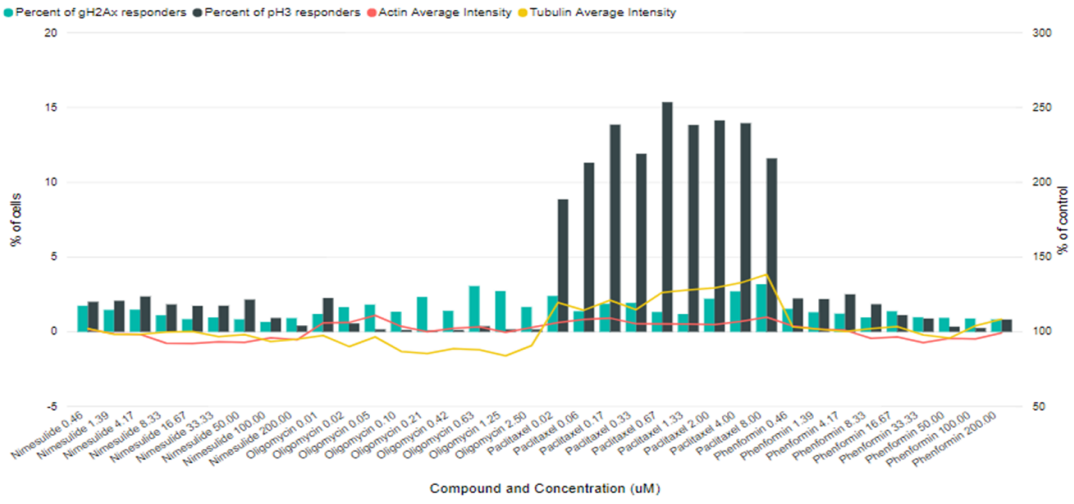
Percent of gH2Ax responders
Percent of pH3 responders
Actin Average Intensity
Tubulin Average Intensity
% of cells
% of control
Nimesulide 0.46
Nimesulide 1.39
Nimesulide 4.17
Nimesulide 8.33
Nimesulide 16.67
Nimesulide 33.33
Nimesulide 50.00
Nimesulide 100.00
Nimesulide 200.00
Oligomycin 0.01
Oligomycin 0.02
Oligomycin 0.05
Oligomycin 0.10
Oligomycin 0.21
Oligomycin 0.42
Oligomycin 0.63
Oligomycin 1.25
Oligomycin 2.50
Paclitaxel 0.02
Paclitaxel 0.06
Paclitaxel 0.17
Paclitaxel 0.33
Paclitaxel 0.67
Paclitaxel 1.33
Paclitaxel 2.00
Paclitaxel 4.00
Paclitaxel 8.00
Phenformin 0.46
Phenformin 1.39
Phenformin 4.17
Phenformin 8.33
Phenformin 16.67
Phenformin 33.33
Phenformin 50.00
Phenformin 100.00
Phenformin 200.00
Compound and Concentration (uM)

24h

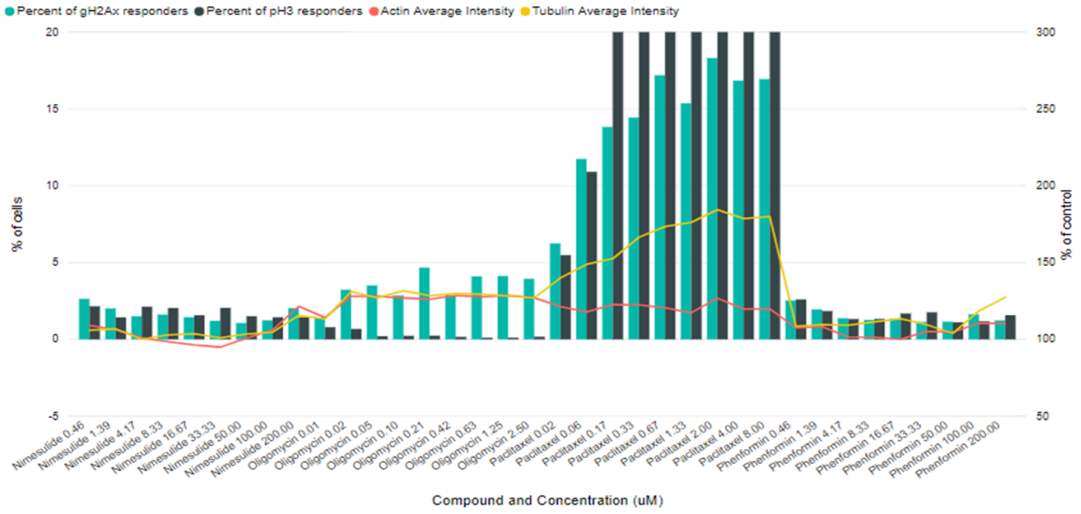
Percent of gH2Ax responders
Percent of pH3 responders
Actin Average Intensity
Tubulin Average Intensity
% of cells
% of control
Nimesulide 0.46
Nimesulide 1.39
Nimesulide 4.17
Nimesulide 8.33
Nimesulide 16.67
Nimesulide 33.33
Nimesulide 50.00
Nimesulide 100.00
Nimesulide 200.00
Oligomycin 0.01
Oligomycin 0.02
Oligomycin 0.05
Oligomycin 0.10
Oligomycin 0.21
Oligomycin 0.42
Oligomycin 0.63
Oligomycin 1.25
Oligomycin 2.50
Paclitaxel 0.02
Paclitaxel 0.06
Paclitaxel 0.17
Paclitaxel 0.33
Paclitaxel 0.67
Paclitaxel 1.33
Paclitaxel 2.00
Paclitaxel 4.00
Paclitaxel 8.00
Phenformin 0.46
Phenformin 1.39
Phenformin 4.17
Phenformin 8.33
Phenformin 16.67
Phenformin 33.33
Phenformin 50.00
Phenformin 100.00
Phenformin 200.00
Compound and Concentration (uM)

6h

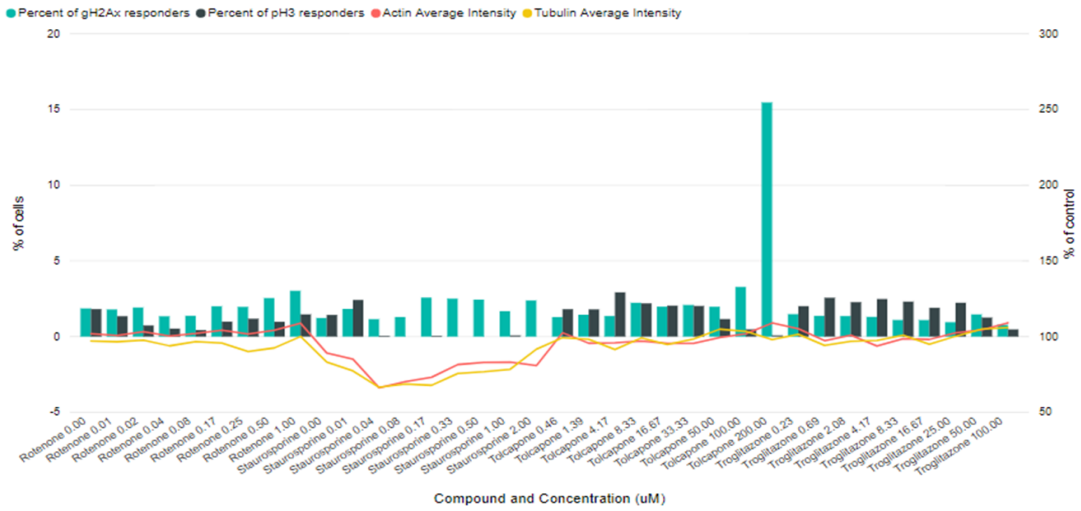
Percent of gH2Ax responders
Percent of pH3 responders
Actin Average Intensity
Tubulin Average Intensity
% of cells
% of control
Rotenone 0.00
Rotenone 0.01
Rotenone 0.02
Rotenone 0.04
Rotenone 0.08
Rotenone 0.17
Rotenone 0.25
Rotenone 0.50
Rotenone 1.00
Staurosporine 0.00
Staurosporine 0.01
Staurosporine 0.04
Staurosporine 0.08
Staurosporine 0.17
Staurosporine 0.33
Staurosporine 0.50
Staurosporine 1.00
Staurosporine 2.00
Tolcapone 0.46
Tolcapone 1.39
Tolcapone 4.17
Tolcapone 8.33
Tolcapone 16.67
Tolcapone 33.33
Tolcapone 50.00
Tolcapone 100.00
Tolcapone 200.00
Troglitazone 0.23
Troglitazone 0.69
Troglitazone 2.08
Troglitazone 4.17
Troglitazone 8.33
Troglitazone 16.67
Troglitazone 25.00
Troglitazone 50.00
Troglitazone 100.00
Compound and Concentration (uM)

24h

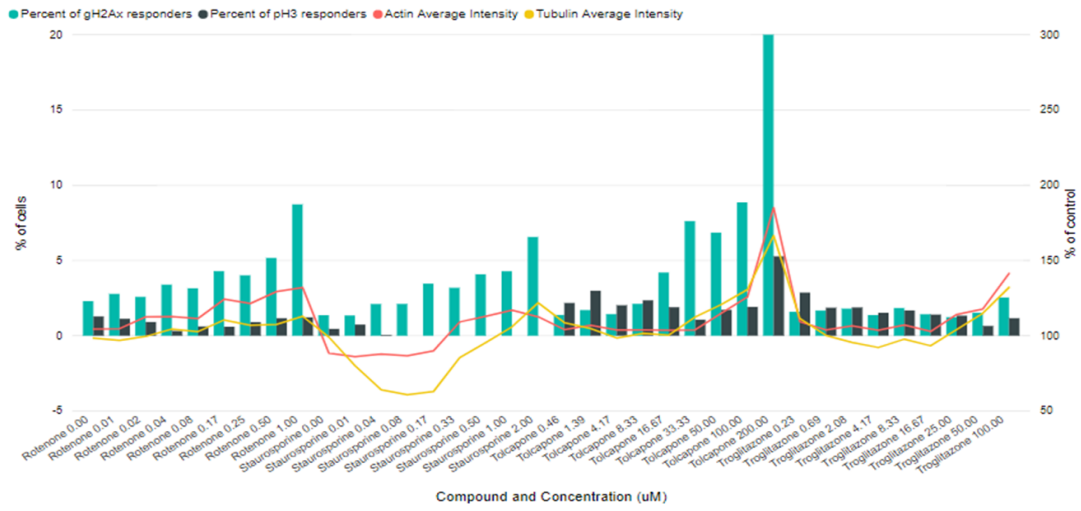
Percent of gH2Ax responders
Percent of pH3 responders
Actin Average Intensity
Tubulin Average Intensity
% of cells
% of control
Rotenone 0.00
Rotenone 0.01
Rotenone 0.02
Rotenone 0.04
Rotenone 0.08
Rotenone 0.17
Rotenone 0.25
Rotenone 0.50
Rotenone 1.00
Staurosporine 0.00
Staurosporine 0.01
Staurosporine 0.04
Staurosporine 0.08
Staurosporine 0.17
Staurosporine 0.33
Staurosporine 0.50
Staurosporine 1.00
Staurosporine 2.00
Tolcapone 0.46
Tolcapone 1.39
Tolcapone 4.17
Tolcapone 8.33
Tolcapone 16.67
Tolcapone 33.33
Tolcapone 50.00
Tolcapone 100.00
Tolcapone 200.00
Troglitazone 0.23
Troglitazone 0.69
Troglitazone 2.08
Troglitazone 4.17
Troglitazone 8.33
Troglitazone 16.67
Troglitazone 25.00
Troglitazone 50.00
Troglitazone 100.00
Compound and Concentration (uM)